JAERI-M
85-026

EVALUATION REPORT ON CCTF CORE-II REFLOOD TEST C2-4 (RUN 62)

—INVESTIGATION OF REPRODUCIBILITY—

March 1985

Tsutomu OKUBO, Tadashi IGUCHI, Kazuharu OKABE
Jun SUGIMOTO, Hajime AKIMOTO and Yoshio MURAO

日本原子力研究所
Japan Atomic Energy Research Institute

JAERI-M レポートは，日本原子力研究所が不定期に公刊している研究報告書です。
入手の問合わせは，日本原子力研究所技術情報部情報資料課（〒319－11 茨城県那珂郡東海村）あて，お申しこしください。なお，このほかに財団法人原子力弘済会資料センター（〒319-11 茨城県那珂郡東海村日本原子力研究所内）で複写による実費頒布をおこなっております。

JAERI-M reports are issued irregularly.
Inquiries about availability of the reports should be addressed to Information Division, Department of Technical Information, Japan Atomic Energy Research Institute, Tokai-mura, Naka-gun, Ibaraki-ken 319-11, Japan.

編集兼発行　日本原子力研究所
印　　刷　山田軽印刷所

JAERI-M 85-026

Evaluation Report on CCTF Core-II Reflood Test C2-4 (Run 62)

— Investigation of reproducibility —

Tsutomu OKUBO, Tadashi IGUCHI, Kazuharu OKABE*,
Jun SUGIMOTO, Hajime AKIMOTO and Yoshio MURAO

Department of Nuclear Safety Research
Tokai Research Establishment, JAERI

(Received January 31, 1985)

This report presents a data evaluation of the CCTF Core-II test C2-4 (Run 62), which was conducted on May 12, 1983. This test was conducted to investigate the reproducibility of tests in the CCTF Core-II test series. Therefore, the initial and boundary conditions of the present test were determined to be the same as those for the previously performed base case test (Test C2-SH1).

Comparing the data of the present test with those of Test C2-SH1, the following results are obtained.

(1) The initial and boundary conditions for the two tests were nearly identical except the temperature of the core barrel and the lower plenum fluid. The difference in the latter is considered to result in the difference in the core inlet subcooling of about 6 K at most.

(2) The system behavior was almost identical.

(3) The core cooling behavior was also nearly identical except a little difference in the rod surface temperature in the upper part of the high power region.

The work was performed undercontract with the Atomic Energy Bureau of Science and Technology Agency of Japan.

* Mitsubishi Atomic Power Industry, Inc.

(4) Taking account that the difference mentioned above in item (3) is small and can be explained qualitatively to be caused by the difference in the core inlet subcooling mentioned above in item (1), it is considered practically that there is the reproducibility of the thermo-hydrodynamic behavior in the CCTF Core-II tests.

Key words: Reactor Safety, LOCA, ECCS, PWR, Reflood, Thermo-hydrodynamics, Two-phase Flow, Heat Transfer, Quenching, CCTF Core-II

大型再冠水円筒第２次炉心試験Ｃ２－４（Run 62）評価報告書
―― 再 現 性 の 検 討 ――

日本原子力研究所東海研究所安全工学部
大久保　努・井口　　正・岡部　一治*
杉本　　純・秋本　　肇・村尾　良夫

（1985年1月31日受理）

本報告書は，1983年5月12日に実施された円筒第２次炉心試験Ｃ２－４（Run 62）の評価を行ったものである。本試験は，円筒第２次炉心試験装置による試験の再現性を検討するために実施された。そのため本試験の条件は，以前に行れた基準試験（試験Ｃ２－ＳＨ１）と同一に設定された。

本試験のデータを試験Ｃ２－ＳＨ１のデータと比較して以下の結果が得られた。

(1) 両試験における初期および境界条件は，炉心バレルおよび下部プレナム水の温度を除けばほぼ同一であった。後者の差が，最大で６Ｋ程度観測された炉心入口サブクーリングの差を生じたと考えられる。

(2) システム挙動は，ほぼ同一であった。

(3) 炉心冷却挙動は，高出力領域の上部における発熱体表面温度にわずかな差が見られた点を除けば，ほぼ同一であった。

(4) 上記(3)の差は小さく，上記(1)で述べた炉心入口サブクーリングの差によって生じている事を定性的に説明できることを考慮すると，実用上，円筒第２次炉心試験の熱水力挙動に再現性があると考えられる。

本報告書は，電源開発促進対策特別会計法に基づき，科学技術庁からの受託によって行った研究の成果である。

＊　三菱原子力工業㈱

Contents

目　　次

Table list

Figure List

1. Introduction

A reflood test program[1] using large scale test facilities has been conducted at the Japan Atomic Energy Research Institute (JAERI). The facilities are the Cylindrical Core Test Facility (CCTF) and the Slab Core Test Facility (SCTF). This report presents the evaluation for the CCTF Core-II base case test, Test C2-4 (Run 62).

The CCTF is an experimental facility designed to model a full-height core section, four primary loops and their components of a pressurized water reactor (PWR). This facility is used to provide information on fluid behaviors in the core, downcomer and upper plenum including the steam and water carryover phenomena, and integral system effects during the refill and reflood phases of a hypothetical loss-of-coolant accident (LOCA) of a PWR.

The objectives of the test program using the CCTF are:

a. Demonstration of capability of emergency core cooling system (ECCS) during refill and reflood period.
b. Verification of reflood analysis codes.
c. Collection of information to improve the thermo-hydrodynamic models in the analysis codes, such as, (a) multi-dimensional core thermo-hydrodynamics including the radial power distribution effect, fall back effect and spatial oscillatory behavior, (b) flow behavior in the upper plenum and hot legs, (c) behavior of accumulated water at the bottom of the upper plenum including possible counter-current flow and sputtering effect, (d) hydrodynamic behavior of the injected ECC water and the water passing through the steam generator, (e) multi-dimensional thermo-hydrodynamic behavior in the hot annular downcomer, and (f) overall oscillatory behavior in the system.

As the first series of the CCTF tests, twenty-seven CCTF Core-I tests were conducted. This series of tests presented a lot of information[2] on the system thermo-hydrodynamic behavior as well as the core behavior during the refill and reflood phases of a LOCA in a PWR. The CCTF Core-I test series was initiated in March 1979 and terminated in April 1981. Subsequently, as the second series of the CCTF tests, the CCTF Core-II test series was initiated in March 1982. The special purposes of the CCTF Core-II test program are to investigate the effects of alternative ECCS such as the combined and the downcomer injections as

well as to extend the experimental range of the Core-I test series.

Test C2-4 (Run 62) was conducted on May 12, 1983 in order to investigate the reproducibility of the CCTF Core-II tests. Therefore, the test conditions of the present test were set to be the same as those for the previously conducted base case test (Test C2-SH1)[3]. In this report, the data of those two tests are compared and discussed.

The selected data of the present test are presented in Appendix B for better understanding of the test results.

2. Test Description

2.1 Test Facility

The CCTF Core-II was designed in consideration of the following objectives and criteria:

a. Design objectives

(1) The facility should provide the capability to reasonably simulate the flow conditions in the primary system of a PWR during the refill and reflood phases of a LOCA.

(2) The downcomer design should provide ECC water flow behavior throughout the test which is reasonably representative of that of the PWR downcomer.

b. Design criteria

(1) The reference reactors are the Trojan reactor in the USA and in certain aspects the Ohi reactor in Japan.

(2) The vertical dimensions and locations of system components are kept as close to those of the reference reactors as possible.

(3) The flow areas of the system components are scaled down in proportion to the scaling factor of core flow area.

(4) The facility is equipped with four loops which are composed of three intact loops and one broken loop.

(5) A 200% cold leg large break is simulated in the broken loop.

(6) The ECCS consists of two accumulator systems (Acc) and alow pressure coolant injection system (LPCI), and the injection locations are the upper plenum and the downcomer as well as the lower plenum and the cold legs.

(7) The maximum allowable pressure of the facility is 588 kPa (6 kg/cm^2 absolute).

(8) The maximum allowable temperature of the simulated fuel rods is 1173 K (900°C).

(9) The maximum allowable temperature of the components in the primary system except the simulated fuel rod assembly is 623 K (350°C).

(10) The reactor vessel contains appreximately 2,000 electrically heated rods simulating the fuel rods.

(11) The design of upper plenum internals is based on that of a new 17×17 type Westinghouse fuel assembly.

(12) The flow resistance of each loop is adjusted by an orifice in the pump simulator.

(13) The containment system consists of two tanks.

A bird's-eye view of the CCTF is shown in Fig. 2.1. The scaled dimensions of the components are given in Table 2.1.

The differences in the design of the Core-II facility from the Core-I are:

(1) Axial peaking factor of heater rods

(2) Local peaking factor of heater rods in a bundle

(3) Upper plenum structures (upper plenum internals, plugging devices in end box region and a upper ring)

(4) Vent valves

(5) Alternative ECCS (downcomer injection and upper plenum injection)

(6) Instruments

2.1.1 Pressure Vessel and Internals

The pressure vessel is of a cylindrical type as shown in Figs. 2.2 and 2.3. The height is the same as the reference reactor pressure vessel. The radial direction is scaled down in proportion to the core flow area scaling, that is, 1/21.44. The upper ring was newly installed in the Core-II facility for the installation of the upper plenum ECC water injection lines and the instruments. The upper plenum injection lines are shown in Figs. 2.4 and 2.5. The upper plenum injection is adopted in some 2-loop PWRs in Japan and the USA. Four vent valves and two downcomer ECC water injection nozzles, which are called Core Flooding Nozzle (CFN), are also newly equipped in the Core-II facility as shown in Figs. 2.2 and 2.3. Vent valves and CFNs are for the simulation of a Babcock & Wilcox (B & W) type PWR. Downcomer injection nozzles also exist in a couple of recent Japanese 2-loop PWRs. The location of Core Flooding Nozzles are shown in Fig. 2.6 in detail.

The cross section of the pressure vessel is shown in Fig. 2.3 and the dimensions are given in Fig. 2.7. The core consists of thirty-two 8×8 electrically heated rod bundles arranged in a cylindrical configuration and simulates a Westinghouse 15×15 type fuel assemblies.

The downcomer is an annulus of 61.5 mm gap. In determining the gap size, the flow area of the core baffle region was added to that of the downcomer region. Thus, the core baffle flow area is included in

the downcomer simulation and is not simulated separately in the vessel inserting stainless steel fillers to prevent fluid flow.

The vessel wall is constructed of carbon steel which is cladded with the 5 mm thick stainless steel plate. The wall is 90 mm thick to simulate the stored energy as reasonably as possible during ECC water injection.

The design of upper plenum internals is based on that of the new Westinghouse 17×17 type fuel assemblies instead of the old type simulated in the Core-I facility. The internals consists of ten control rod guide tubes, ten support columns and twelve open boles as shown in Fig. 2.8. The radius of each internals is scaled down by factor 8/15 from that of an actual reactor. They are illustrated in Fig. 2.9. Flow resistance baffles are inserted into the control rod guide tubes. The baffles consist of two kinds of baffle plates and a shaft. The baffle plates are shown in Fig. 2.10.

End boxes are attached beneath the UCSP. The structure for one heater rod bundle is shown in Fig. 2.11. Plugging devices are installed newly in the Core-II facility as shown in Figs. 2.11 and 2.12 to simulate the flow resistance more correctly.

2.1.2 Heater Rod Assembly

The heater rod assembly simulating the fuel assembly consists of thirty-two 8×8 array rod bundle. Each bundle consists of fifty-seven electrically heated rods and seven non-heated rods as shown in Fig. 2.13. The core is usually subdivided into three regions to achieve a desired radial power distribution. This is shown in Fig. 2.3. The high, medium and low power regions are named A, B and C regions, respectively. The local peaking factor of heated rods in a bundle is unity, that is, all heated rods in a bundle have the same power density in the Core-II facility.

A heater rod consists of a nichrome heating element, magnesium oxide (MgO) and boron nitride (BN) insulators, and Inconel-600 sheath. BN is used for only central part of the heated region and MgO for the other part as shown in Fig. 2.14. The heated length and the outer diameter of the heater rods are 3.66 m and 10.7 mm, respectively, which are identical to the corresponding dimensions of actual PWR fuel rods. The sheath wall thickness is 1.0 mm and is thicker than the actual fuel

cladding, because of the requirements for thermocouple installation. The heating element is a helical coil with a varying pitch to generate a 17-step chopped consine axial power profile as shown in Fig. 2.15. The peaking factor is 1.40, instead of 1.492 for a Core-I rod.

Non-heated rods are either stainless steel pipes or solid bars of 13.8 mm O.D. The pipes are utilized for installation of instruments such as superheated steam probes and thermocouples. The bars are used for supporting the assembly loads.

The heated rods and non-heated rods are held in radial position by gird spacers which are located at six elevations along the axial length as shown in Fig. 2.15. A grid spacer is a lattice structure composed of stainless steel plates of 0.4 mm and 0.8 mm thick and 40 mm high. The rod pitch is 14.3 mm which is the same as that of the reference PWR.

The heater rods penetrate through the bottom plate of the vessel to facilitate lead out of the power cables from the bottom of the vessel. The outer diameter of the rods in the lower plenum is reduced to 8.6 mm. Three phase electric current is used for heating the heater rods and the electrical neutral point is at the top of the rods where they are interconnected to each other.

2.1.3 Primary Loops and ECCS

Primary loops consist of three intact loops and a broken loop. Each loop consists of hot leg and cold leg pipings, a steam generator simulator and a pump simulator. The 200 percent cold leg large break is simulated for the broken loop. The broken cold leg is connected to two containment tanks through blowdown valves. The primary loop arrangement is shown in Figs. 2.16 and 2.17.

The inner diameter of the piping is scaled down in proportion to the core flow area scaling. The length of each piping section is almost the same as the corresponding section of the reference PWR.

The steam generator simulators are of the U-tube and shell type as shown in Fig. 2.18. The tube length is about 5 m shorter than in the reference PWR. The vertical hight of the steam generator simulators is also about 5 m lower than in the reference PWR. The primary coolant passes through the tube side and the secondary coolant is stagnant in the shell side. The steam generator simulators of two loops are housed in a single shell assembly which has two compartment, one simulator for

each loop in one compartment. The wall thickness of the U-tube is 2.9 mm compared to 1.27 mm of the reference PWR, because of a higher pressure difference between the primary and secondary sides in the simulator.

The pump simulator consists of the casing and duct simulators and an orifice plate as shown in Fig. 2.19. The loop flow resistance is simulated with the orifice plate. Each orifice plate has a hole with diameter and thickness of 95 mm and 10 mm, respectively.

ECCS consists of two Accs and a LPCI. The injection points are at each cold leg, lower plenum, upper plenum and downcomer. The upper plenum and downcomer injection system was newly installed after Test C2-2 (Run 56) for the alternative ECCS tests. In the new injection system, two accumulator tanks are used for ECC water injection.

2.1.4 Instrumentation

The instrumentation is divided into two groups. One of them is JAERI-supplied instruments measuring the temperatures, absolute pressures, differential pressures, water levels and flow rates. Thermo-couples measure the temperatures of the rod surface, fluid and structure. The absolute pressures are measured in the upper and lower plena, steam generator plena and containment tanks. The differential pressure measurements are carried out at many locations covering the whole system almost completely. In the ECC water supply tanks and the containment tank 1, the liquid levels are measured. The flow meters measure the ECC water flow rates. Furthermore, flow rates in the downcomer, loop seal pipings and the vent line from the containment tank 2 to the atmosphere are measured with drag disk flow meters, pitot tubes and a venturi tube, respectively. The total number of the JAERI-supplied instruments is 1338 channels as summarized in Table 2.2 and the signals from these instruments are recorded on a magnetic tape.

The other group of the instrumentation is the USNRC-supplied instruments. They are the advanced instrumentation for the two-phase flow measurement. The kinds and quantities of those are tabulated in Table 2.3. The total number is 540 channels.

2.2 Test Conditions and Procedures

2.2.1 Test Conditions

The summary of the test conditions are presented in Table 2.4. The test conditions of the present test were set to be the same as those for the base case test (Test C2-SH1).

2.2.2 Test Procedures

In preparation for the test, the accumulator tanks, the LPCI tank, the saturated water tank and the secondary sides of the steam generator simulators were filled with water which was purified with ion exchange resin. After all the components and instruments were inspected for mechanical and electrical leakages, the instruments were checked for zero points and sensitivity.

After these preparatory operation, the primary system was heated with the preheaters to its specified temperature (393 K) and pressurized to a specified pressure (200 kPa) by substituting steam for nitrogen gas in the system. The water in the accumulator tanks was electrically heated to its specified temperature (308 K) and pressurized with nitrogen gas to provide sufficient head to drive the injection flow required. The water in the LPCI tank was also heated to its specified temperature (308 K) and was circulated through the circulation line including the LPCI line so as to preheat the line to the same temperature as the water. The water in the saturated water tank was heated up near saturation temperature (393 K) of the expected primary system pressure (200 kPa). The water in the secondary side of each steam generator simulator was also heated and pressurized to the specified temperature (539 K) and pressure (5.3 MPa).

After establishing the initial conditions of the test, electric power for preheating was turned off and the lower plenum was filled to a specified level (0.9 m) directly from the saturated water tank. When the water level in the lower plenum reached the specified level and other initial conditions of the test stabilized at the allowable tolerance, electric power was applied to the heater rods in the core and the data recording was started. This is the initiation of the test, *i.e.* 0 s. The temperature rise of the rods were monitored by using

computer. When a specified clad temperature (995 K) was reached, Acc injection (0.105 m^3/s) into the lower plenum was initiated. This specified initial clad temperature (995 K) of the heater rods for initiation of coolant injection was predetermined by interpolation between the clad temperature (393 K) after preheating and the cald temperature (1073 K) assumed for the time of bottom of core recovery (BOCREC). Decay of power input to the rods was programed to begin at the time of BOCREC. The specified power decay was obtained by normalizing the decay curve of the ANS standard $\times 1.2 + {}^{238}U$ capture decay $\times 1.1$ at 30 seconds after shutdown.

At a specified time, Acc injection location was switched from the lower plenum to three intact cold legs. Since the BOCREC was scheduled to occur a few seconds before this time, some amount of steam generated in the core was expected to flow in the primary loops prior to switching of the Acc injection location. This procedure was for preventing an unrealistic condensation from occurring at the cold legs. At a specified time (23 s) after the initiation of Acc injection, the Acc injection mode was transferred to the LPCI injection mode. A specified LPCI injection rate (0.011 m^3/s) was maintained constantly until the ECC injection was turned off.

The generated steam and the entrained water flowed via broken and intact loops to the containment tank 2. The steam was then vented to the atmosphere to maintain the pressure in the containment tank constant at the specified initial pressure (200 KPa).

When all thermocouples on the surface of heater rods indicated quenching of the rods, the power supply to heater rods and the ECC water injection were turned off. After this the data recording was ended terminating the test.

The chronology of events is presented in Table 2.5.

Table 2.1 CCTF component scaled dimensions

COMPONENT		PWR	JAERI	RATIO
PRESSURE VESSEL				
VESSEL INSIDE DIAMETER	(mm)	4394 (173")	1084	
VESSEL THICKNESS	(mm)	216 (8 1/2")	90	
CORE BARREL OUTSIDE DIAMETER	(mm)	3874	961	
CORE BARREL INSIDE DIAMETER	(mm)	3760	929	
THERMAL SHIELD OUTSIDE DIAMETER	(mm)	4170		
THERMAL SHIELD INSIDE DIAMETER	(mm)	4030		
DOWNCOMER LENGTH	(mm)	4849	4849	1/1
DOWNCOMER GAP	(mm)	114.3	61.5	
DOWNCOMER (+ BUFFLE) FLOW AREA	(m^2)	4.23	0.197	1/21.44
LOWER PLENUM VOLUME	(m^3)	29.6	1.38	1/21.44
UPPER PLENUM VOLUME	(m^3)	43.6	2.04	1/21.44
FUEL (HEATER ROD) ASSEMBLY				
NUMBER OF BUNDLES	(—)	193	32	
ROD ARRAY	(—)	15 × 15	8 × 8	
ROD HEATED LENGTH	(mm)	3660	3660	1/1
ROD PITCH	(mm)	14.3	14.3	1/1
FUEL ROD OUTSIDE DIAMETER	(mm)	10.72	10.7	1/1
THIMBLE TUBE DLAMETER	(mm)	13.87	13.8	1/1
INSTRUMENT TUBE DIAMETER	(mm)	13.87	13.8	1/1
NUMBER OF HEATER RODS	(—)	39372	1824	1/21.58
NUMBER OF NON-HEATED RODS	(—)	4053	224	1/18.09
CORE FLOW AREA	(m^2)	5.29	0.25	1/21.2
CORE FLUID VOLUME	(m^3)	17.95	0.915	1/19.6
PRIMARY LOOP				
HOT LEG INSIDE DIAMETER	(mm)	736.6 (29")	155.2	1/4.75
HOT LEG FLOW AREA	(m^2)	0.426	0.019	1/22.54
HOT LEG LENGTH	(mm)	3940	3940	1/1
PUMP SUCTION INSIDE DIAMETER	(mm)	787.4 (31")	155.2	1/5.07
PUMP SUCTION FLOW AREA	(m^2)	0.487	0.019	1/25.77
PUMP SUCTION LENGTH	(mm)	7950	7950	1/1

Table 2.1 (Cont'd)

COMPONENT		PWR	JAERI	RATIO
COLD LEG INSIDE DIAMETER	(mm)	698.5 (27.5")	155.2	1/4.50
COLD LEG FLOW AREA	(m^2)	0.383	0.019	1/20.26
COLD LEG LENGTH	(mm)	5600	5600	1/1
STEAM GENERATOR SIMULATOR				
NUMBER OF TUBES	(—)	3388	158	1/21.44
TUBE LENGTH (AVERAGE)	(m)	20.5	15.2	1/1.35
TUBE OUTSIDE DIAMETER	(mm)	22.225 (0.875")	25.4	
TUBE INSIDE DIAMETER	(mm)	19.7 (0.05")	19.6	1/1
TUBE WALL THICKNESS	(mm)	1.27	2.9	
HEAT TRANSFER AREA	(m^2)	4784 (51500 ft^2)	192	1/24.92
TUBE FLOW AREA	(m^2)	1.03	0.048	1/21.44
INLET PLENUM VOLUME	(m^3)	4.25	0.198	1/21.44
OUTLET PLENUM VOLUME	(m^3)	4.25	0.198	1/21.44
PRIMARY SIDE VOLUME	(m^3)	30.50 (1077 ft^3)	1.2	1/25.41
SECONDARY SIDE VOLUME	(m^3)	157.33 (5556 ft^3)	2.5	1/62.93
CONTAINMENT TANK - I	(m^3)		30	
CONTAINMENT TANK - II	(m^3)		50	
STORAGE TANK	(m^3)		25	
ACC. TANK	(m^3)		5	
SATURATED WATER TANK	(m^3)		3.5	
ELEVATION				
BOTTOM OF HEATED REGION IN CORE	(mm)	0	0	
TOP OF HEATED REGION IN CORE	(mm)	3660	3660	0
TOP OF DOWNCOMER	(mm)	4849	4849	0
BOTTOM OF DOWNCOMER	(mm)	0	0	0
CENTERLINE OF COLD LEG	(mm)	5198	4927	- 271
BOTTOM OF COLD LEG (INSIDE)	(mm)	4849	4849	0
CENTERLINE OF LOOP SEAL LOWER END	(mm)	2056	2047	- 9
BOTTOM OF LOOP SEAL LOWER END	(mm)	1662	1959	+ 297

Table 2.1 (Cont'd)

COMPONENT		PWR	JAERI	RATIO
CENTER OF HOT LEG	(mm)	5198	4927	- 271
BOTTOM OF HOT LEG (INSIDE)	(mm)	4830	4849	+ 19
BOTTOM OF UPPER CORE PLATE	(mm)	3957	3957	0
TOP OF LOWER CORE PLATE	(mm)	- 108	- 50	+ 58
BOTTOM OF TUBE SHEET OF STEAM GENERATOR SIMULATOR	(mm)	7308	7307	- 1
LOWER END OF STEAM GENERATOR SIMULATOR PLENUM	(mm)	5713	5712	- 1
TOP OF TUBES OF STEAM GENERATOR SIMULATOR (avg)	(mm)	17952.7	14820	

Table 2.2 List of items measured with JAERI-supplied instruments

Item	Number of channels
Rod surface temperature	673
Core fluid temperature	40
Core barrel wall temperature	10
UP fluid temperature	120
UP wall temperature	36
DC fluid temperature	20
DC wall temperature	40
LP fluid temperature	8
LP wall temperature	4
SG primary side fluid temperature	24
SG secondary side fluid temperature	66
Primary loop piping fluid temperature	94
Primary loop piping wall temperature	4
Water supply tank fluid temperature	12
Core differential pressure	28
DC differential pressure	20
UP differential pressure	8
LP differential pressure	1
SG primary side differential pressure	8
Primary loop differential pressure	52
Pressure	15
Water level	7
Flow rate	39
Electric power	9
Total	1338

Note

UP : Upper plenum, DC : Downcomer

LP : Lower plenum, SG : Steam generator

Table 2.3 List of USNRC-provided instruments

Instrument	Number of sets	Number of sensors
DC FDG	18	162
DC VOP	1	1
DC drag disk	4	8
Core velocimeter	4	4
Core flag probe	12	24
Core LLD	6	96
LP LLD	3	15
End box turbine meter	8	8
UP turbine meter	4	4
UP FDG	11	110
UP film probe	2	4
UP prong probe	2	4
UP VOP	1	1
VV turbine meter	2	2
VV string probe	2	2
HL film probe	2	4
HL VOP	1	1
Reference probe	1	1
Spool piece	8	89
Total	92	540

Note

DC : Downcomer, FDG: Fluid distribution grid,
VOP: Video optical probe, LLD: Liquid level detector,
LP : Lower plenum, UP : Upper plenum,
VV : Vent valve

Table 2.4 Summary of test conditions

1. Test type: Reproducibility
2. Test No.: C2-4 (Run 62)
3. Test Date: May 12, 1983
4. Power: Total; 9.37 MW, Average linear; 1.40 kW/m
5. Radial power distribution:

   A : B : C

   1.92 : 1.67 : 1.07 kW/m
6. Pressure (MPa):

   Upper plenum ; 0.26

   Containment ; 0.20
7. Temperature (K):

   Downcomer wall; 467, Vessel internals; 394

   Primary piping; 394, Lower plenum liquid; 394

   ECC liquid; 308, Steam generator secondary; 539
8. ECC injection type: Cold leg injection
9. Pump K-factor: ~15
10. ECC injection rates and duration:

    Acc; 91 × 10^{-3} m^3/s from 99.5 to 111.0 s (at half maximum)

    LPCI; 11 × 10^{-3} m^3/s from 120.0 to 1005.0 s

    ECC injection to lower plenum; from 84.5 to 97.0 s
11. Initial water level in lower plenum: 0.81 m
12. Power decay: ANS × 1.2 + Actinide × 1.1 (30 s after scram)
13. Peak clad temperature at BOCREC: 1072 K

Table 2.5 Chronology of events for test

Event	Time (s)
Test initiated (Heater rods power on) (Data recording initiated)	0.0
Accumulator injection initiated	84.5
Power decay initiated	93.5
Bottom of core recovery (BOCREC)	94.0
Accumulator injection switched from lower plenum to cold legs	97.0
LPCI injection initiated	120.0
All heater rods quenched	652.0
Power off	1005.0
LPCI injection ended	1005.0
Test ended (Data recording ended)	1035.0

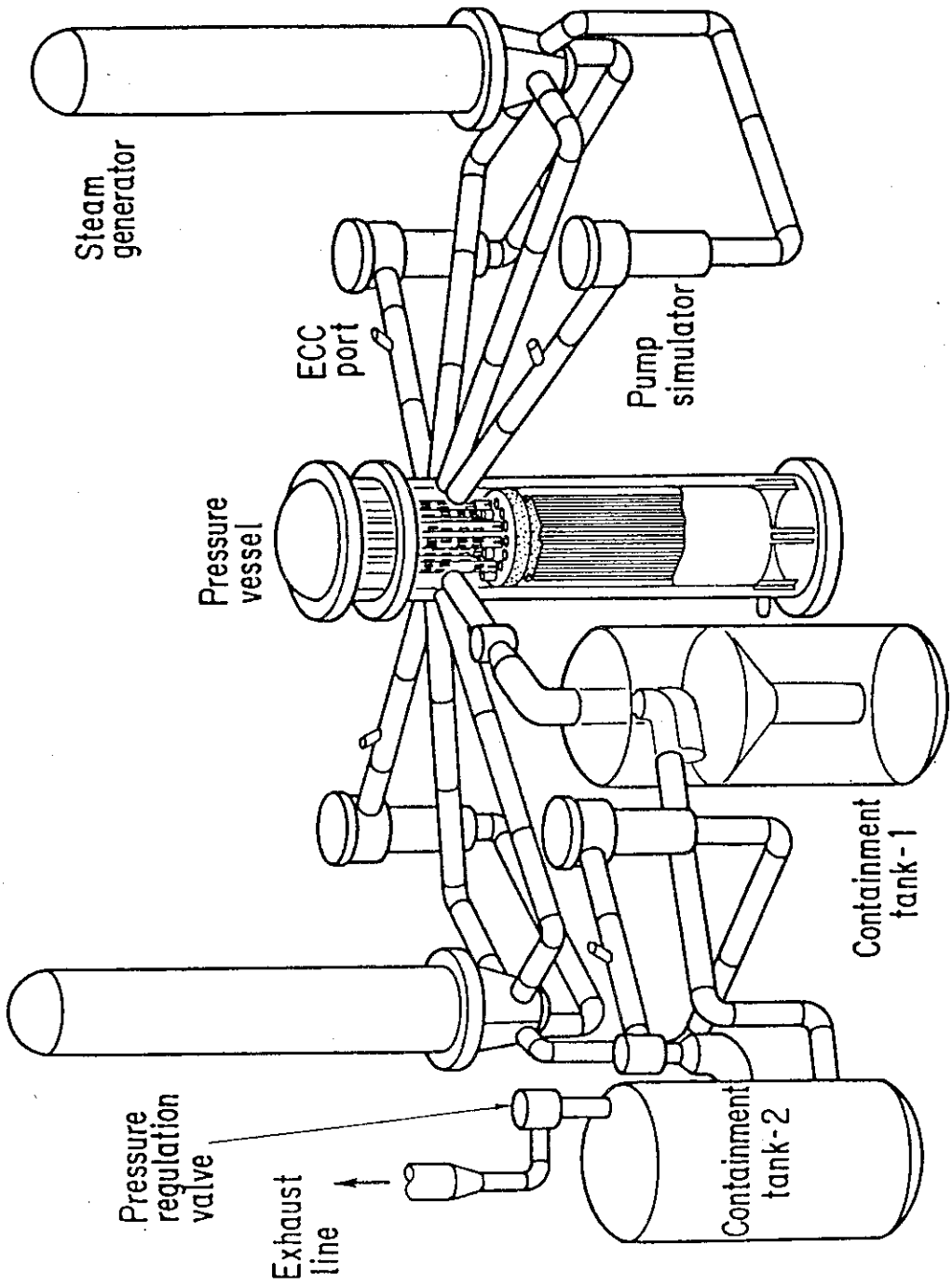

Fig. 2.1 Bird's-eye view of CCTF

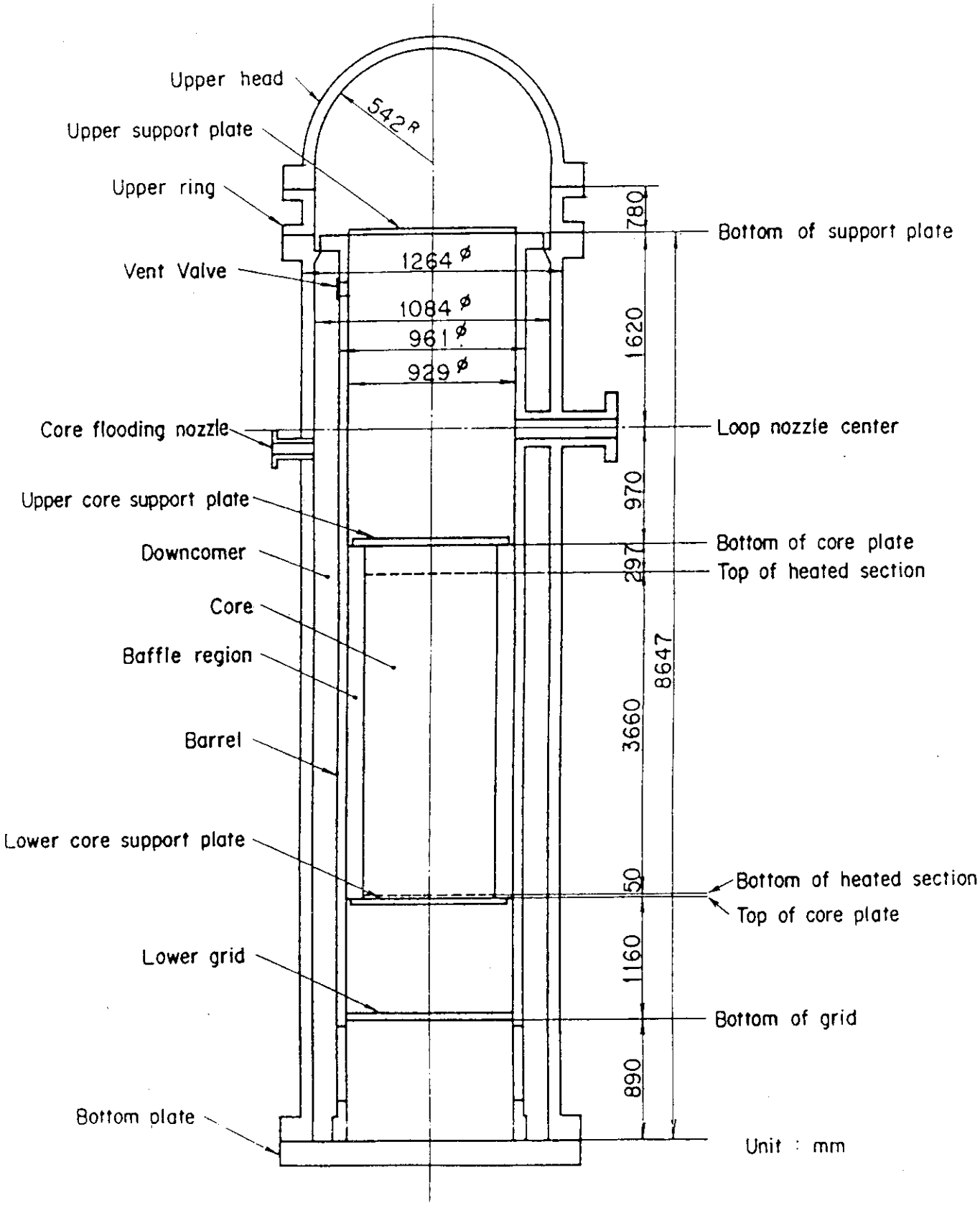

Fig. 2.2 CCTF Core-II pressure vessel

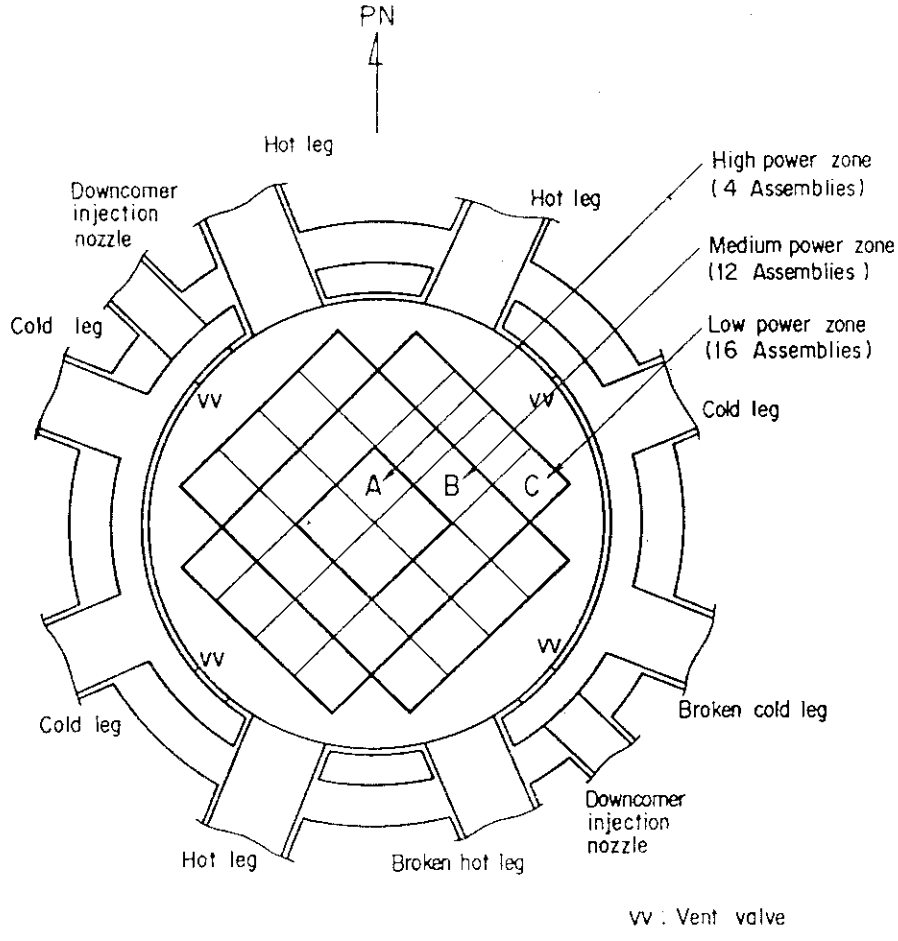

Fig. 2.3 Cross section of CCTF Core-II pressure vessel

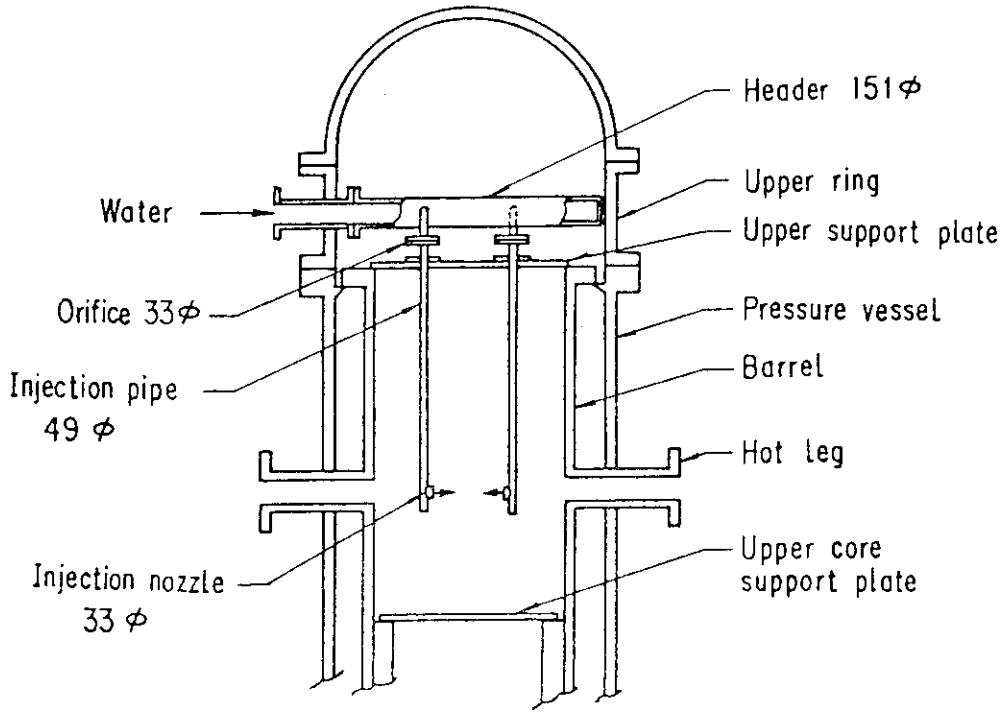

Fig. 2.4 Configuration of upper plenum injection pipe

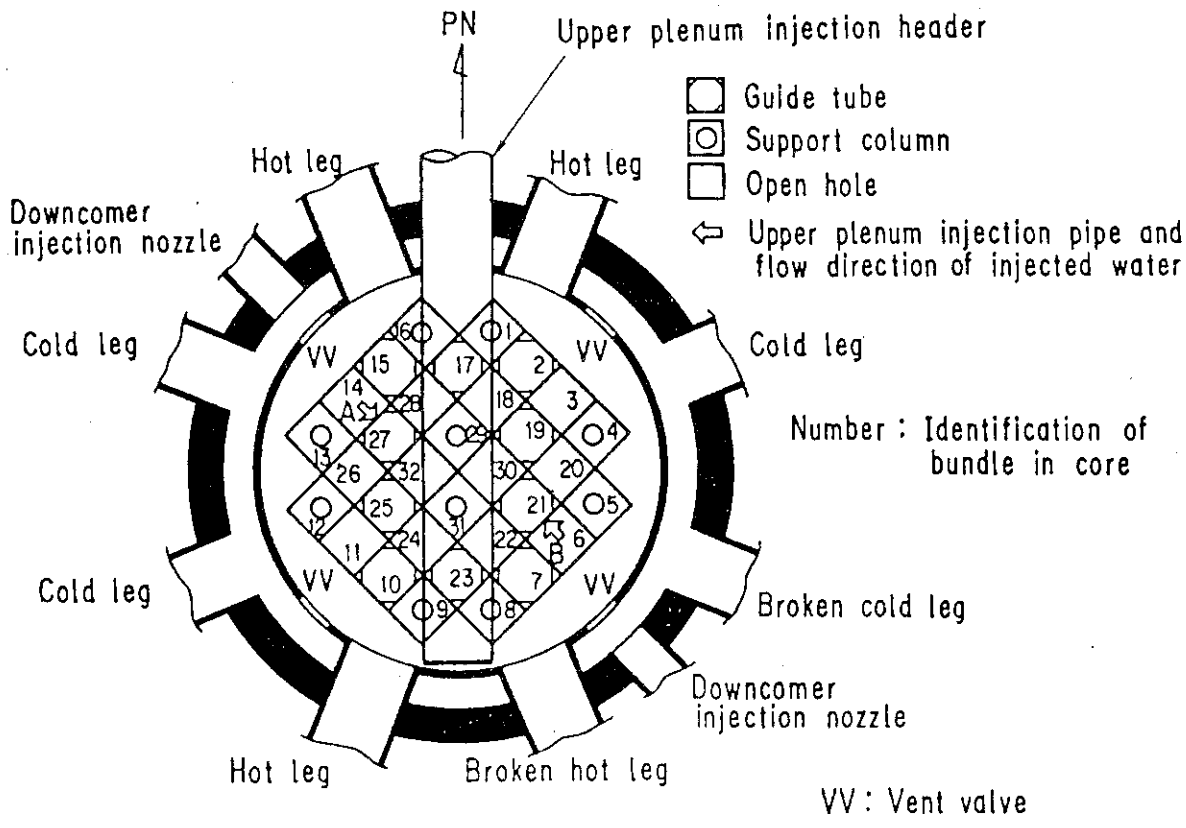

Fig. 2.5 Arrangement and location of upper plenum injection pipe

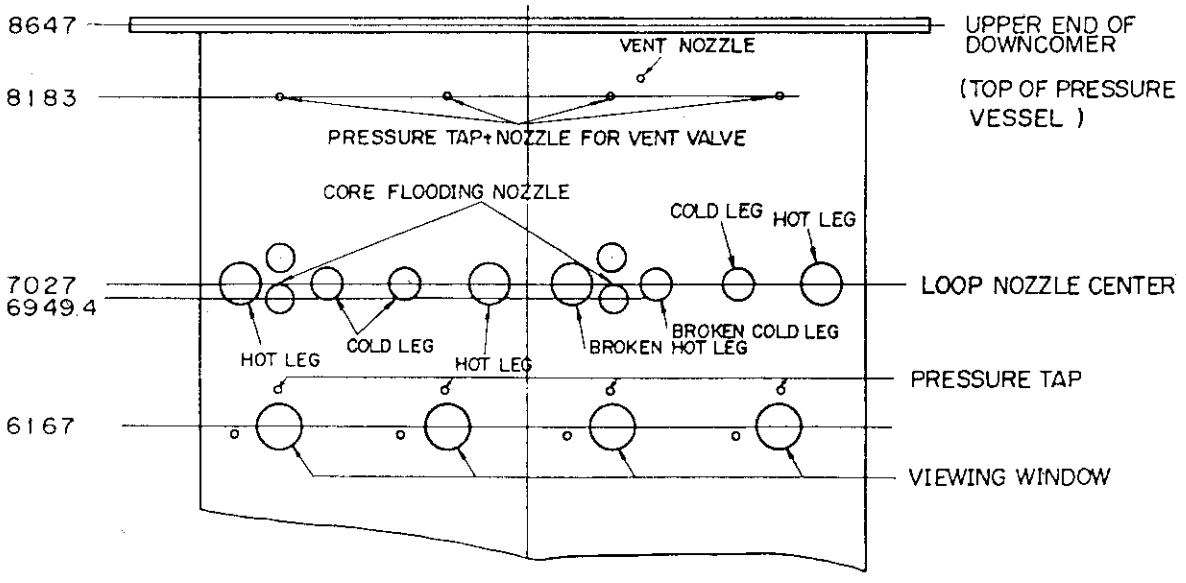

Fig. 2.6 Location of Core Flooding Nozzles

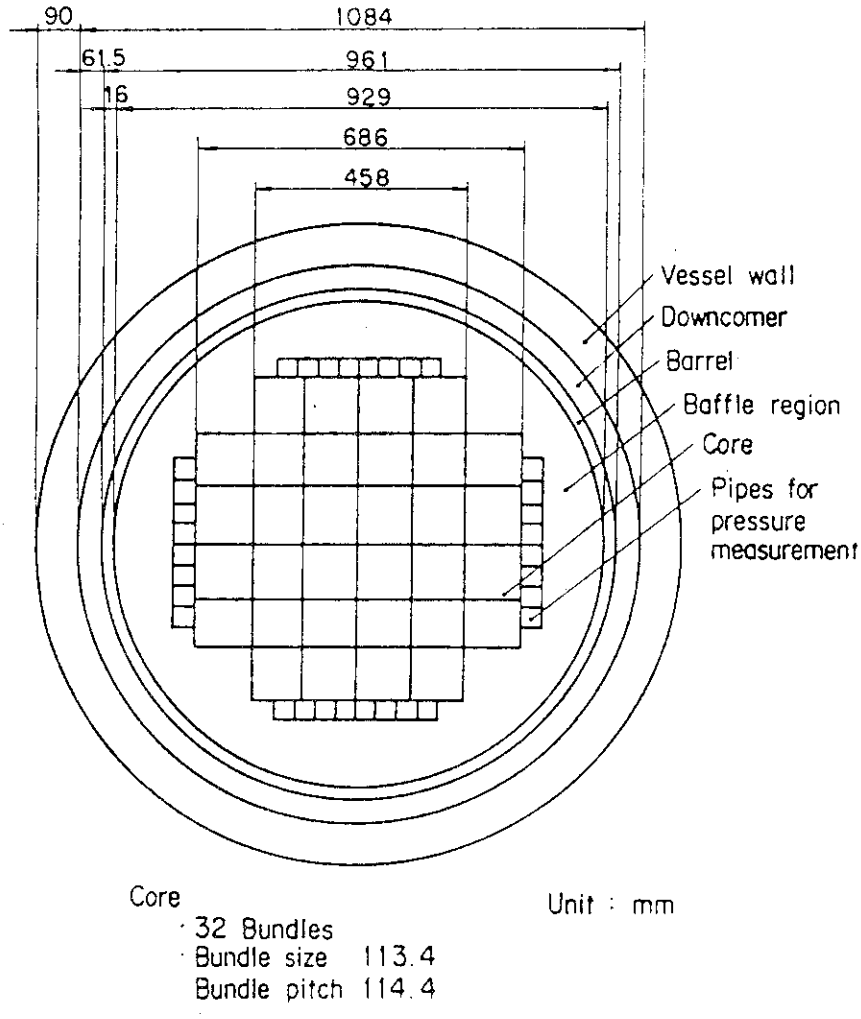

Fig. 2.7 Dimension of CCTF Core-II pressure vessel cross section

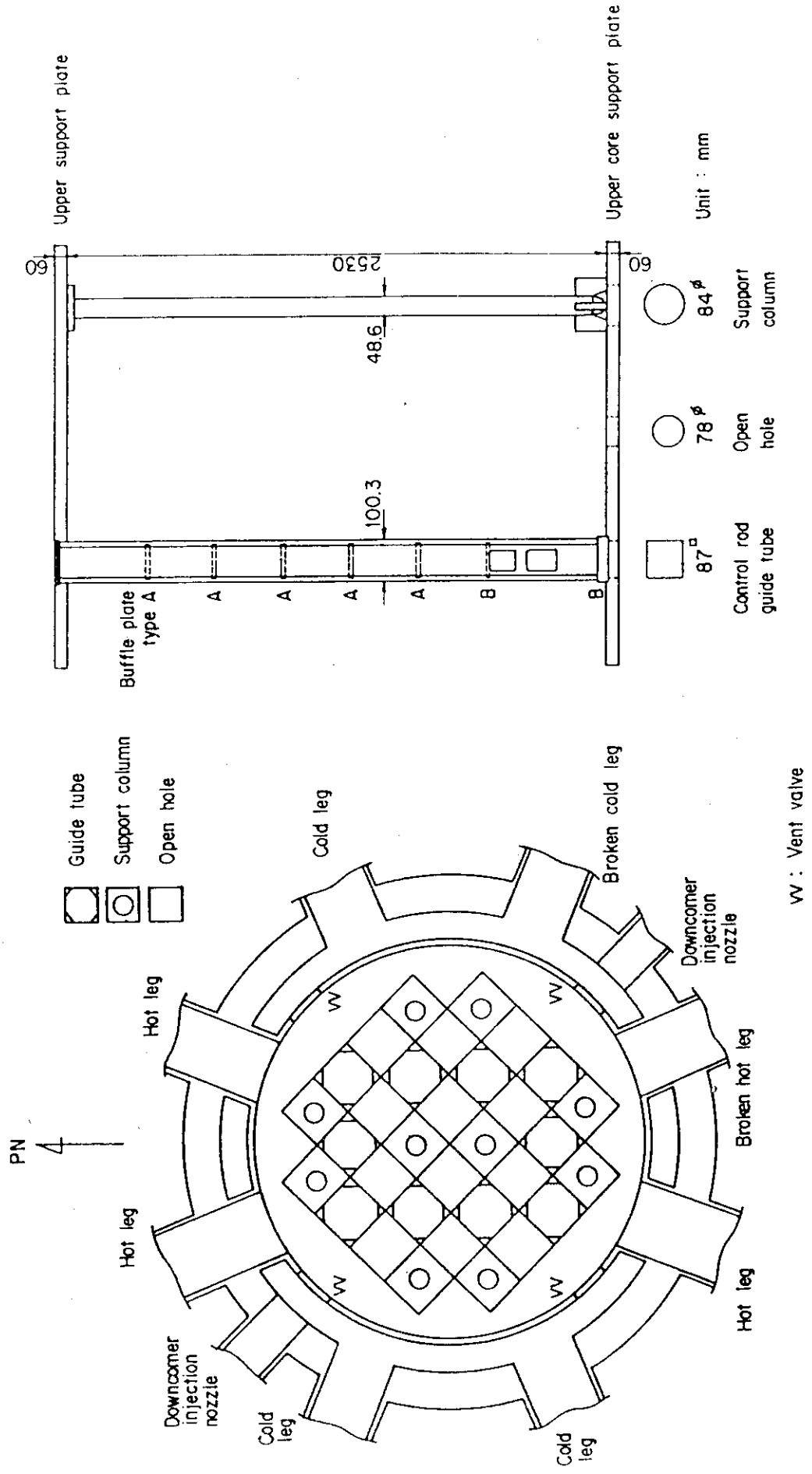

Fig. 2.8 Arrangement of upper plenum internals

Fig. 2.9 Upper plenum internals

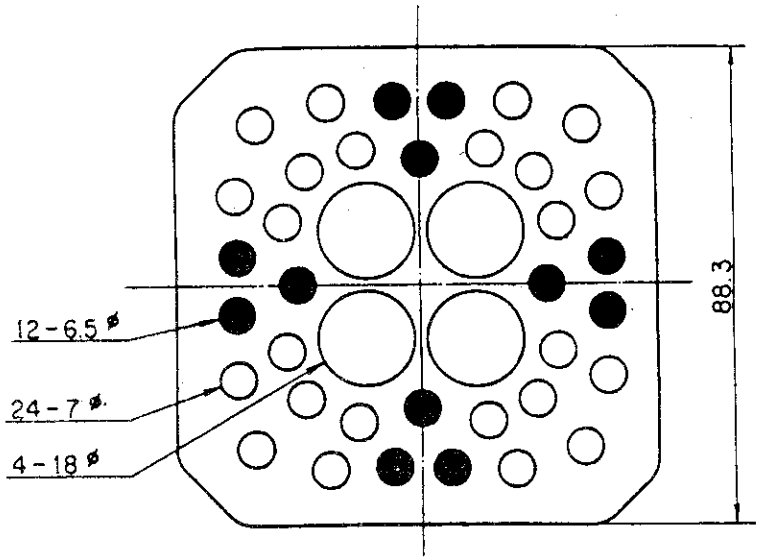

Type A

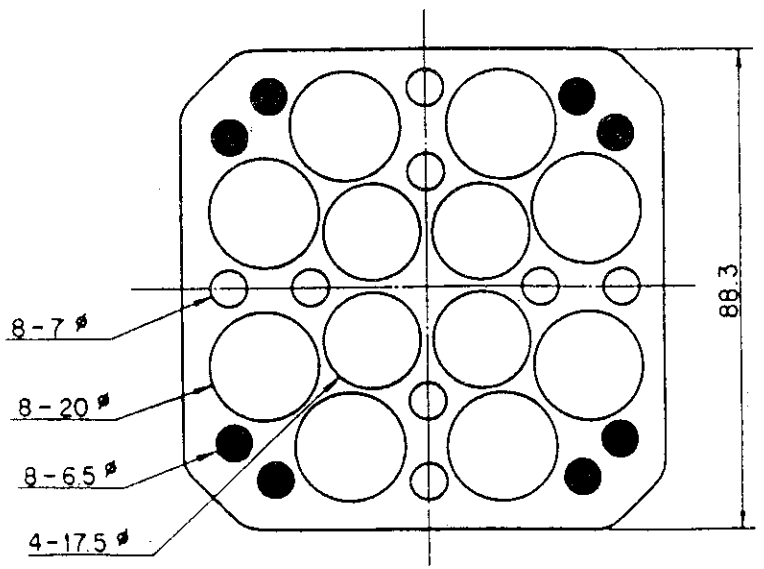

Type B

Unit : mm

Fig. 2.10 Buffle plates in control rod guide tube

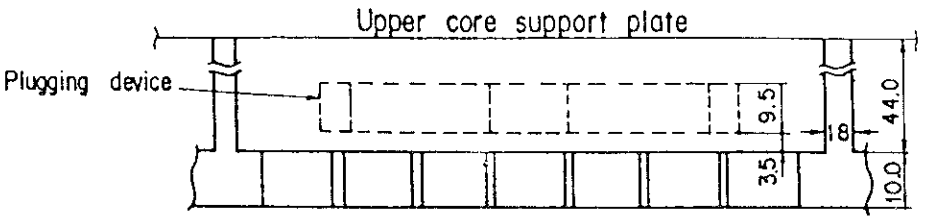

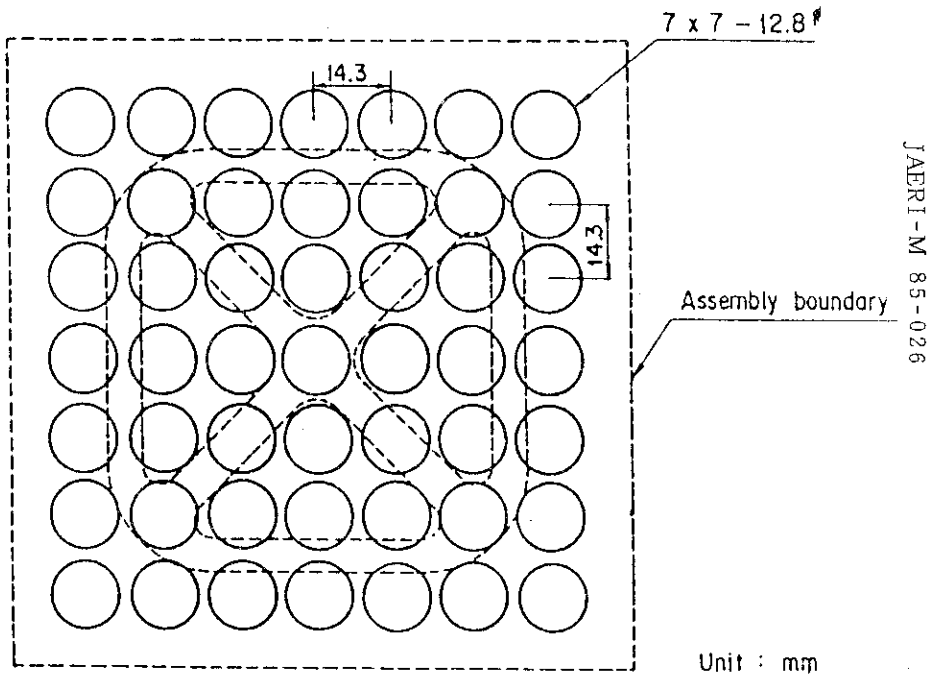

Unit : mm

Fig. 2.11 End box

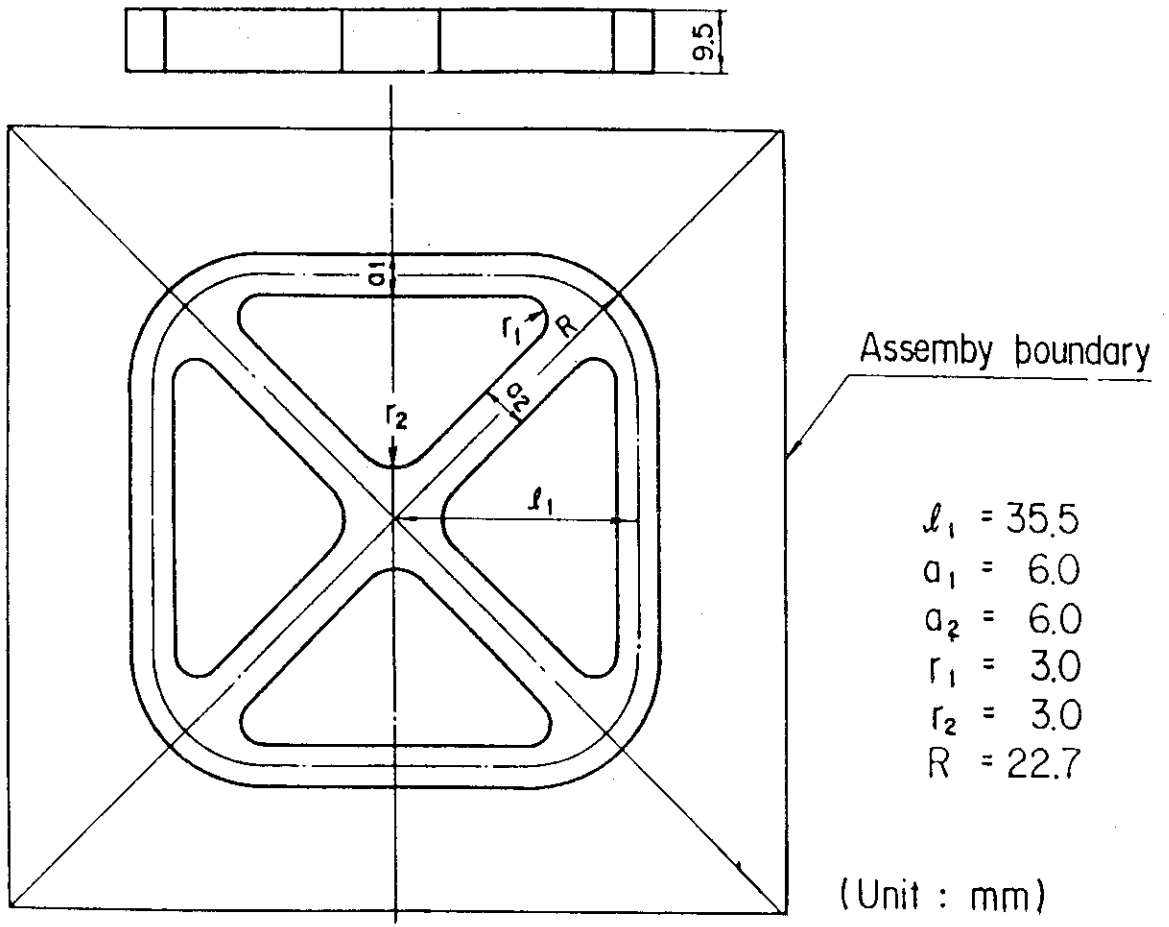

Fig. 2.12 Dimensions of plugging device

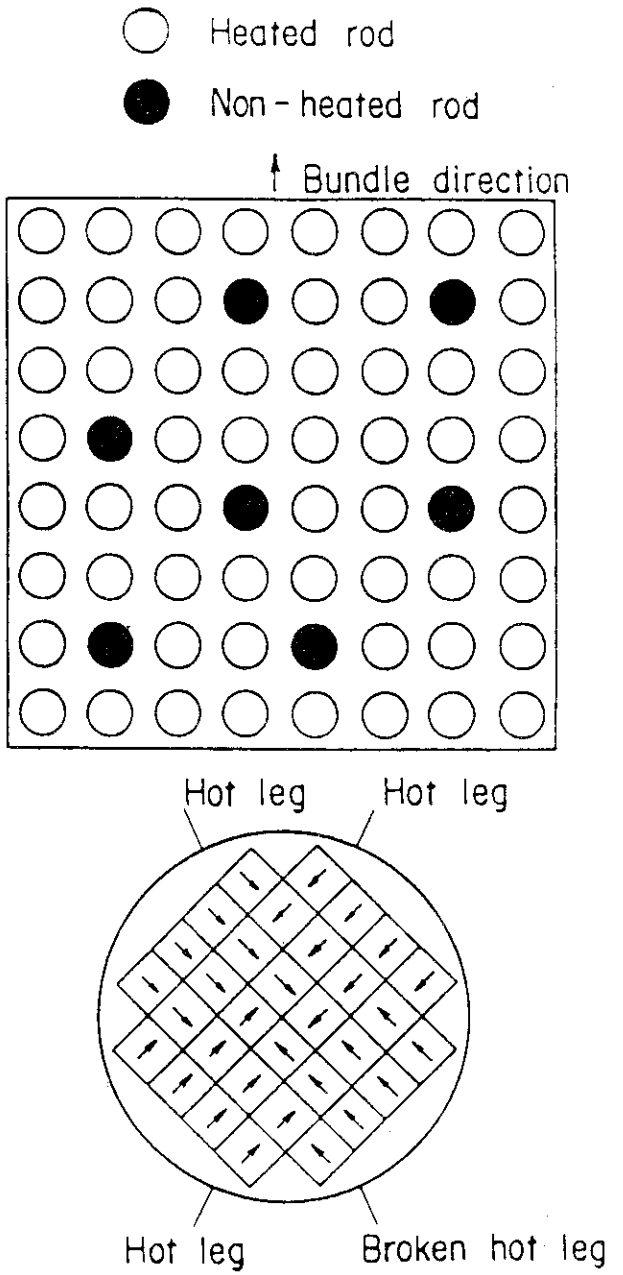

Fig. 2.13 Arrangement of non-heated rods and bundle direction

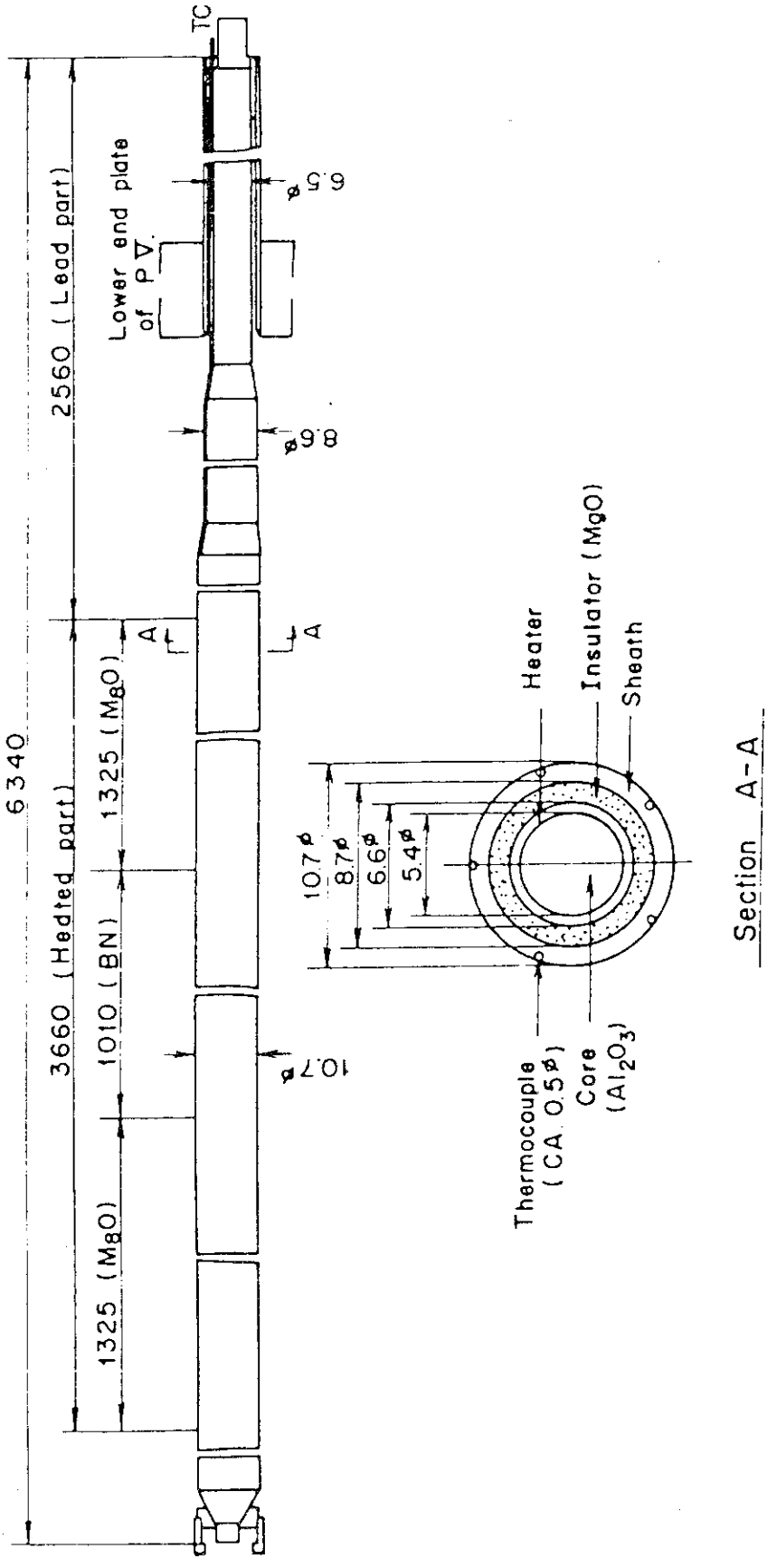

Fig. 2.14 Heater rod

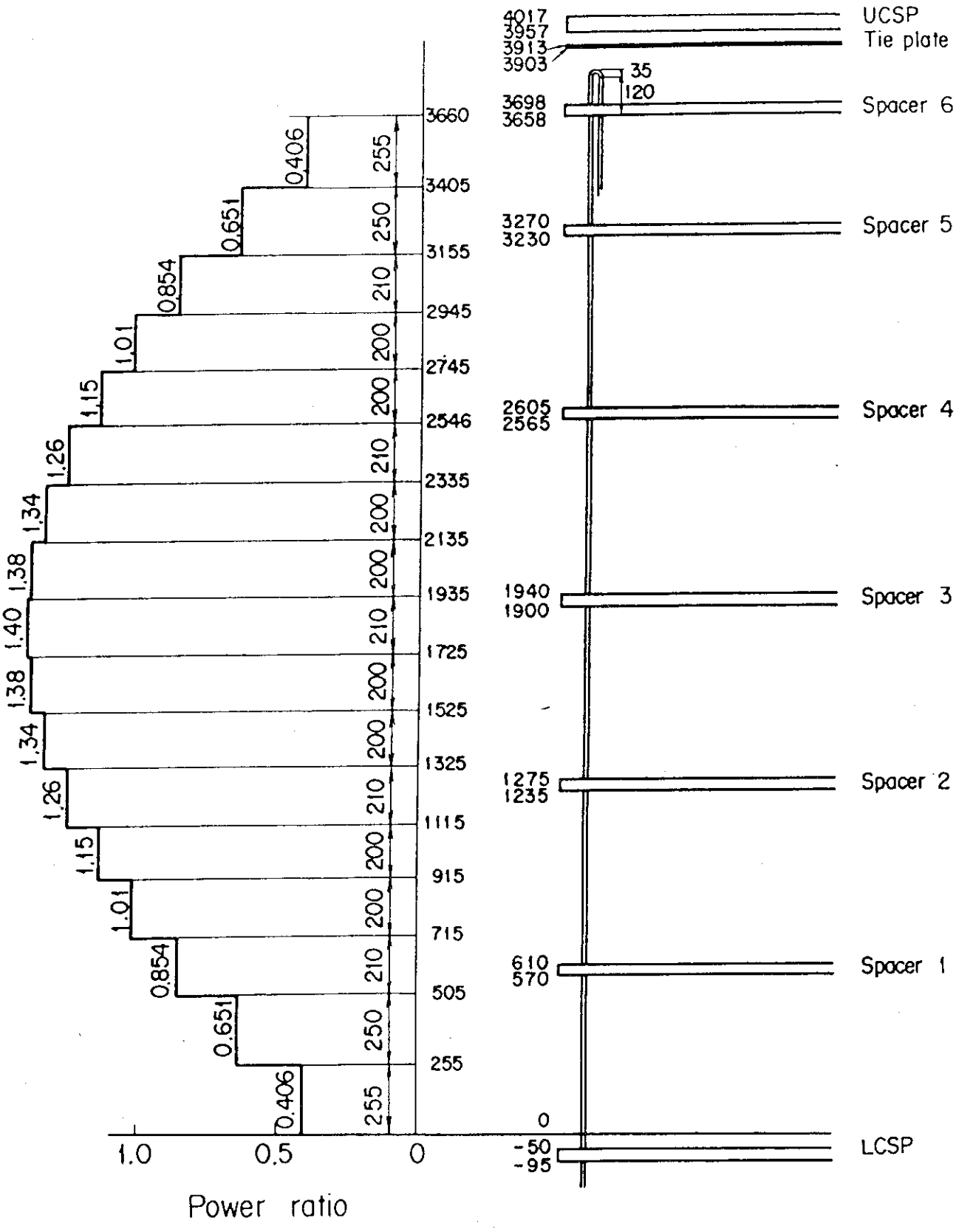

F Fig. 2.15 Axial power profile of CCTF Core-II heater rod

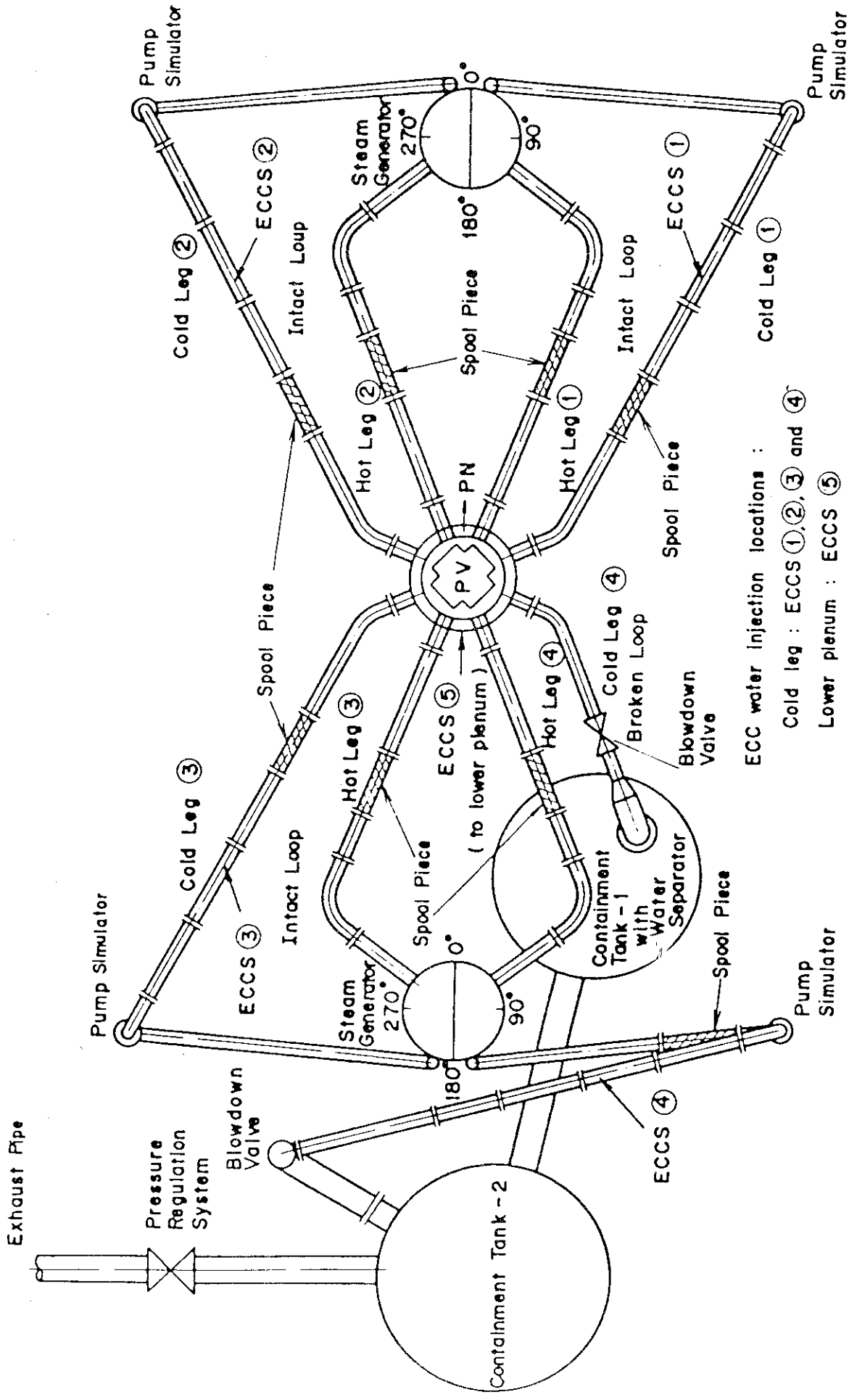

Fig. 2.16 Top view of primary loop pipings

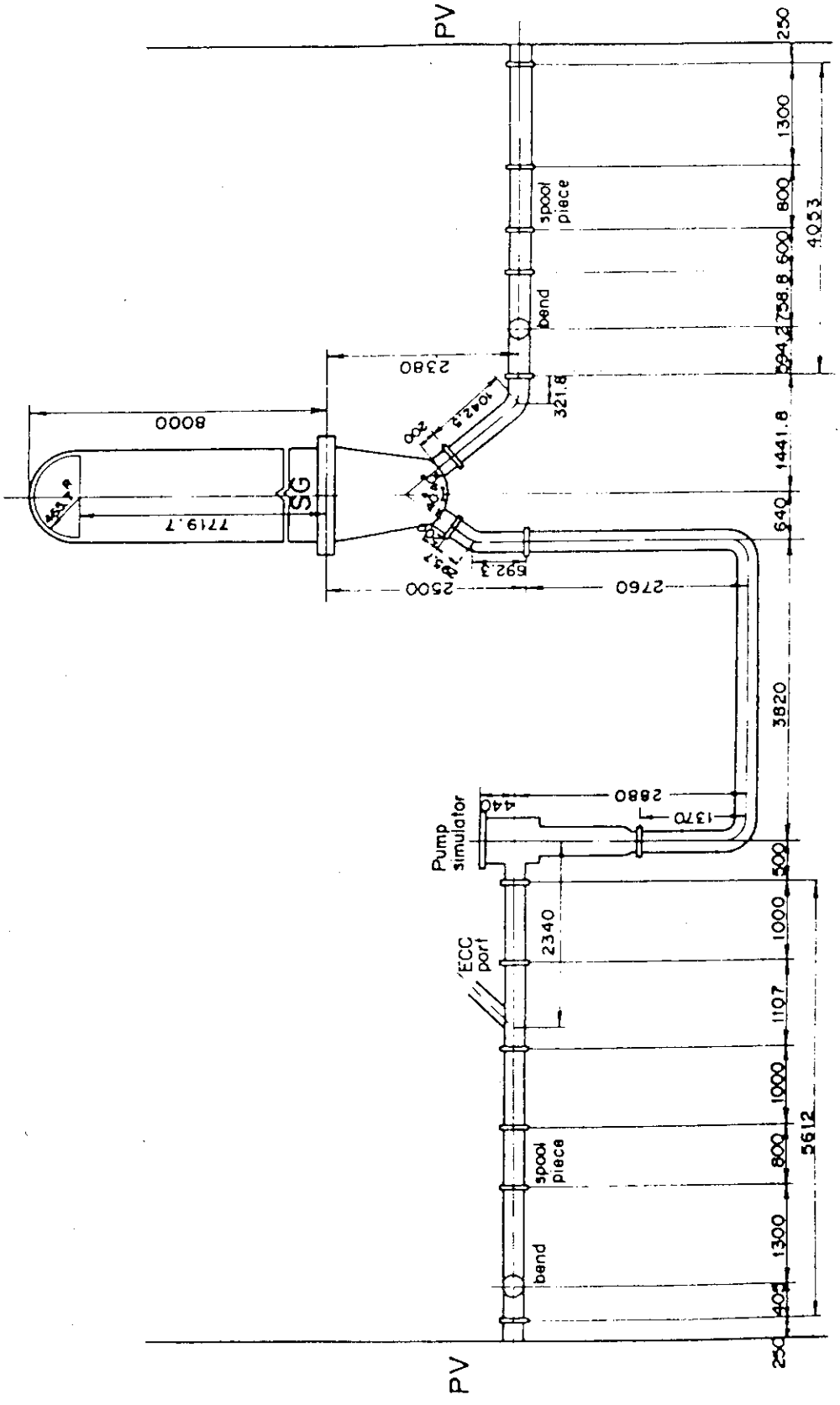

Fig. 2.17 Dimensions of primary loop

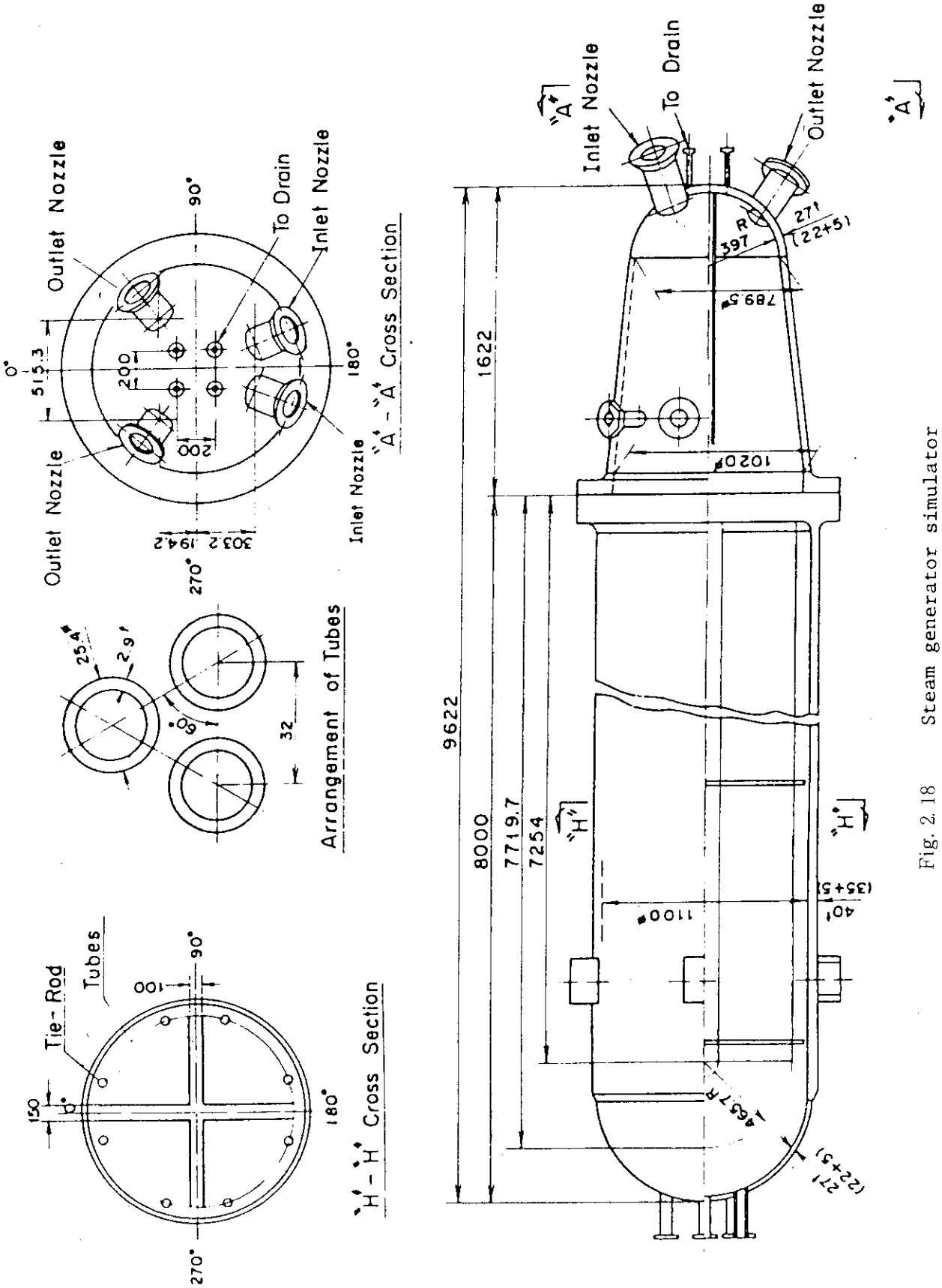

Fig. 2.18 Steam generator simulator

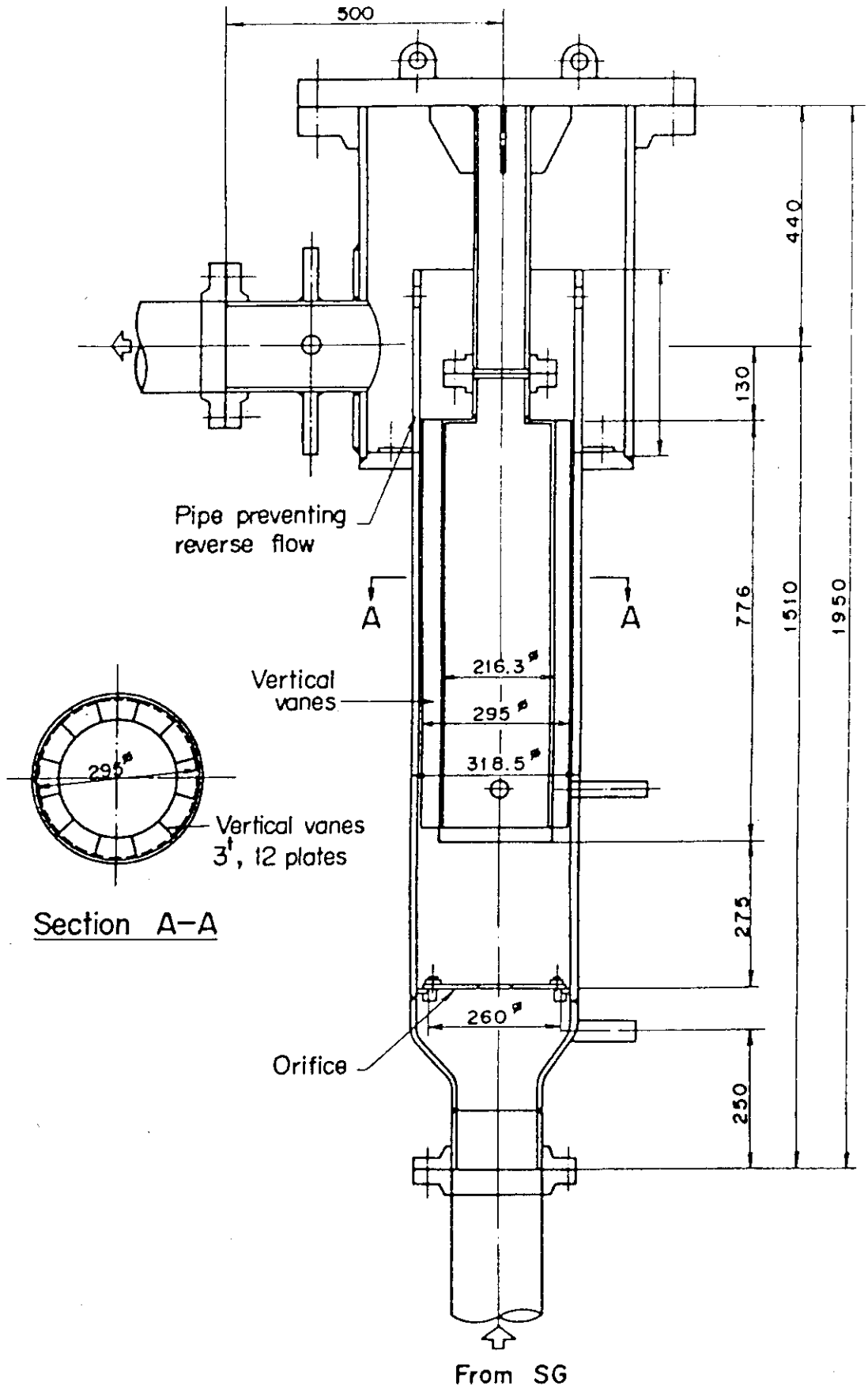

Fig. 2.19 Pump simulator

3. Test Results and Discussion

3.1 Comparison of Initial and Boundary Conditions

In this section, the initial and boundary conditions for the present test are compared with those for Test C2-SH1 in order to confirm that they are identical. The initial conditions for these two tests are compared in Table 3.1. The boundary conditions, such as the ECC water injection rate and temperatures and the containment tank pressure, are compared in Figs. 3.1 through 3.4.

Table 3.1 indicates that the initial conditions for both tests are almost identical except the temperatures of the lower plenum water and the core barrel wall (downcomer side). The difference in the lower plenum water temperature was caused by the insufficient preheating of the water supply piping connected to the lower plenum in Test C2-SH1. The difference in the core barrel wall temperature was caused by the pressurization of the system up to 4 bars prior to the initiation of Test C2-SH1 in order to prevent the glasses of view windows from collecting moisture. Since the pressure was reduced to 2 bars afterward, the temperature of the primary loop piping wall decreased to the saturation temperature for 2 bars. However, the temperature of the core barrel wall did not decrease, probably because of the influence of the superheated downcomer wall, which was heated up to 471 K.

The difference in the lower plenum water temperature is expected to result in the difference in the core inlet subcooling. Also, the difference in the core barrel wall temperature is expected to result in the difference in the downcomer water temperature, and hence, the downcomer differential pressure. The magnitudes of difference in those data are investigated in the following section.

Figure 3.1 is the comparison of the Acc injection rates and shows almost the same history. Figures 3.2 and 3.3 are the comparisons of the ECC water injection rates and temperatures at three intact cold leg ECC ports. These figures show that those data are almost identical between the two tests. Figure 3.4 shows the comparison of the pressure of the containment tank 2 and indicates the system pressures are almost identical.

3.2 System Behavior

The downcomer differential pressures are compared in Fig. 3.5. They are almost identical to each other. Figures 3.6(a) through (e) show the downcomer fluid temperatures. They are also almost identical to each other except for the initial period. As mentioned in the previous section, the initial temperature of the core barrel wall was higher by about 20 K in Test C2-SH1. However, the effects of this difference are not noticeable in the downcomer differential pressure and fluid temperatures as shown in Figs. 3.5 through 3.6(e). The sectional downcomer differential pressures are also presented in Figs. 3.7(a) through (e), which show the almost identical behavior between the two tests.

The core differential pressures are compared in Fig. 3.8 and the sectional core differential pressures are compared in Fig. 3.9(a) through (f). As described later, there was a trouble in the core differential pressure measurement for Test C2-SH1 and the data above 1.83 m are judged to be unreliable before 200 s. After 200 s the core differential pressures are almost identical between the two tests. The sectional differential pressures are almost identical below 1.83 m elevation through the whole transient. Above 1.83 m elevation, however, the behaviors of the differential pressure for Test C2-SH1 are unreasonable and different from those for Test C2-4 in the early period. This was caused by the trouble in the core differential pressure measurement system as explained below.

The core differential pressure data above 1.83 m elevation are presented in Figs. 3.10(a) through (c) for Test C2-SH1. There observed significant zero-shift of the data in these figures at 0 s and the data at the different orientation differ from each other in the period before 200 s. However, except for the data at the orientation 6 shown in Figs. 3.10(a) and (b), the data of the other three orientations become almost the same after 120 s and 200 s for Figs. 3.10(a) and (b) and Fig. 3.10(c), respectively, and in this period these data are almost identical to those for Test C2-4 as shown in Figs. 3.9(d) through (f). Therefore, judging from the information above, the trouble seems to be as follows. In test C2-SH1, the system was pressurized at 4 bars and then depressurized to 2 bars before the initiation of test. This procedure seems to cause the flashing or vaporization of some water

filled in the pipings for the differential pressure measurement in the upper region of the core, resulting in the significant zero-shift mentioned above. As the reflooding proceeds, however, the water in the core seems to fill the piping gradually and then the differential pressure measurement seems to recover by 200 s.

Figure 3.11 shows the comparison of the upper plenum differential pressures (above UCSP). They are almost identical. Figures 3.12 and 3.13 show the intact and broken loop differential pressures, respectively. Also, Fig. 3.14 shows the pressure losses through the broken cold leg. They are almost identical between the two tests. Figure 3.15 shows the comparison of the upper plenum pressure and they are nearly identical.

Figure 3.16 shows the core flooding rate evaluated by the mass balance calculation. Although the peak value for Test C2-SH1 is slightly smaller, they are generally almost identical. It should be noted that these core flooding rates were calculated with the core differential pressure data shown in Fig. 3.8, and hence, the value for Test C2-SH1 is not correct in the early period. Figures 3.17 and 3.18 show the core inlet fluid temperature and subcooling, respectively. The core inlet subcooling for Test C2-SH1 is larger than for Test C2-4. This is probably because the initial fluid temperature in the lower plenum was about 40 K lower in Test C2-SH1 as mentioned in the previous section. However, the megnitude of difference in the core inlet subcooling is about 6 K at most.

3.3 Core Cooling Behavior

The quench envelopes are compared in Fig. 3.19. This figure indicates the quenching occurs at almost the same time between the two tests. This figure shows the average quench times for the three (A, B and C) power regions. The standard deviations (σ_{n-1}) of the quench time are presented in Figs. 3.20(a) and (b) as well as the average values.

Figures 3.21(a) through (c) show the comparisons of the rod surface temperatures in A, B and C regions, respectively. The data in the upper part (above 2.44 m elevation) of A region differ slightly between the two tests and the data for the present test are slightly lower. Figure 3.22 shows the rod surface temperatures above 3.05 m elevation, indicating the same trend of the comparison. Figure 3.23 shows the comparisons

of the heat transfer coefficients in the high power region (A region), corresponding to Fig. 3.21(a). The reason for the difference in the rod surface temperature might be the difference in the core inlet subcooling shown before (Fig. 3.18), as described in the following.

In Fig. 3.24, the core inlet subcooling for the two tests in the CCTF Core-I test series are compared. These tests are Tests C1-2 and C1-3[4]. Except for the core inlet subcooling, the conditions for core cooling were almost identical between the two tests[4]. The temperature histories are compared in Fig. 3.25 in order to show the effects of core inlet subcooling on core cooling in the typical CCTF tests. The figure indicates that the turnaround temperature is slightly lower for the lower core inlet subcooling test (Test C1-2), whereas the quench time is later. The slightly better core cooling around the turnaround time for the lower core inlet subcooling case can be explained to result from the larger generation of vapor and liquid entrainments due to its lower subcooling. However, this effects on core cooling is considered to become recessive as core cooling advances and be replaced by another effect, that is, the retarded core cooling caused by the slower propagation of quench front due to higher carryover rate[4].

Concerning to Tests C2-4 and C2-SH1, the slightly better core cooling around the turnaround time is also obseved in Test C2-4 (Fig. 3.21(a)), in which the core inlet subcooling is lower (Fig. 3.18). Figure 3.26 shows the comparison of core outlet steam mass flow rate measured with spool pieces in hot legs. From this figure, it is comfirmed that the core outlet steam mass flow rate is higher in Test C2-4. However, the differences in the temperature shown in Fig. 3.21(a) are larger than in Fig. 3.25. This might result from the higher initial rod surface temperature, that is, the higher initial stored energy, in Tests C2-4 and C2-SH1 than in Tests C1-2 and C1-3. After the turnaround time the rod surface temperatures for Test C2-4 become closer to those for Test C2-SH1. However, in general, the temperatures for Test C2-4 do not become higher than those for Test C2-SH1. This might be because the difference in core inlet subcooling, and hence, core outlet steam mass flow rate becomes very small at later times as shown in Figs. 3.18 and 3.26.

3.4 Investigation of Reproducibility

As presented in Section 3.1, the initial and boundary conditions are almost identical between the two tests except the initial temperatures of the lower plenum fluid and the core barrel wall. The former seems to cause a little difference in the core inlet subcooling, which is 6 K at most.

As discussed in Section 3.2, the system behavior is nearly identical. The core cooling behavior is also almost identical as discussed in Section 3.3 except a little difference in the rod surface temperatures at the upper part in the high power region. Furthermore, the magnitude of this difference is small and can be explained qualitatively to be caused by the difference in the core inlet subcooling mentioned above. Therefore, it can be practically concluded that there is the reproducibility of the thermo-hydrodynamic behavior in the CCTF Core-II tests.

Table 3.1 Comparison of initial conditions

		Planned	Measured (Test C2-SH1)	Measured (Test C2-4)
Power				
Total (MW)	:	9.345	9.354	9.365
Average linear (kW/m)	:	1.40	1.40	1.40
Radial power distribution	:	1.36:1.20:0.76	1.37:1.20:0.76	1.37:1.20:0.76
Pressure (MPa)				
System	:	0.2	0.2	0.2
Steam generator secondary	:	5.2	5.2	5.1
Temperature (K)				
Downcomer wall	:	471	469	467
Core barrel wall	:	393	423	404
Primary piping wall	:	393	401	394
Steam generator secondary	:	539	546	539
Peak clad at ECC initiation	:	995	1001	1013
Peak clad at BOCREC	:	1073	1066	1072
Lower plenum filled liquid	:	393	355	394
ECC liquid	:	308	308	308
Water level (m)				
Lower Plenum	:	0.90	0.95	0.81
Steam generator secondary	:	7.4	7.5	7.4

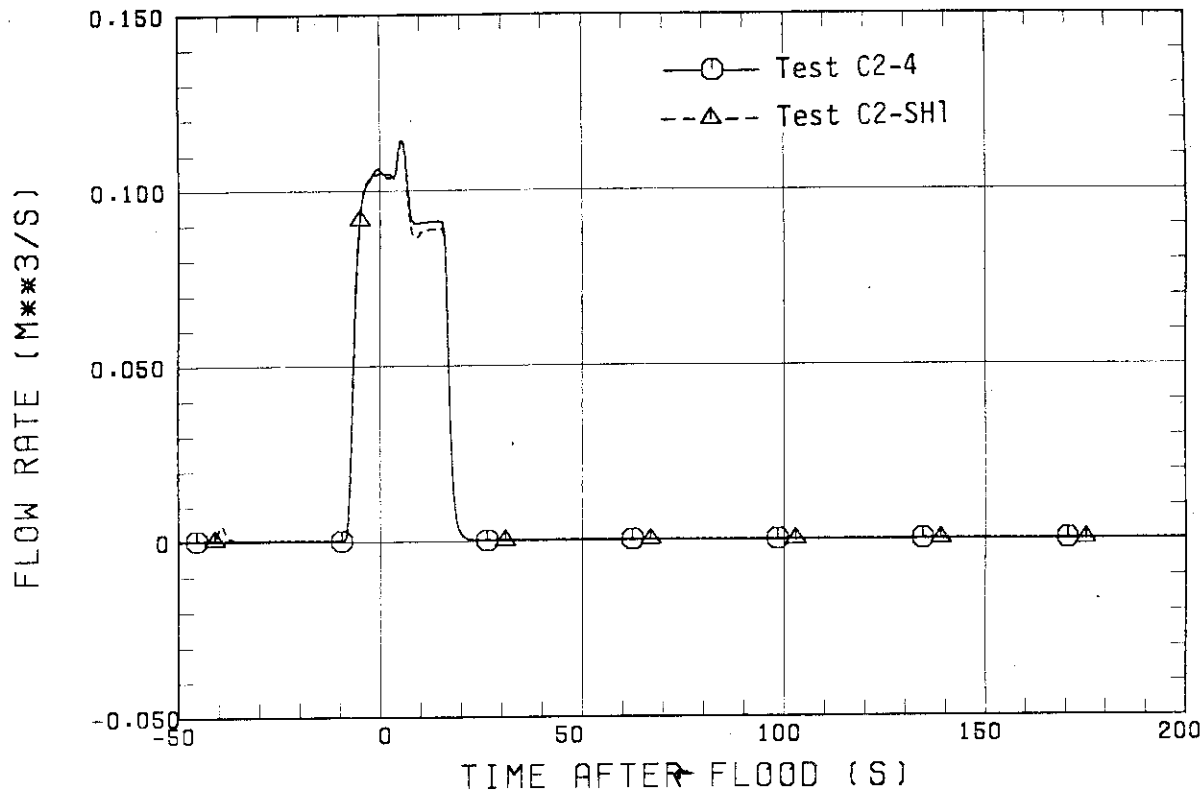

Fig. 3.1 Acc injection rates

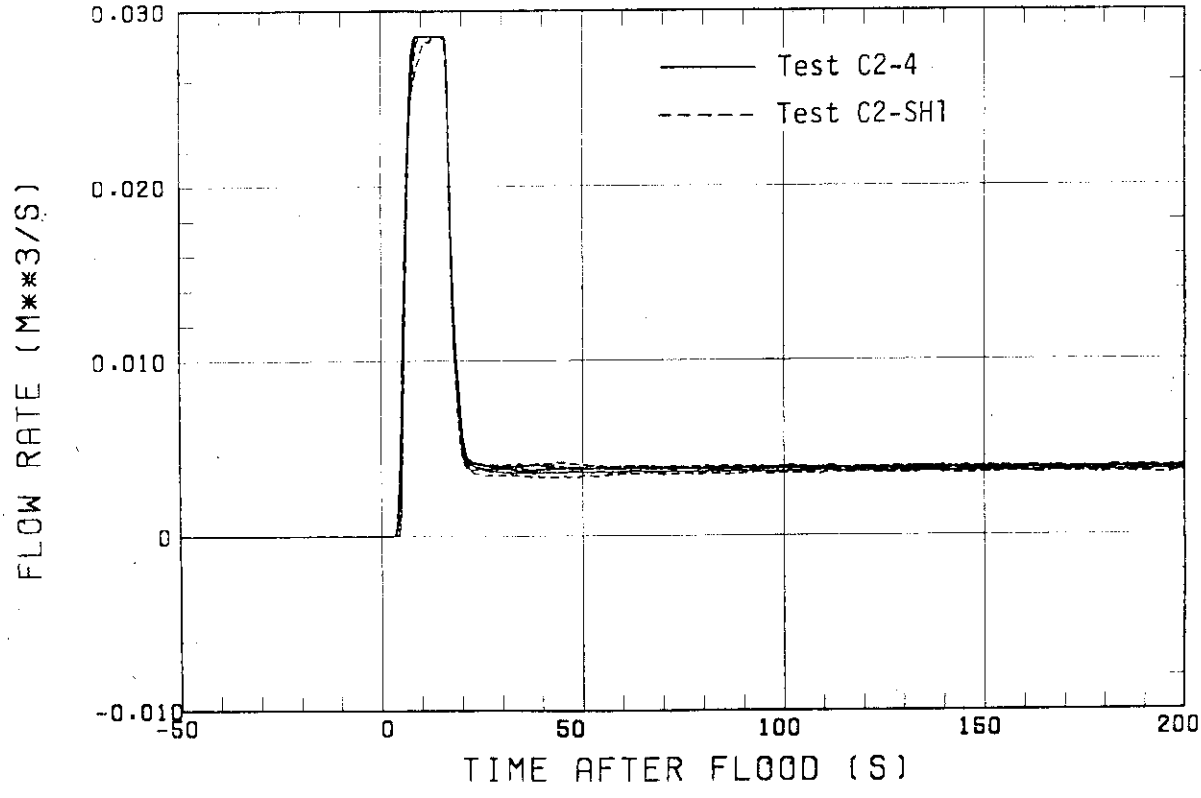

Fig. 3.2 ECC injection rates at intact cold legs

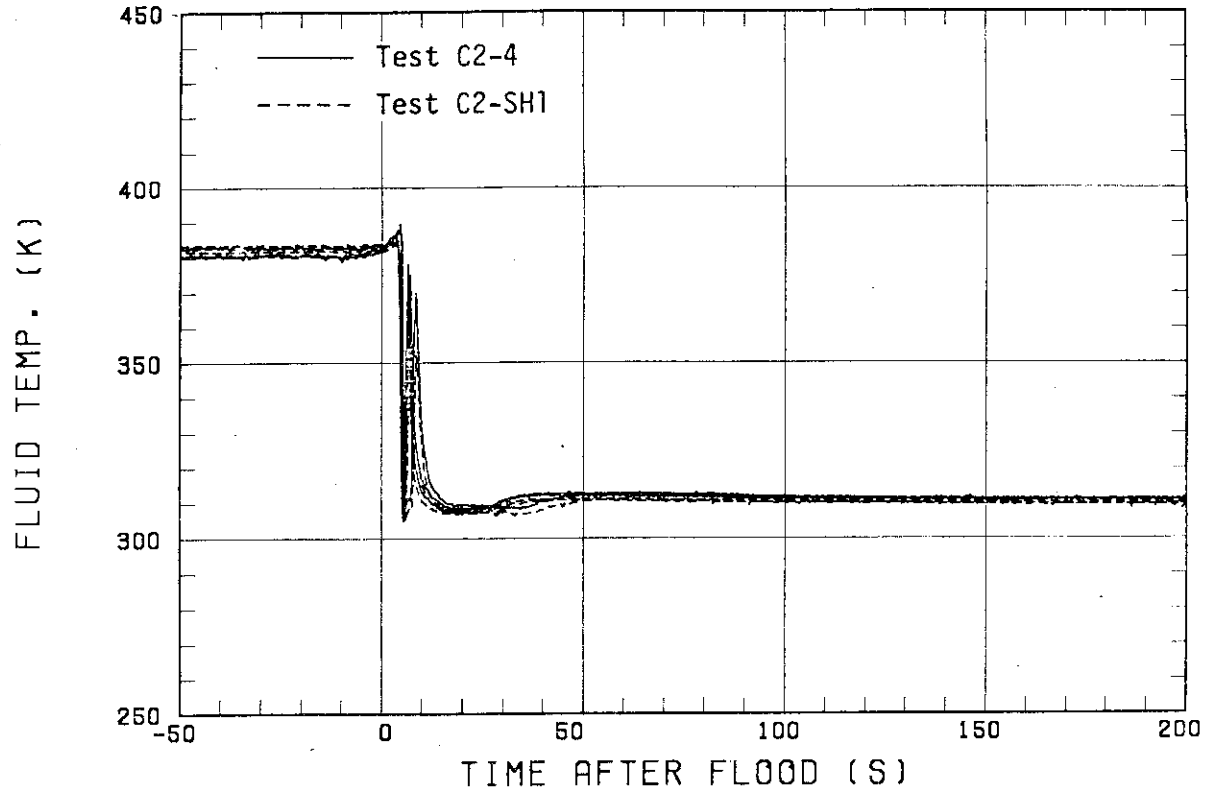

Fig. 3.3 ECC water temperatures at intact cold legs

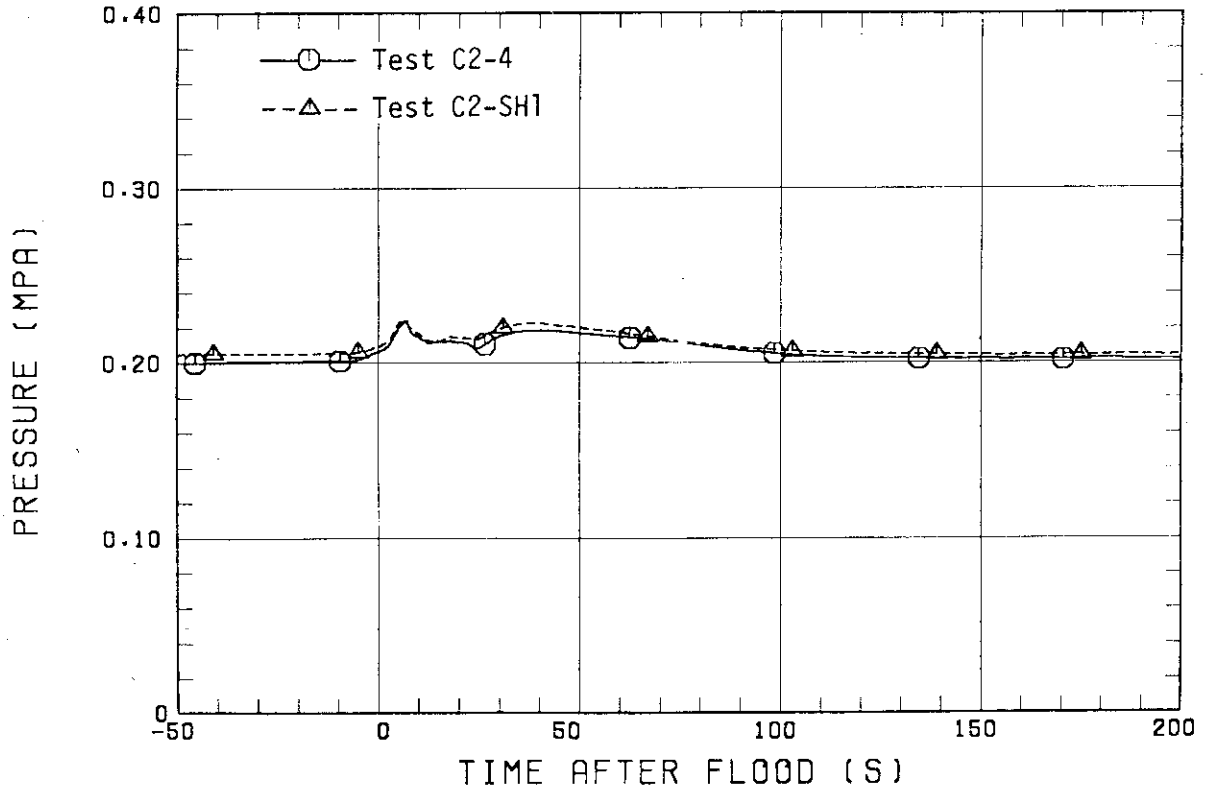

Fig. 3.4 Pressures of Containment tank 2

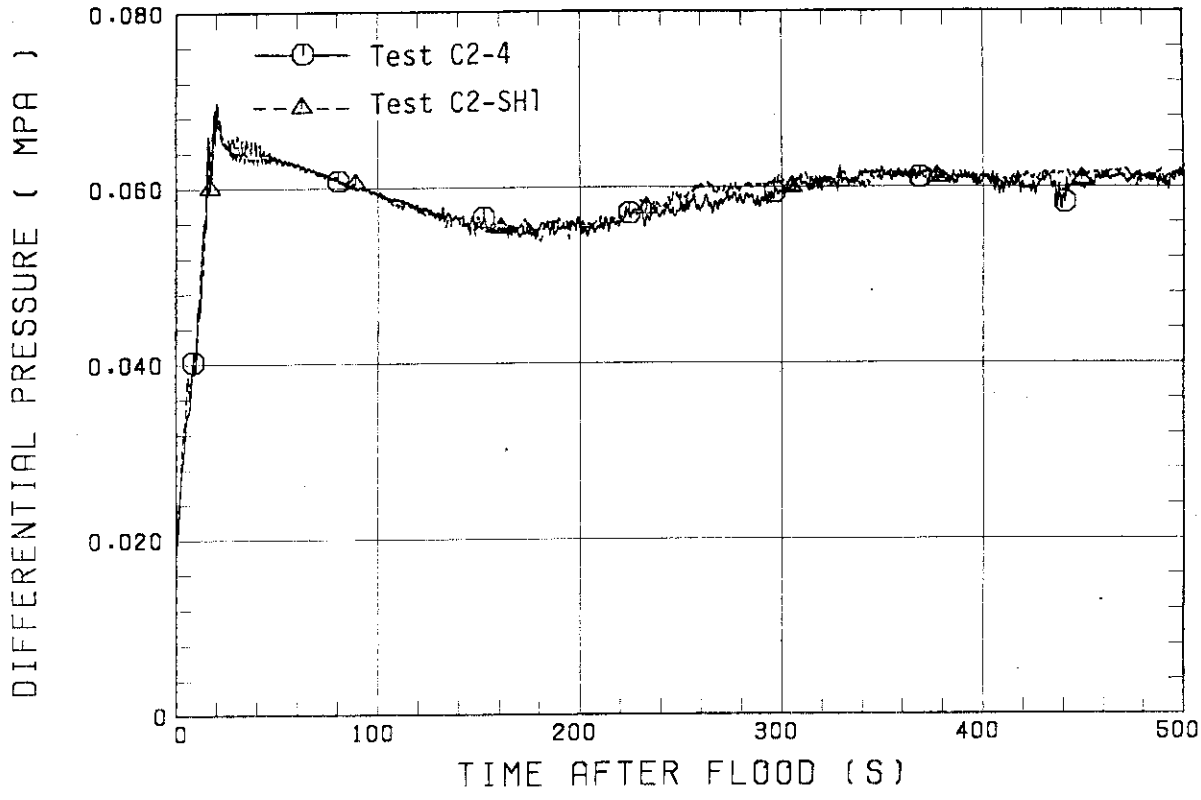

Fig. 3.5 Downcomer differential pressures

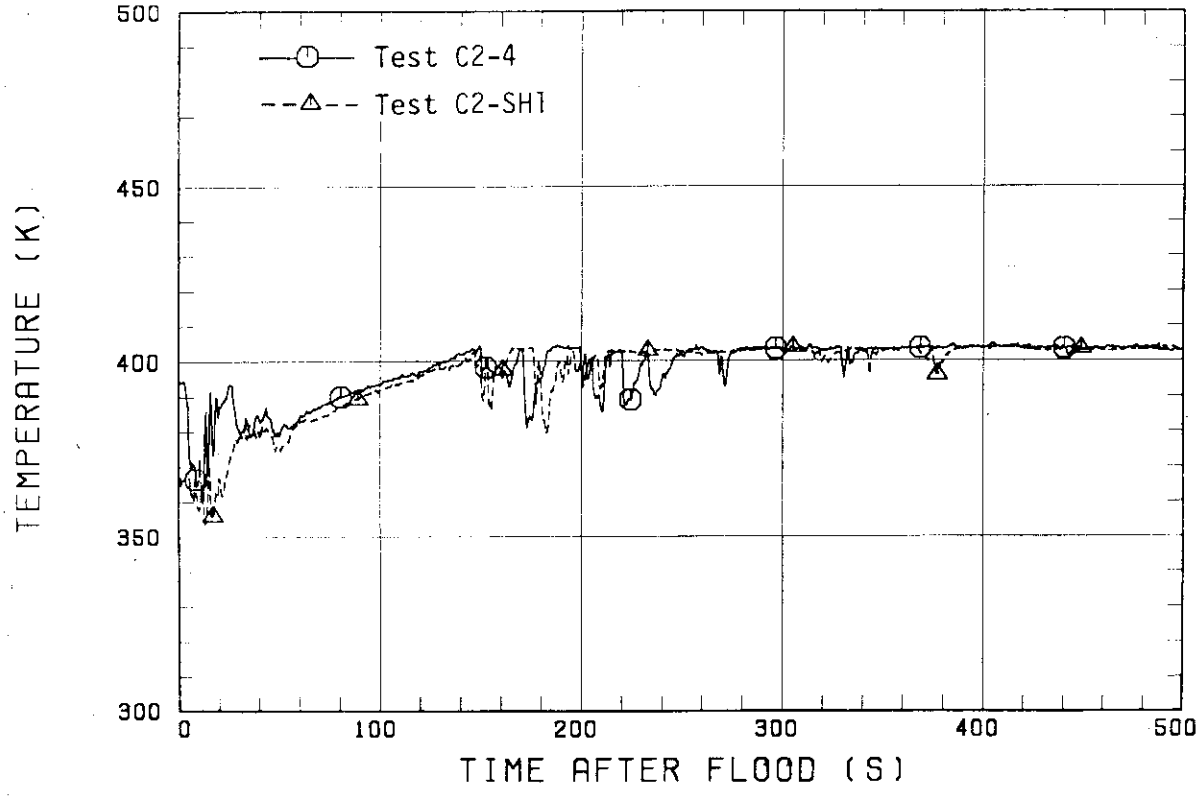

Fig. 3.6(a) Downcomer fluid temperatures at 0.983 m

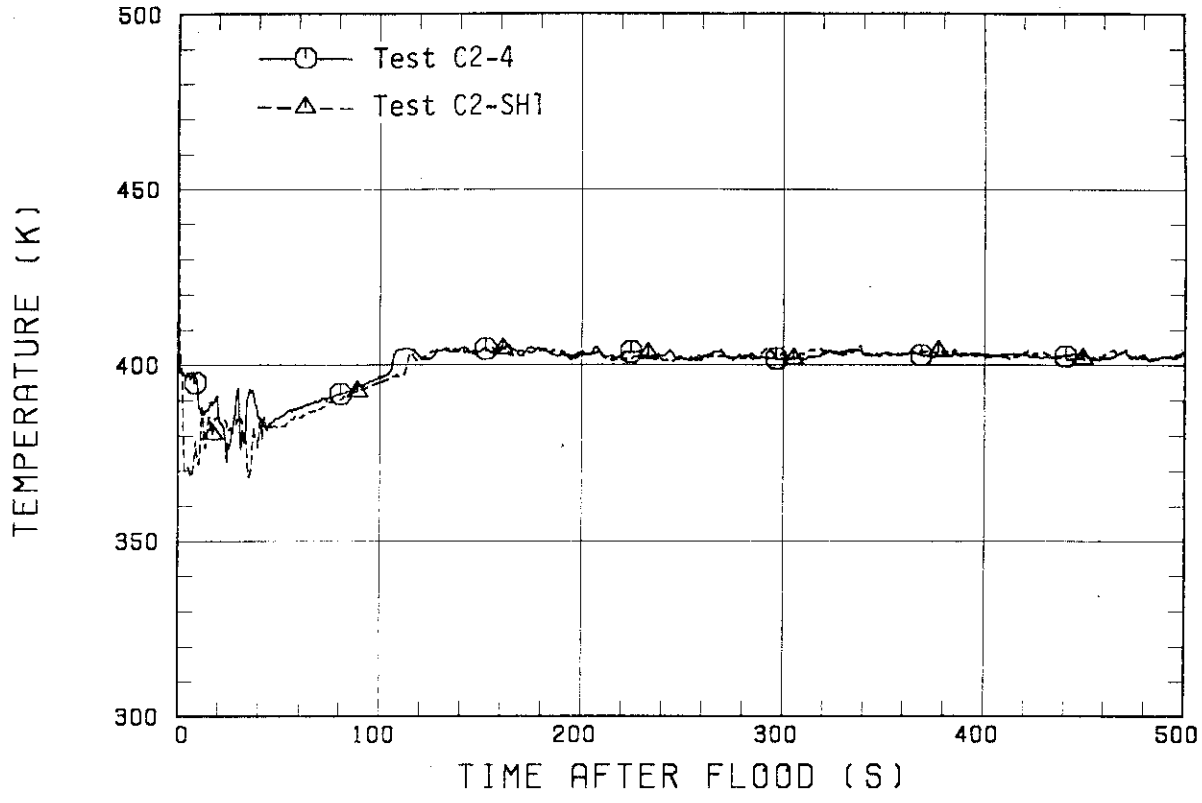

Fig. 3.6(b) Downcomer fluid temperatures at 2.423 m

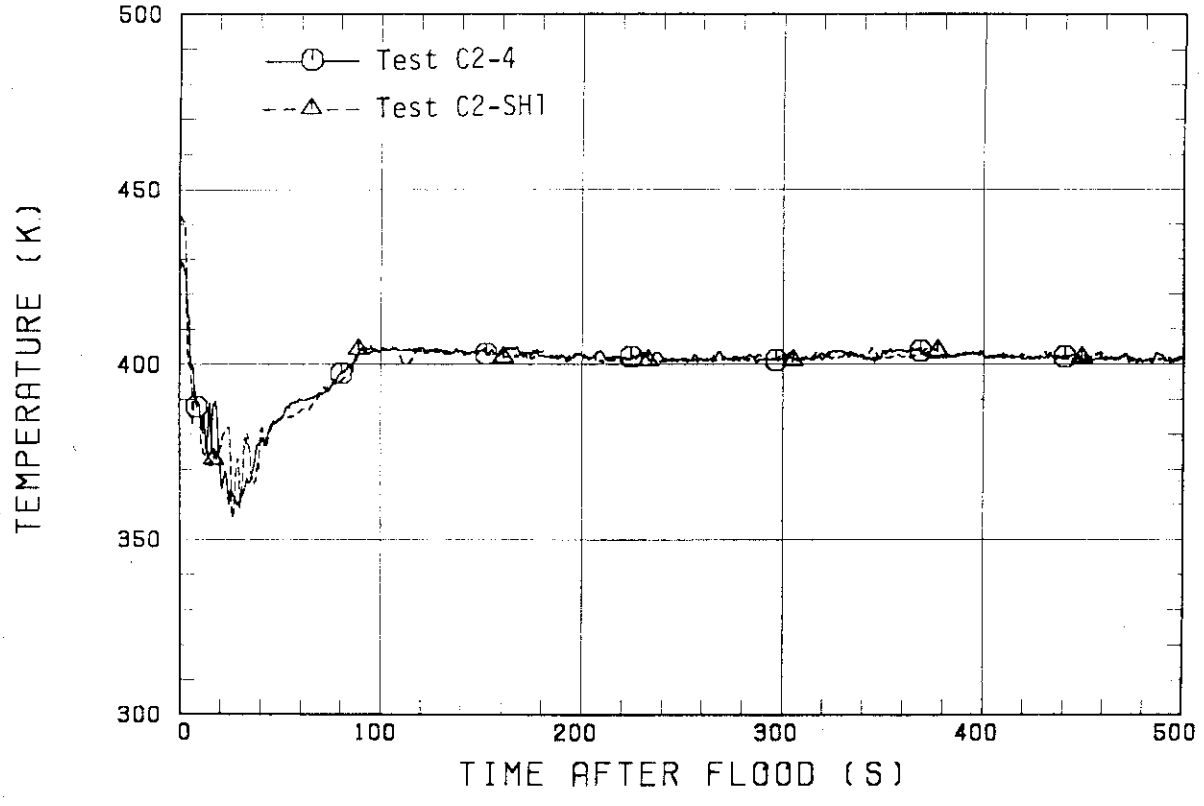

Fig. 3.6(c) Downcomer fluid temperatures at 3.863 m

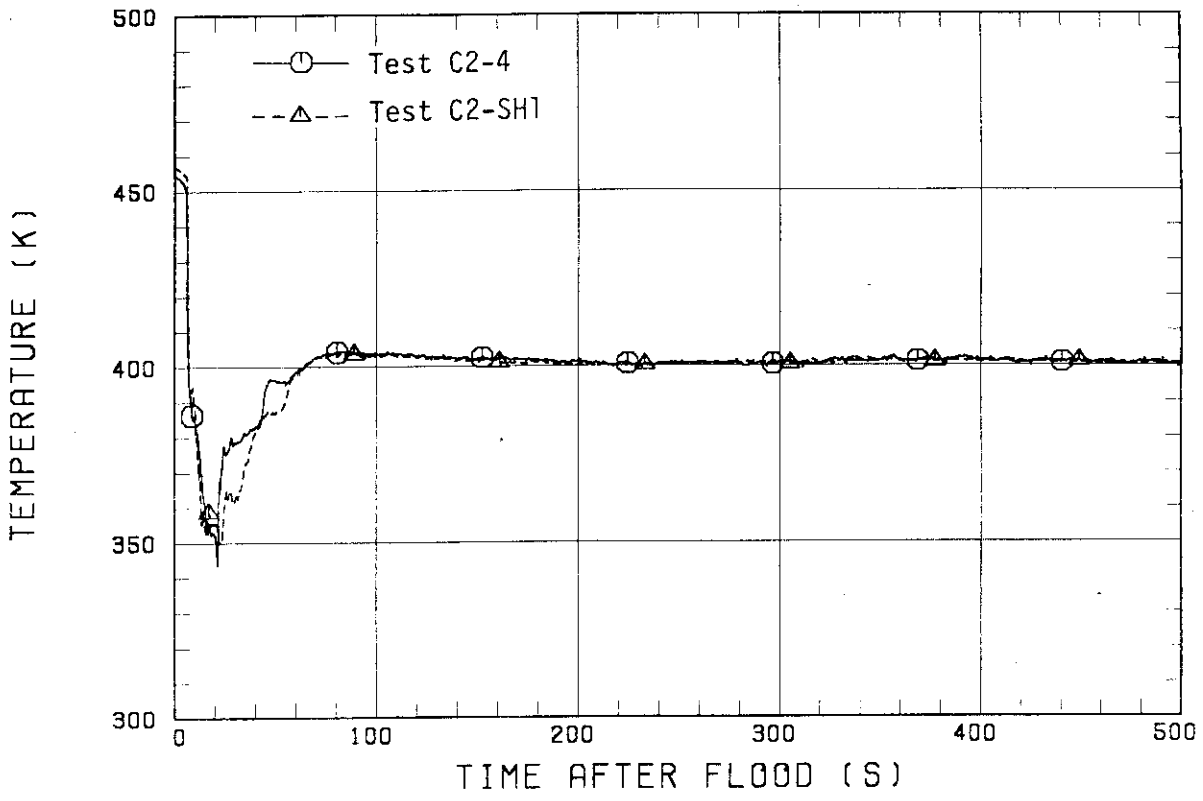

Fig. 3.6(d) Downcomer fluid temperatures at 5.303 m

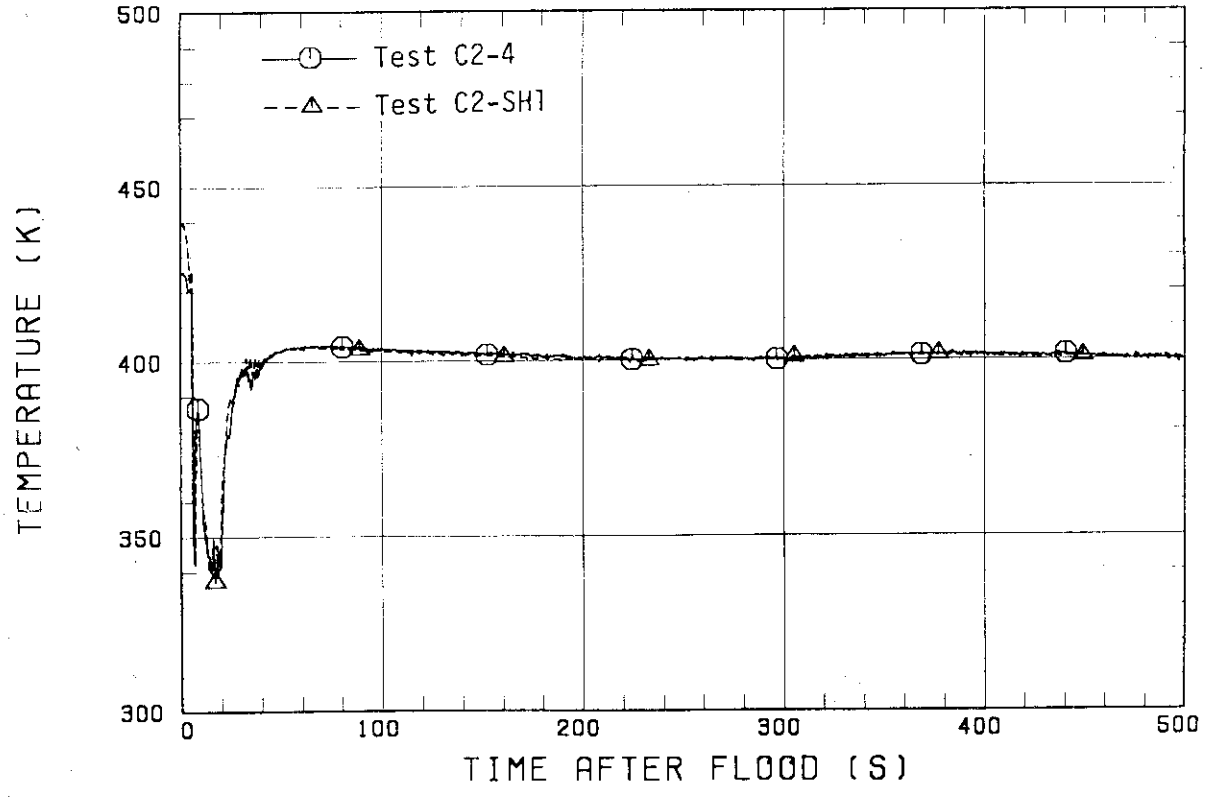

Fig. 3.6(e) Downcomer fluid temperatures at 6.743 m

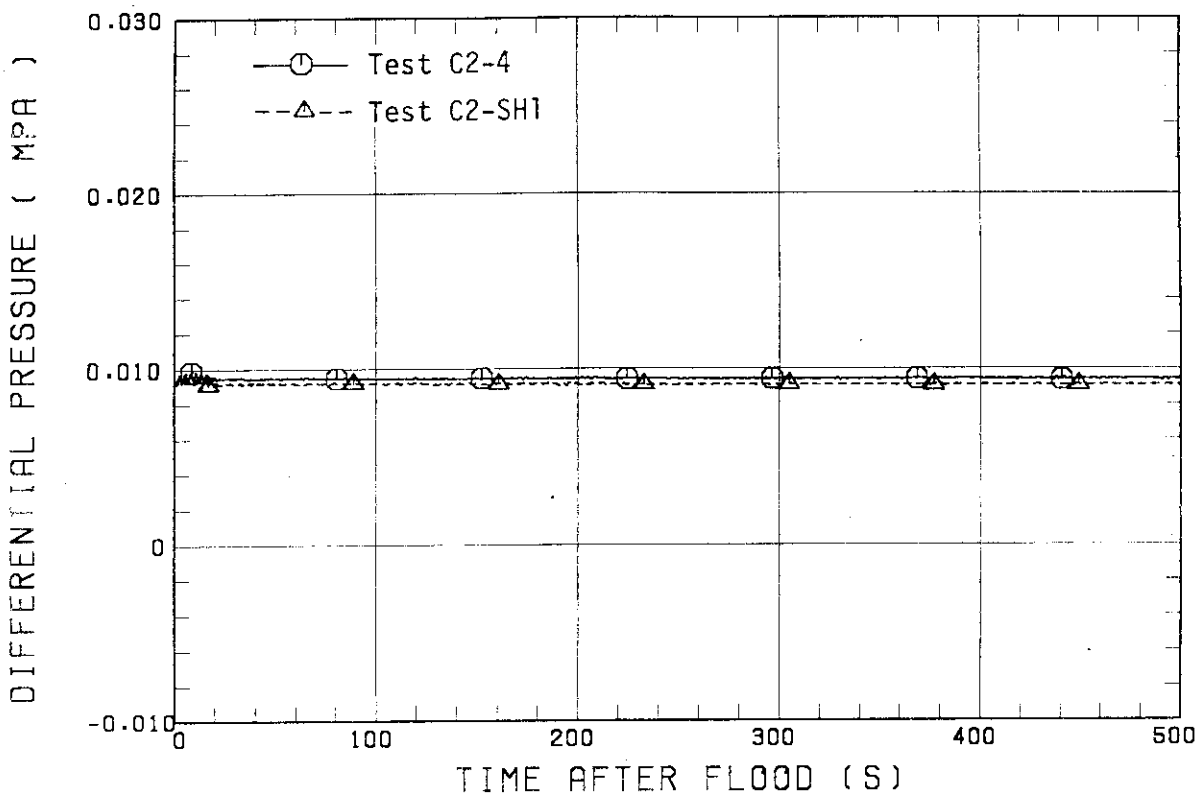

Fig. 3.7(a) Downcomer sectional differential pressures between 0 and 0.983 m elevations

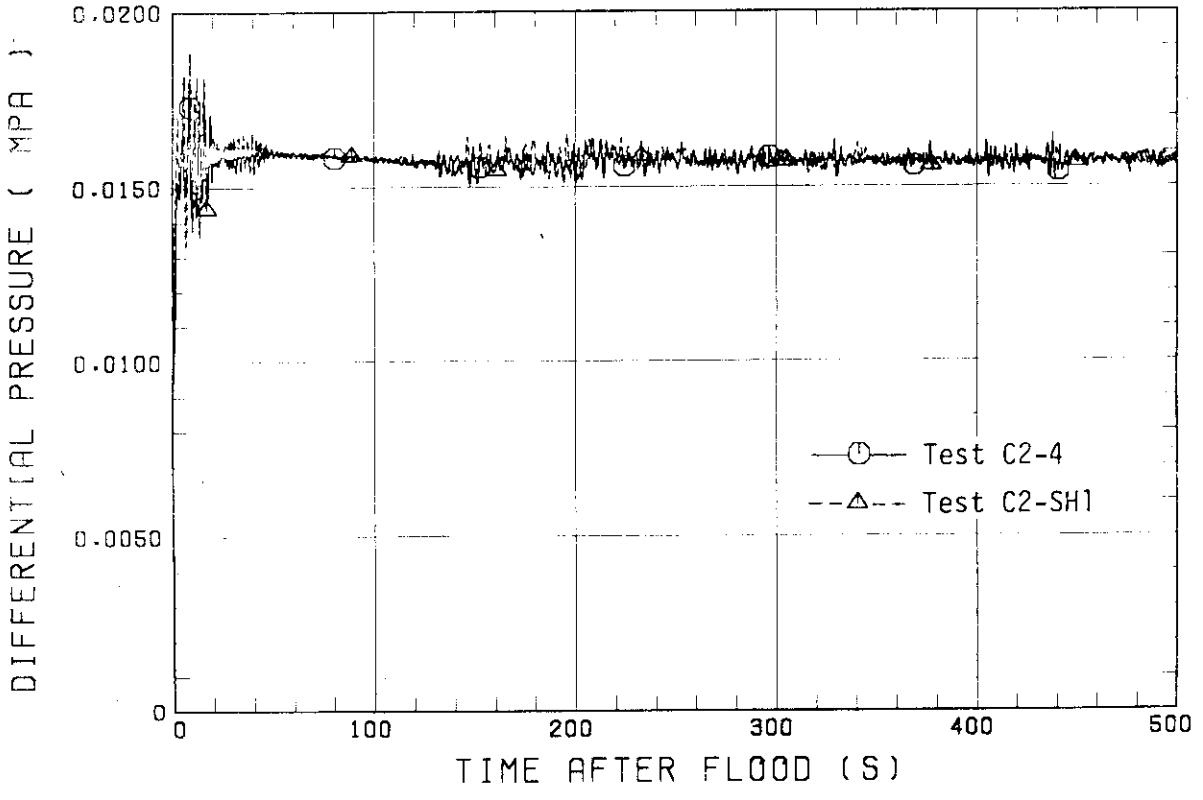

Fig. 3.7(b) Downcomer sectional differential pressures between 0.983 and 2.683 m elevations

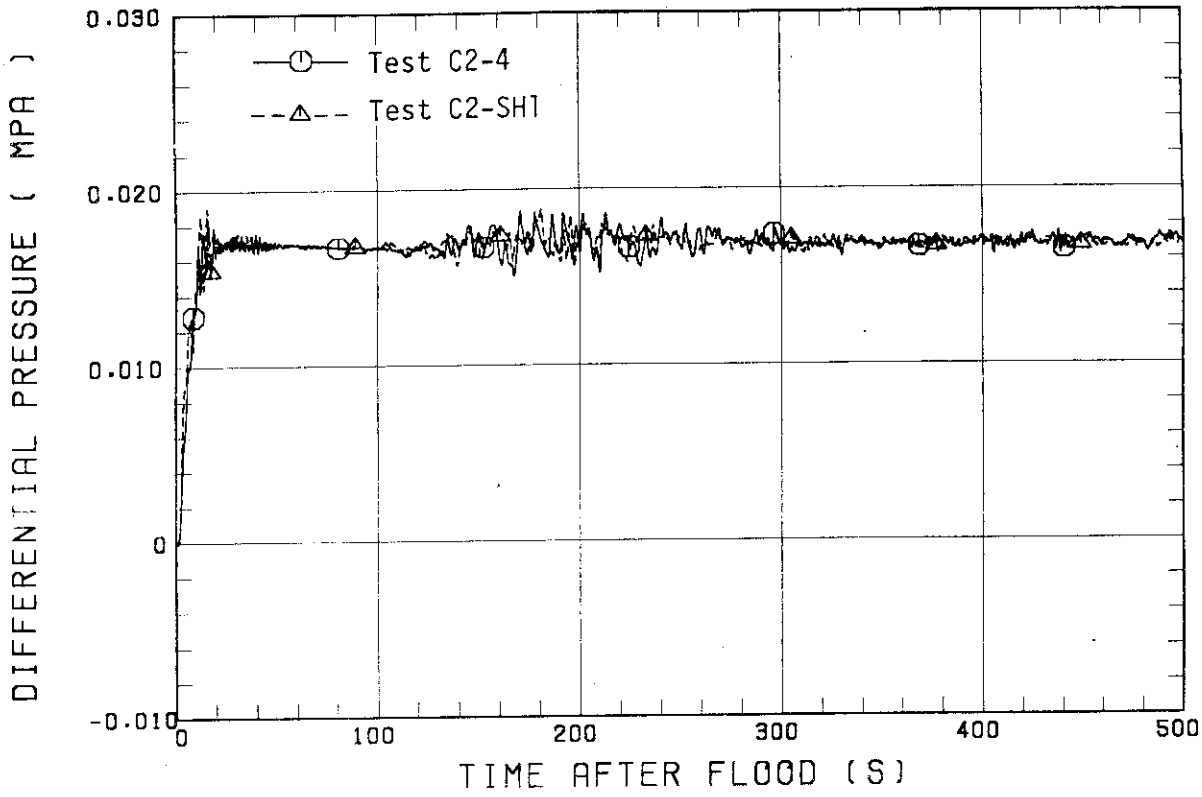

Fig. 3.7(c) Downcomer sectional differential pressures between 2.683 and 4.483 m elevations

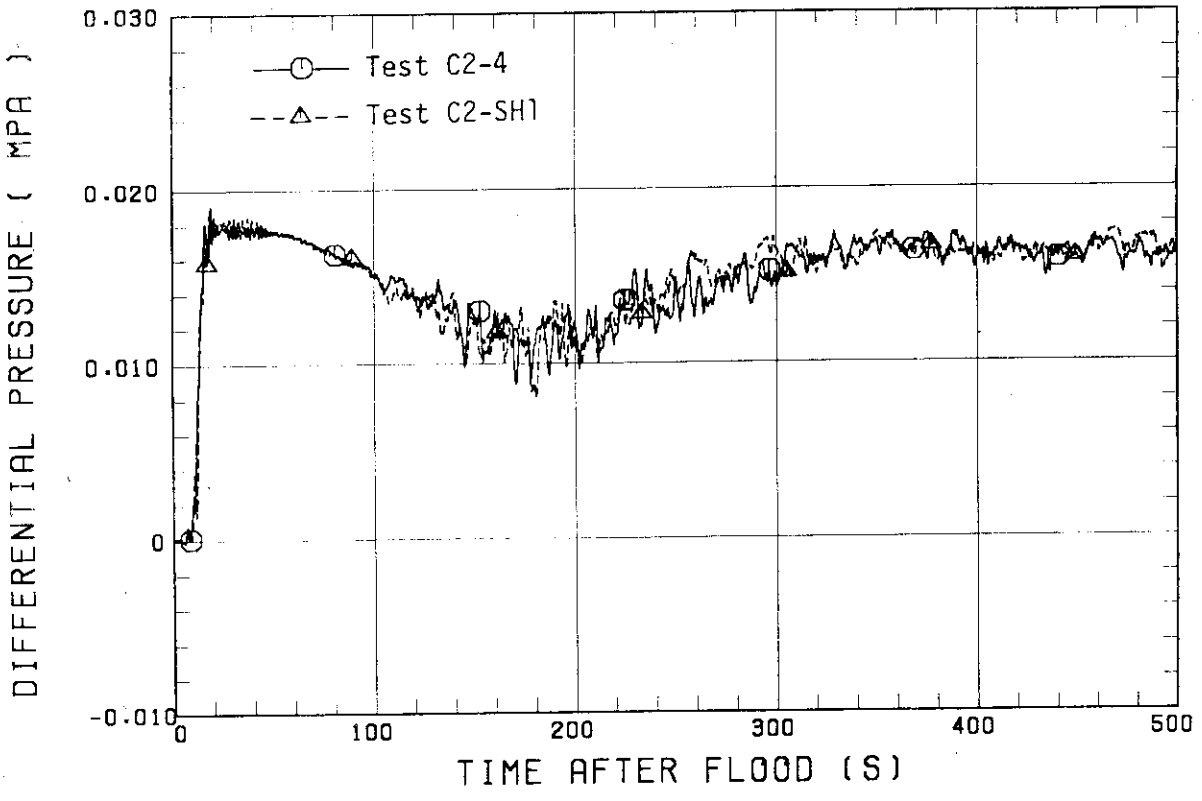

Fig. 3.7(d) Downcomer sectional differential pressures between 4.483 and 6.383 m elevations

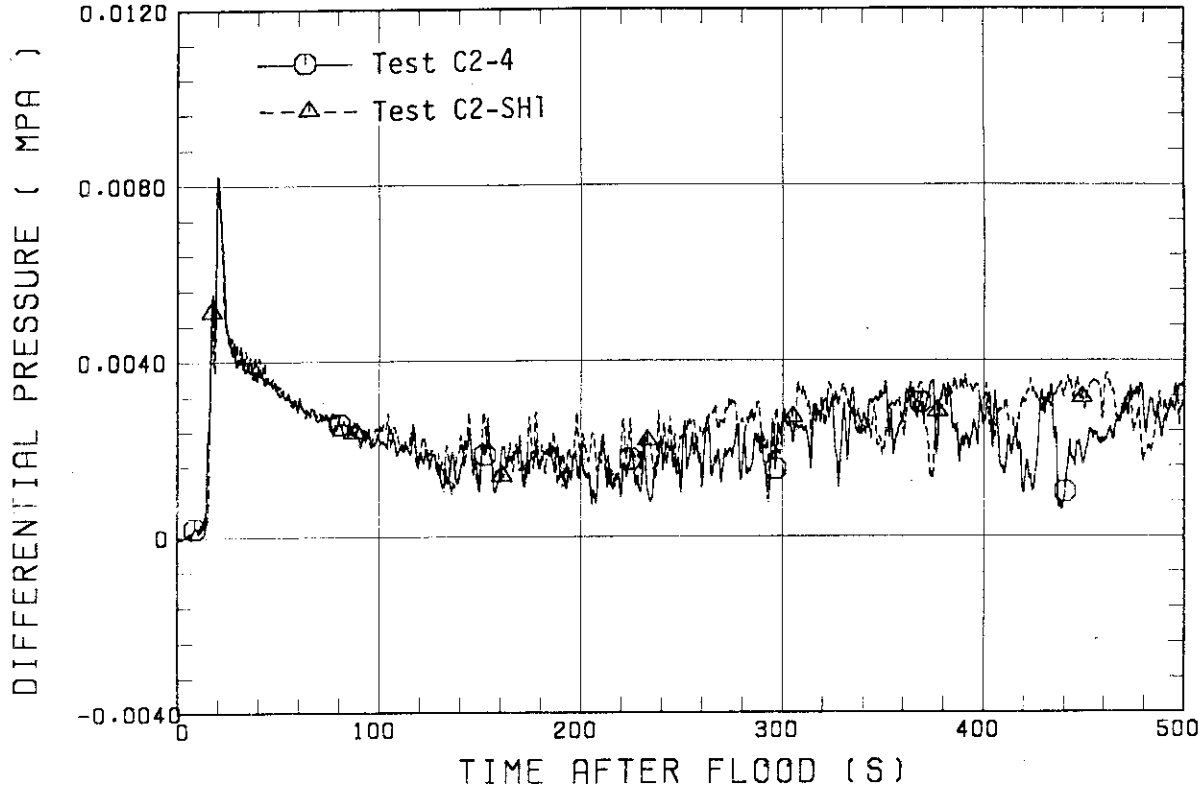

Fig. 3.7(e) Downcomer sectional differential pressures between 6.383 and 8.183 m elevations

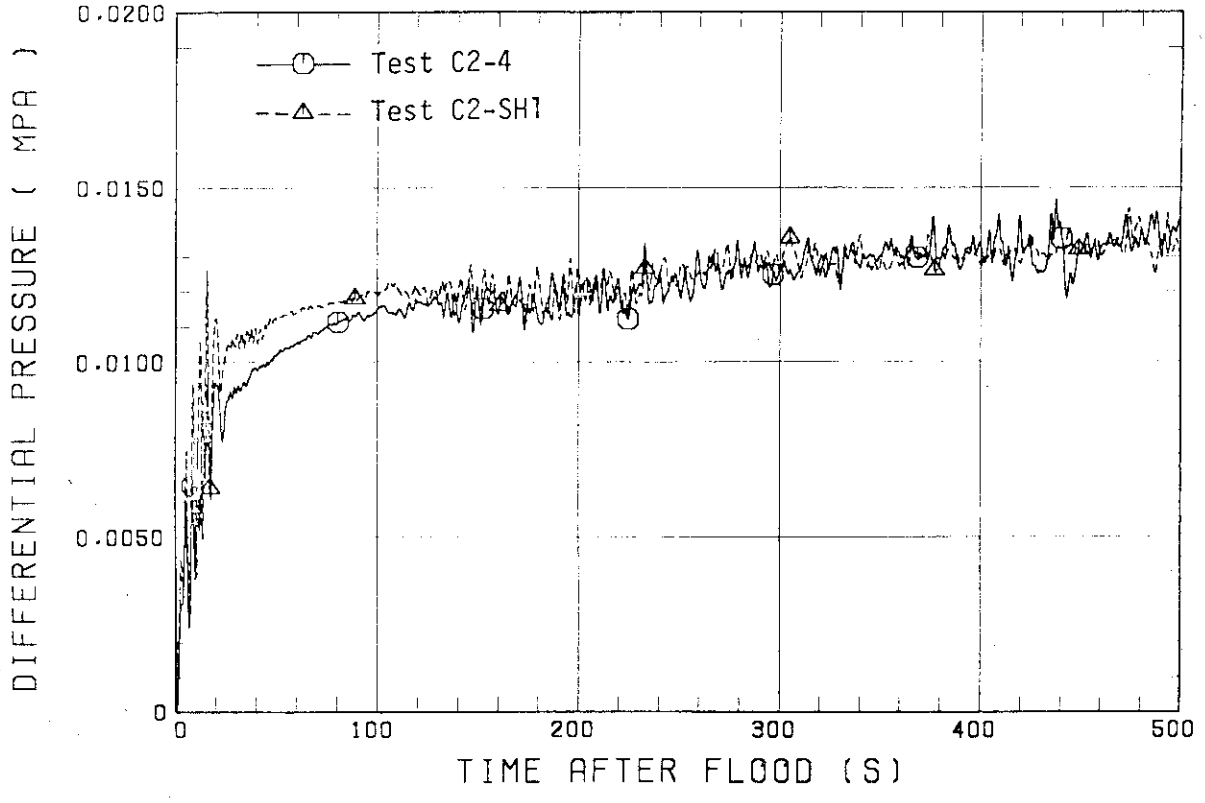

Fig. 3.8 Core differential pressures

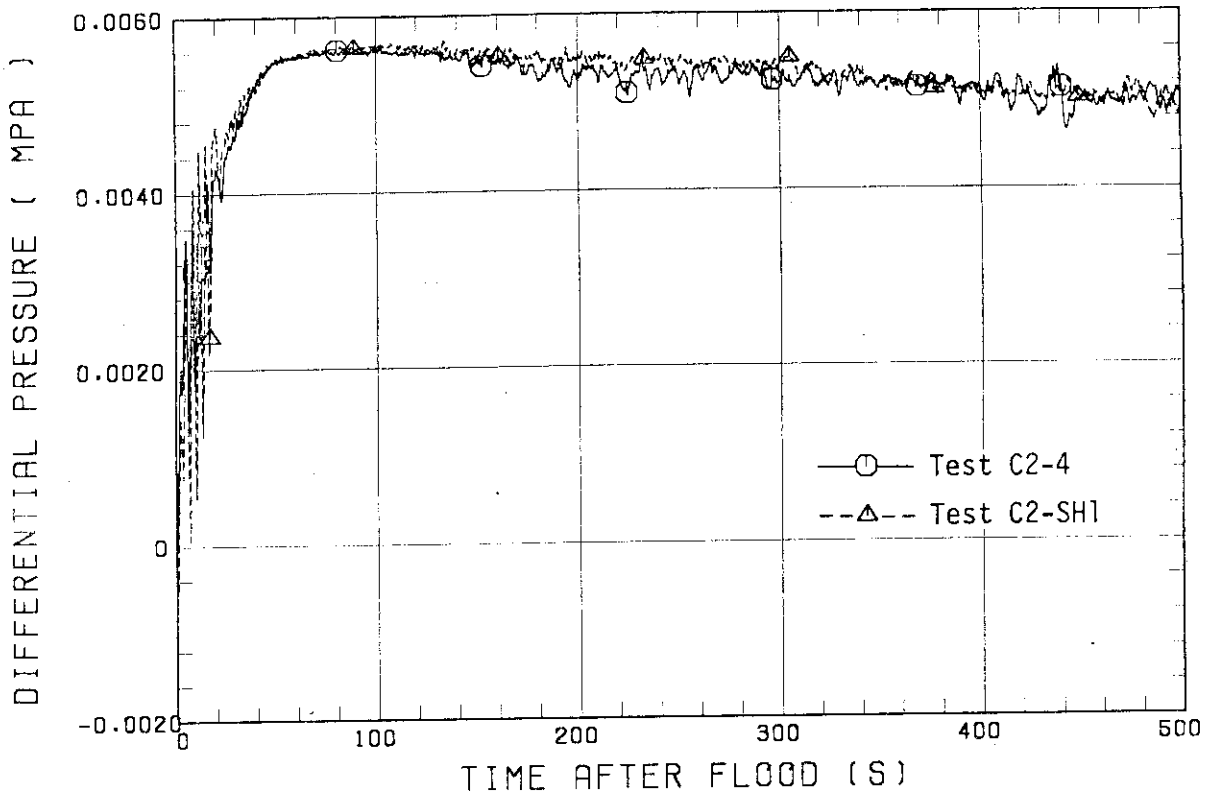

Fig. 3.9(a) Core sectional differential pressures between 0 and 0.61 m elevations

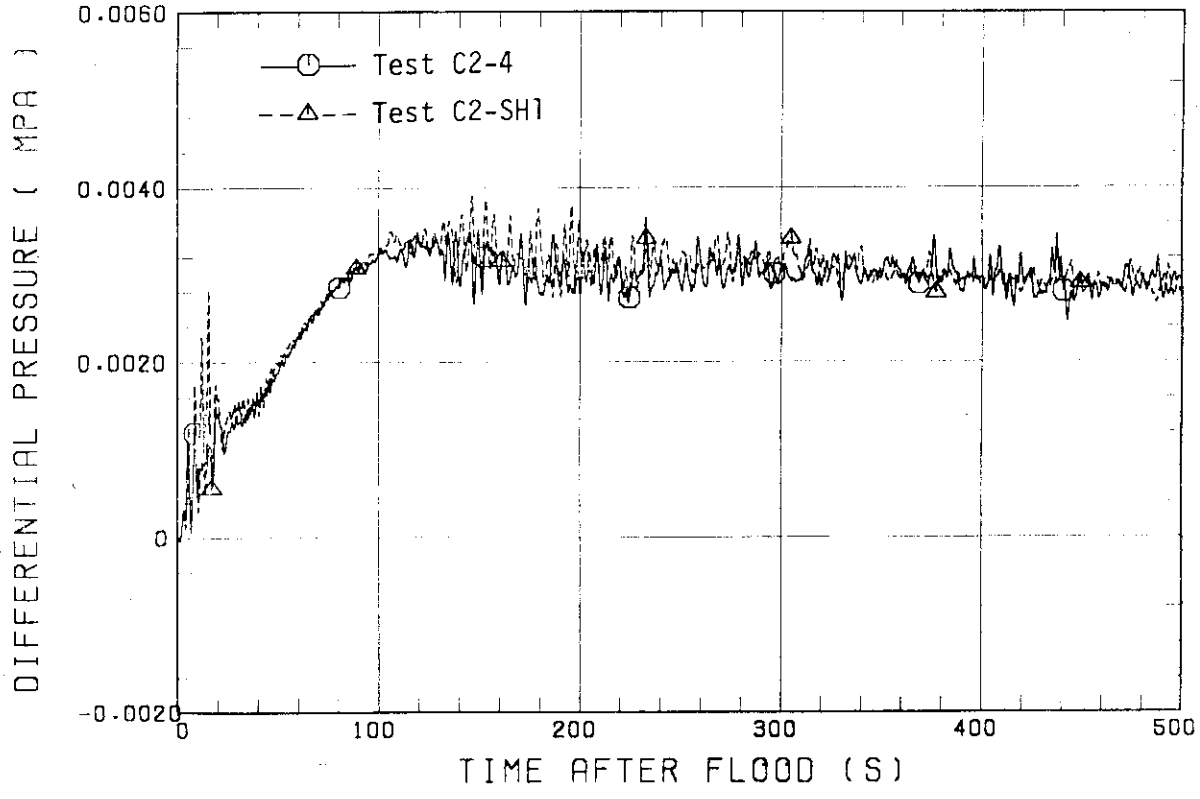

Fig. 3.9(b) Core sectional differential pressures between 0.61 and 1.22 m elevations

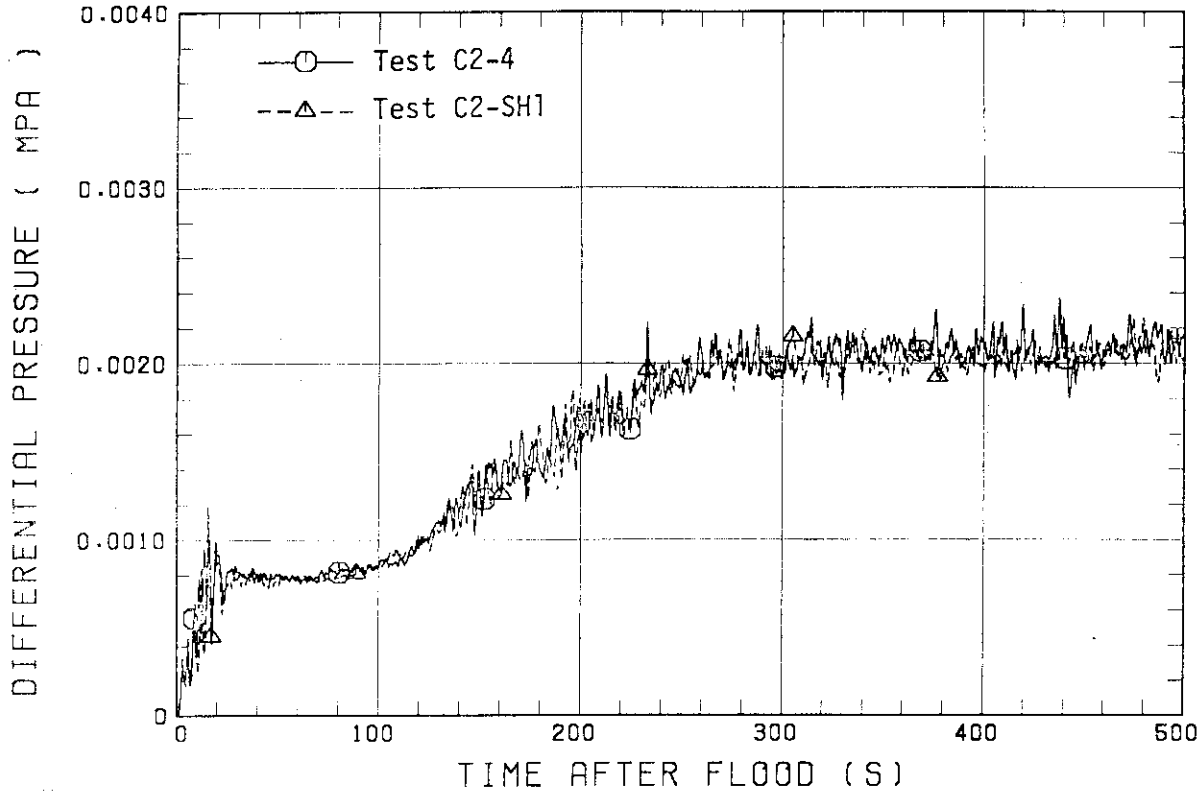

Fig. 3.9(c) Core sectional differential pressures between 1.22 and 1.83 m elevations

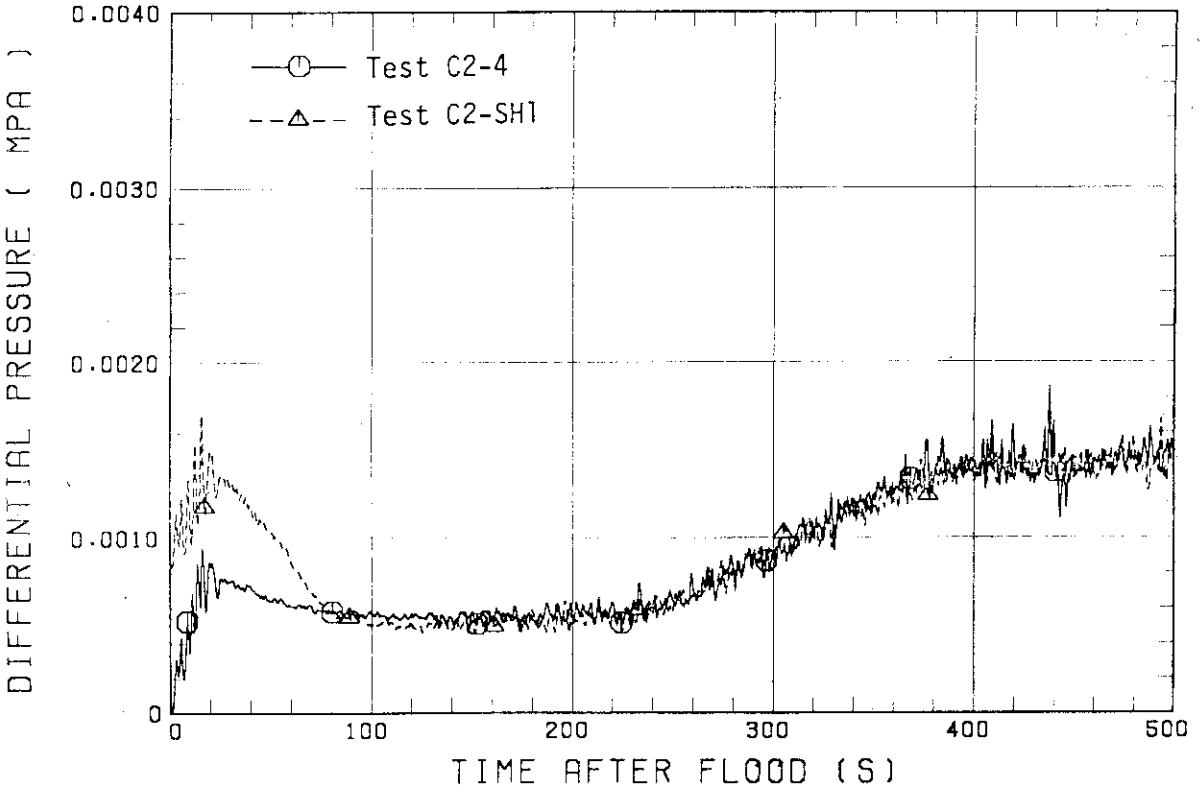

Fig. 3.9(d) Core sectional differential pressures between 1.83 and 2.44 m elevations

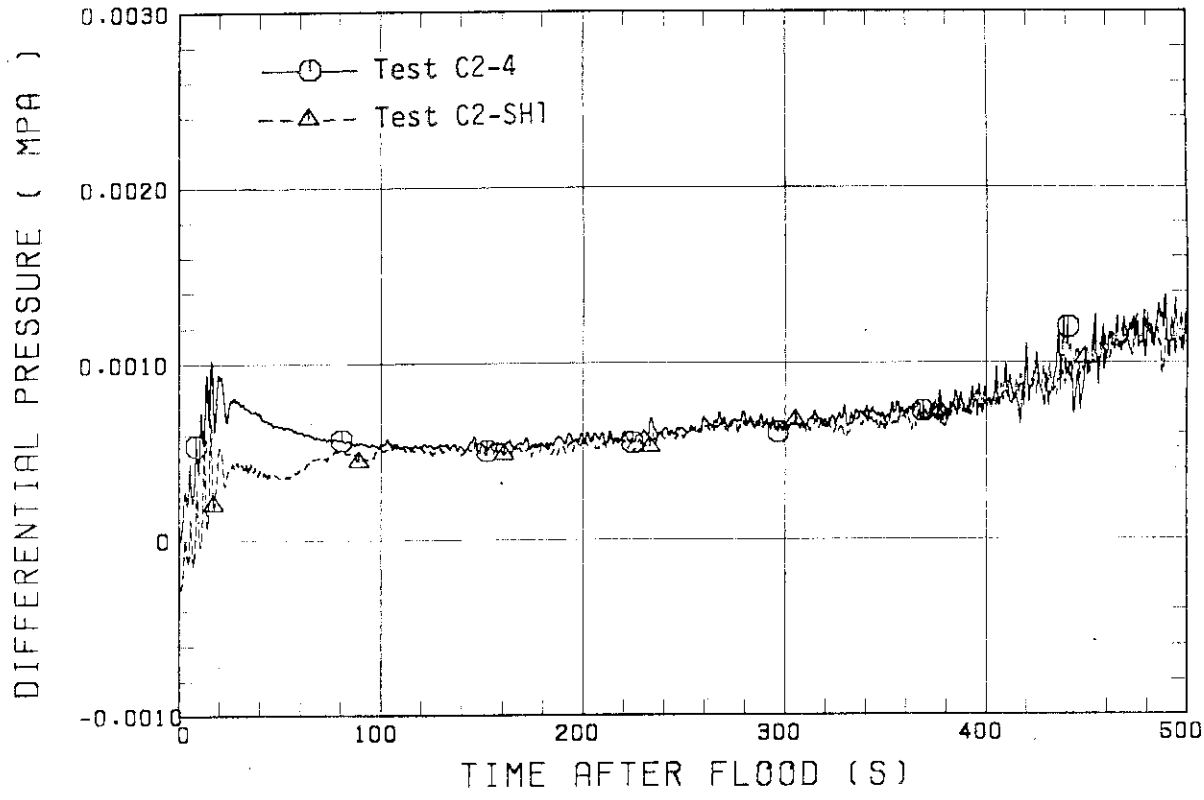

Fig. 3.9(e) Core sectional differential pressures between 2.44 and 3.05 m elevations

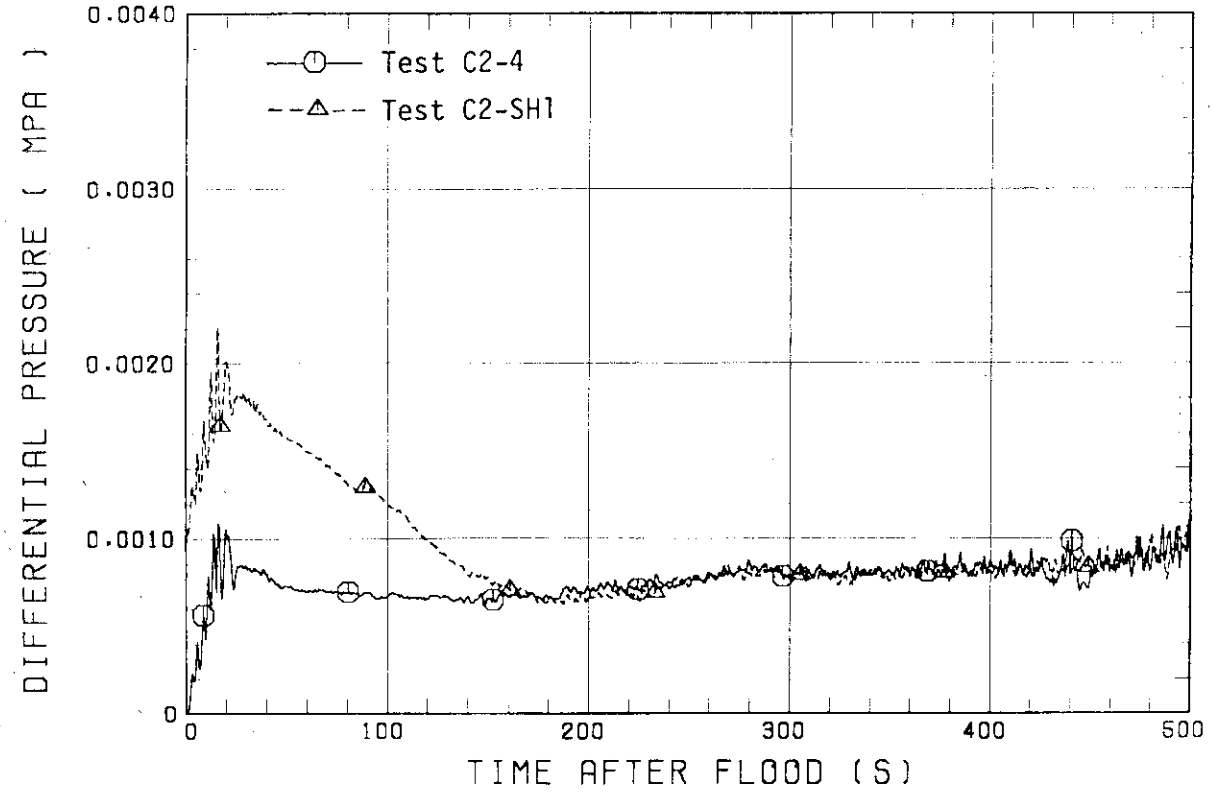

Fig. 3.9(f) Core sectional differential pressures between 3.05 and 3.66 m elevations

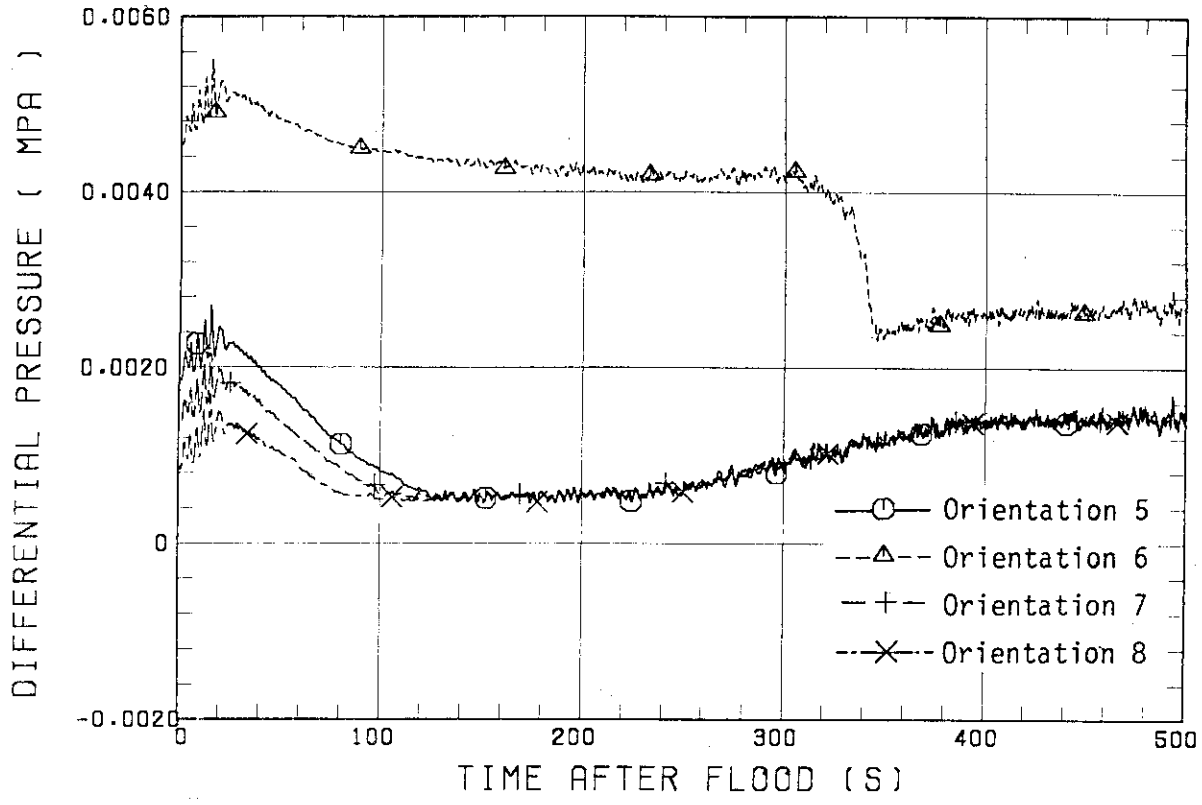

Fig. 3.10(a) Core sectional differential pressures between 1.83 and 2.44 m elevations for Test C2-SH1

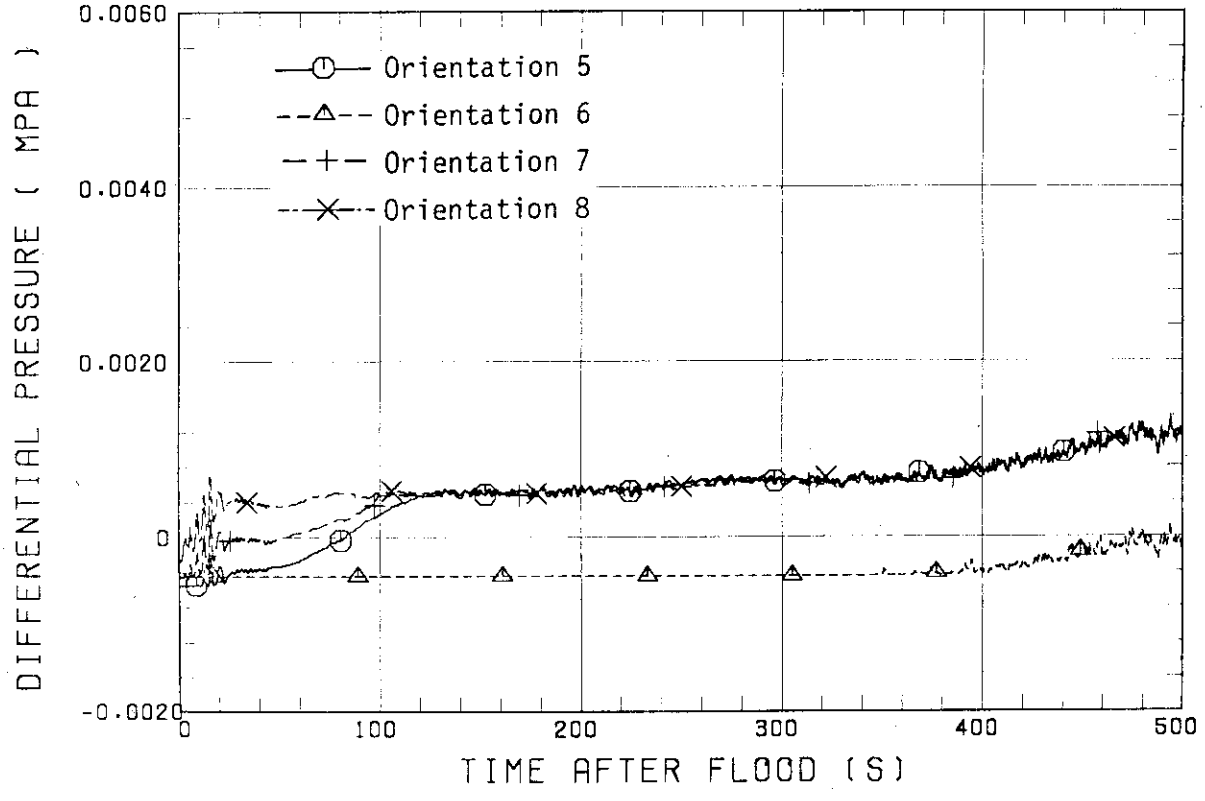

Fig. 3.10(b) Core sectional differential pressures between 2.44 and 3.05 m elevations for Test C2-SH1

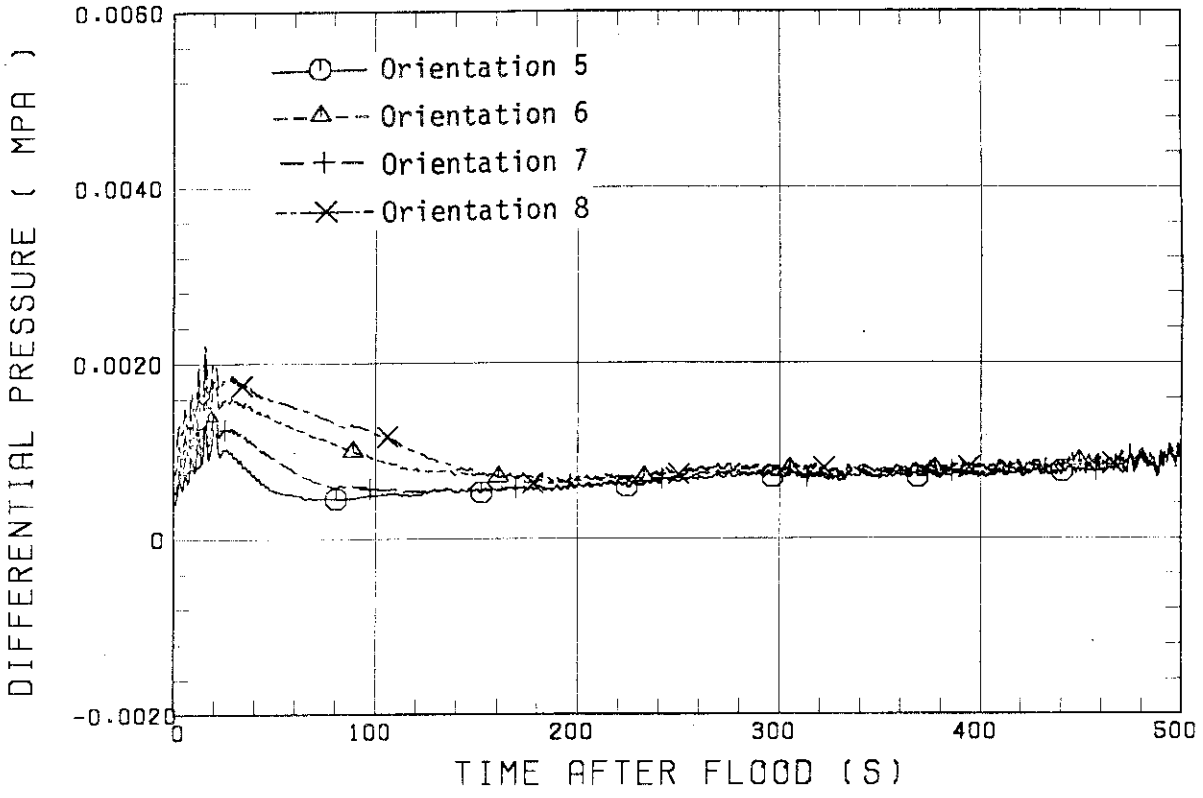

Fig. 3.10(c) Core sectional differential pressures between 3.05 and 3.66 m elevations for Test C2-SH1

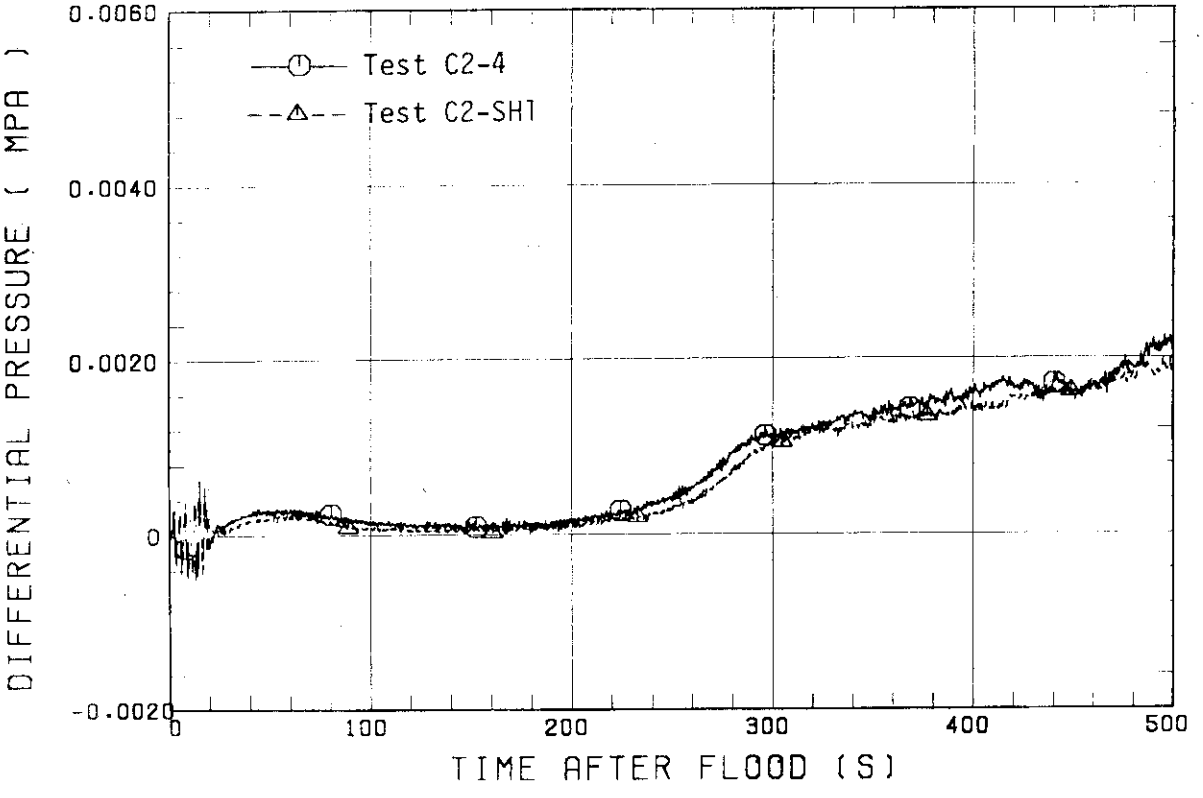

Fig. 3.11 Upper plenum differential pressures above UCSP

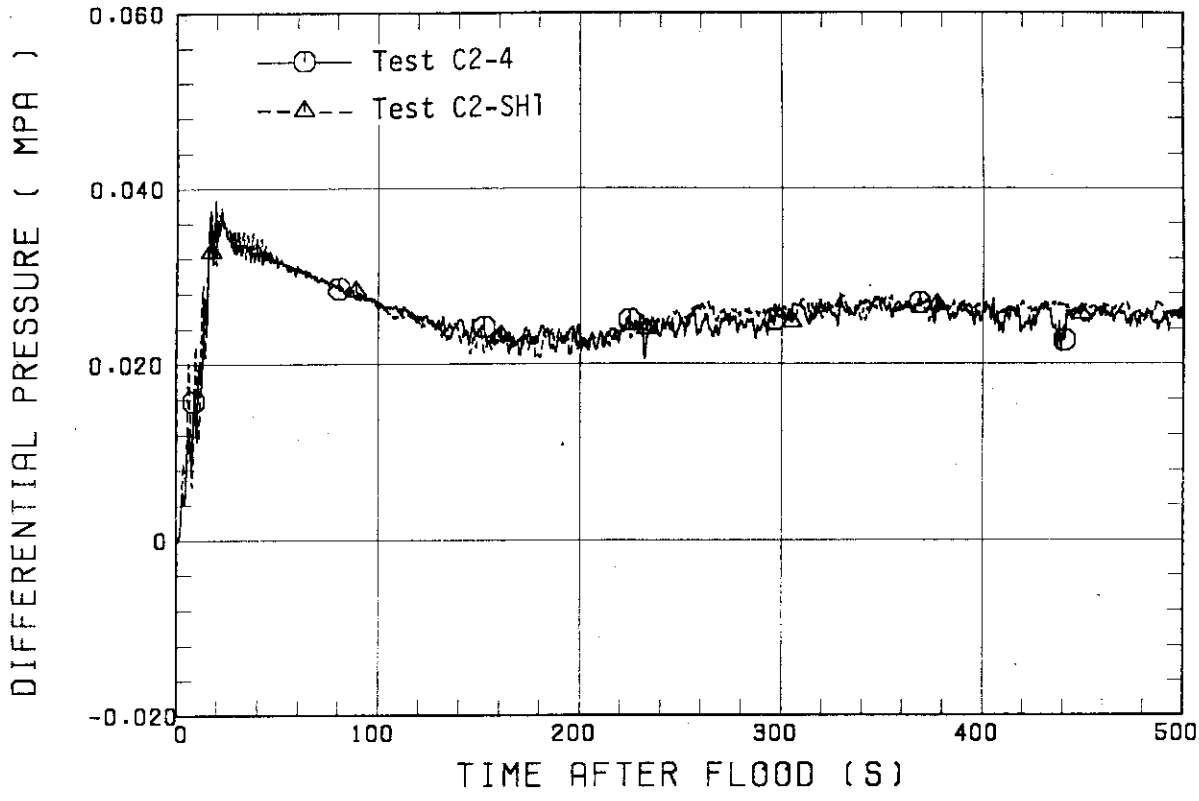

Fig. 3.12 Intact loop differential pressures

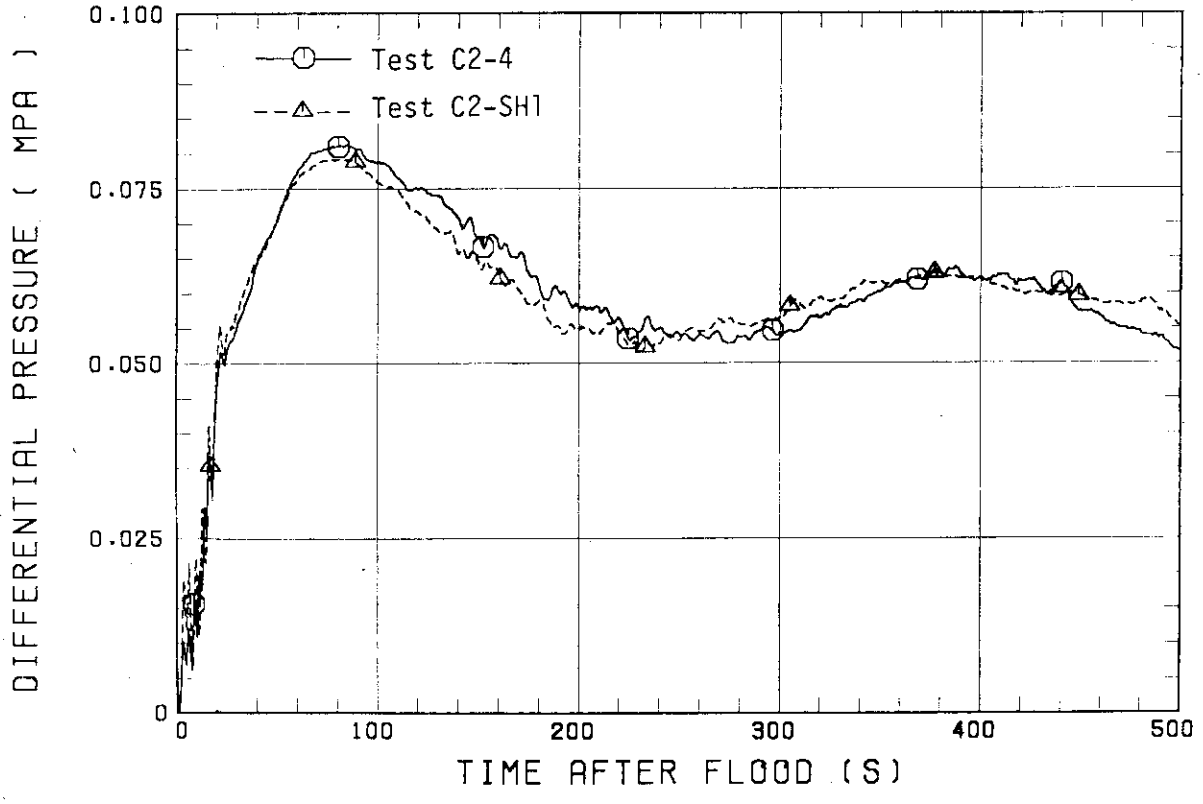

Fig. 3.13 Broken loop differential pressures

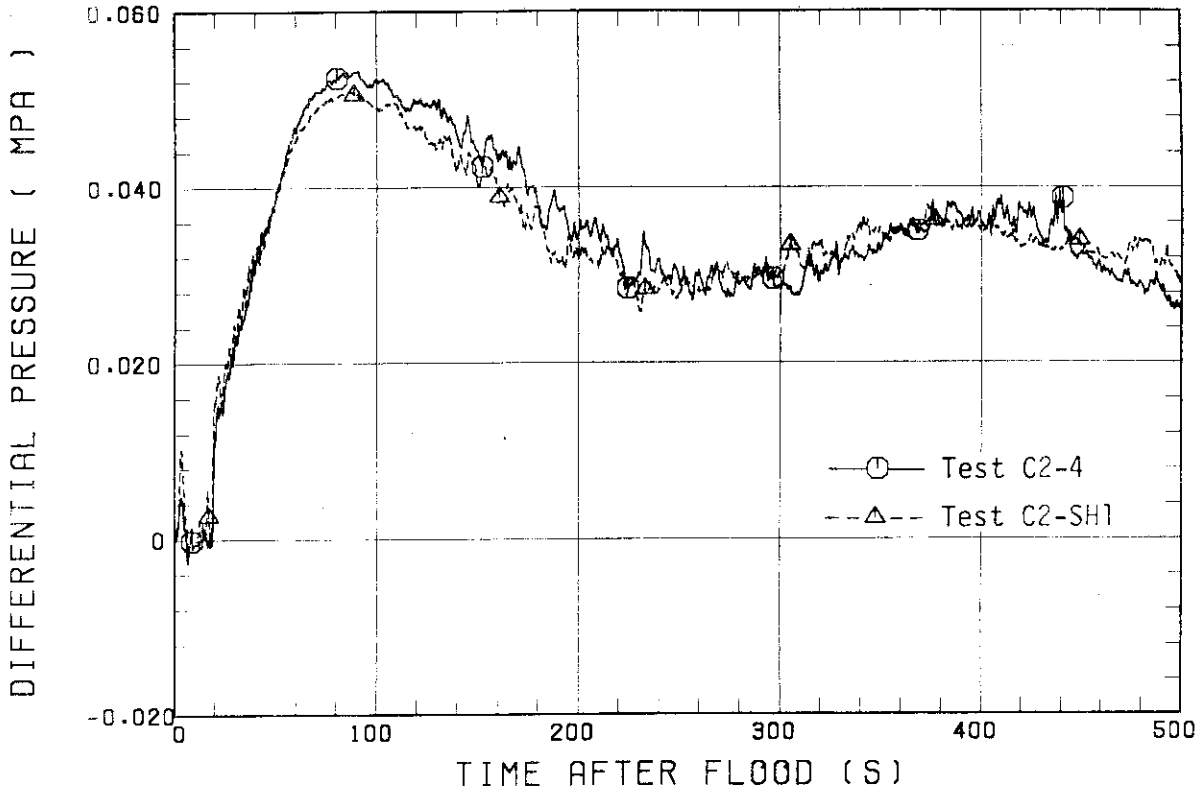

Fig. 3.14 Pressure losses through broken cold leg

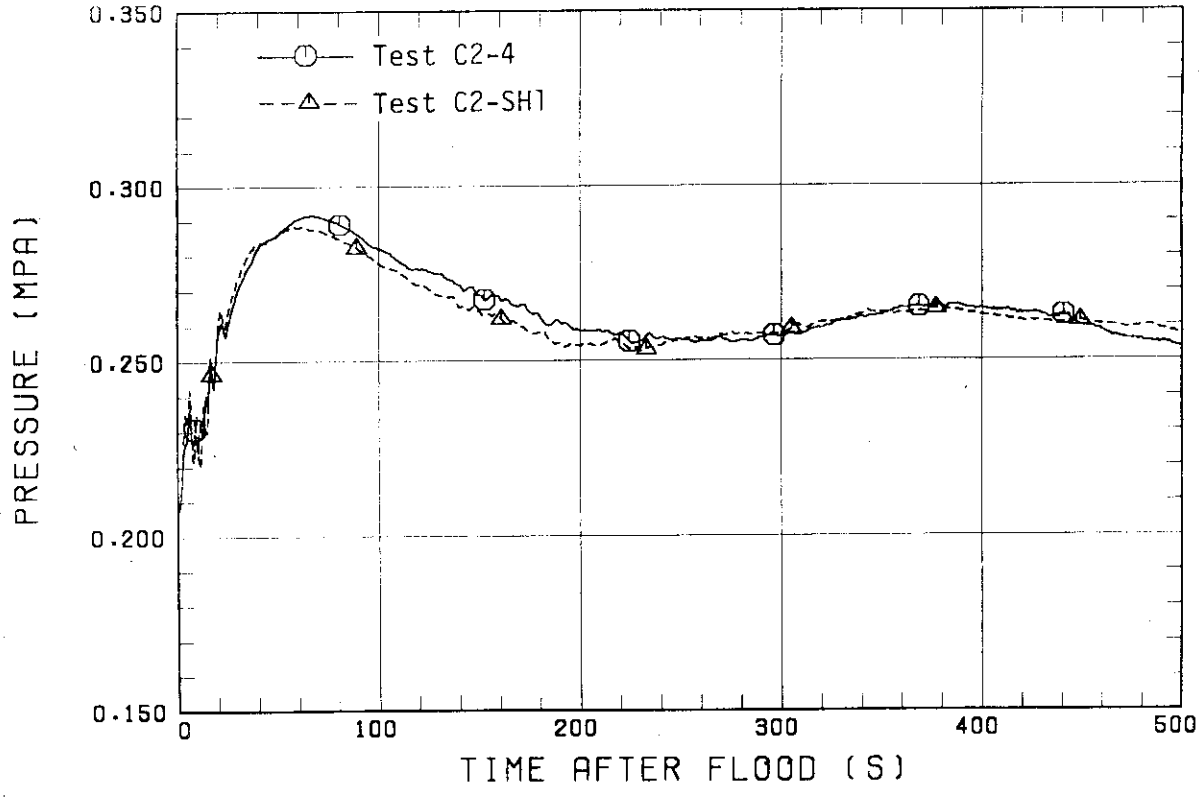

Fig. 3.15 Upper plenum pressures

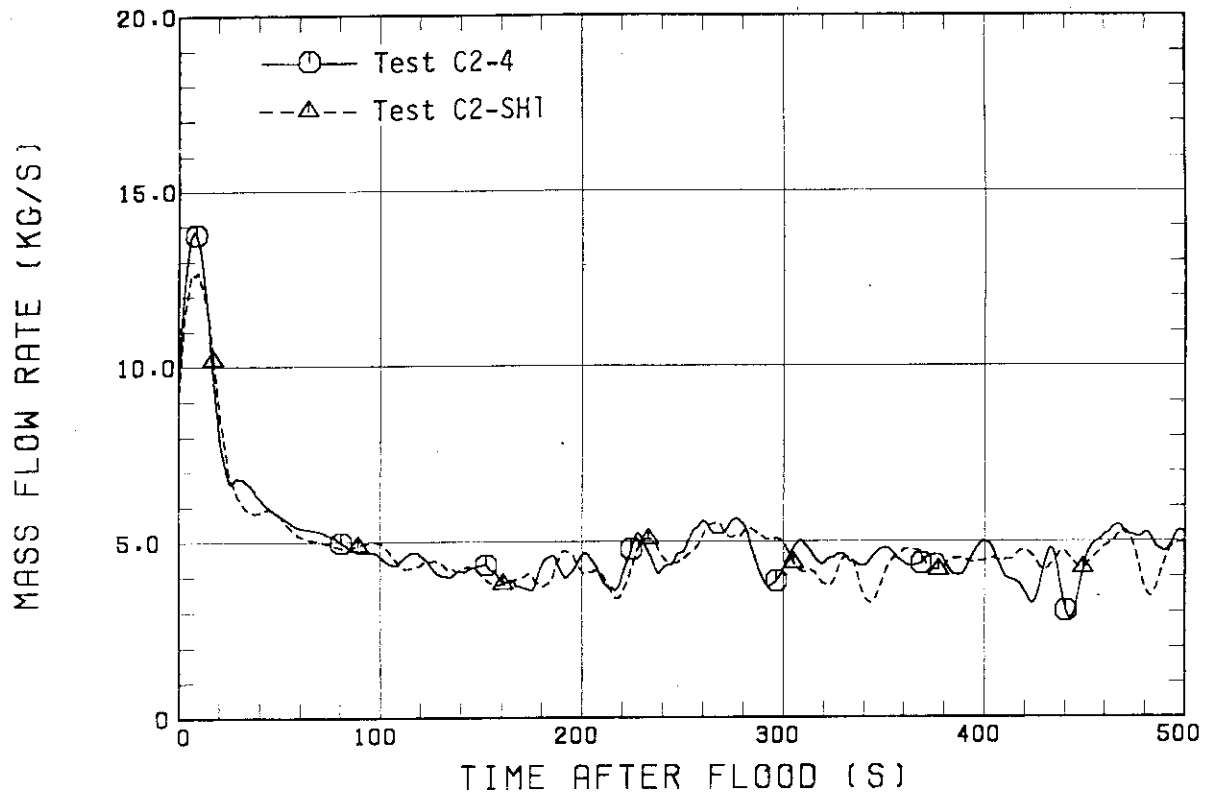

Fig. 3.16 Evaluated core flooding rates

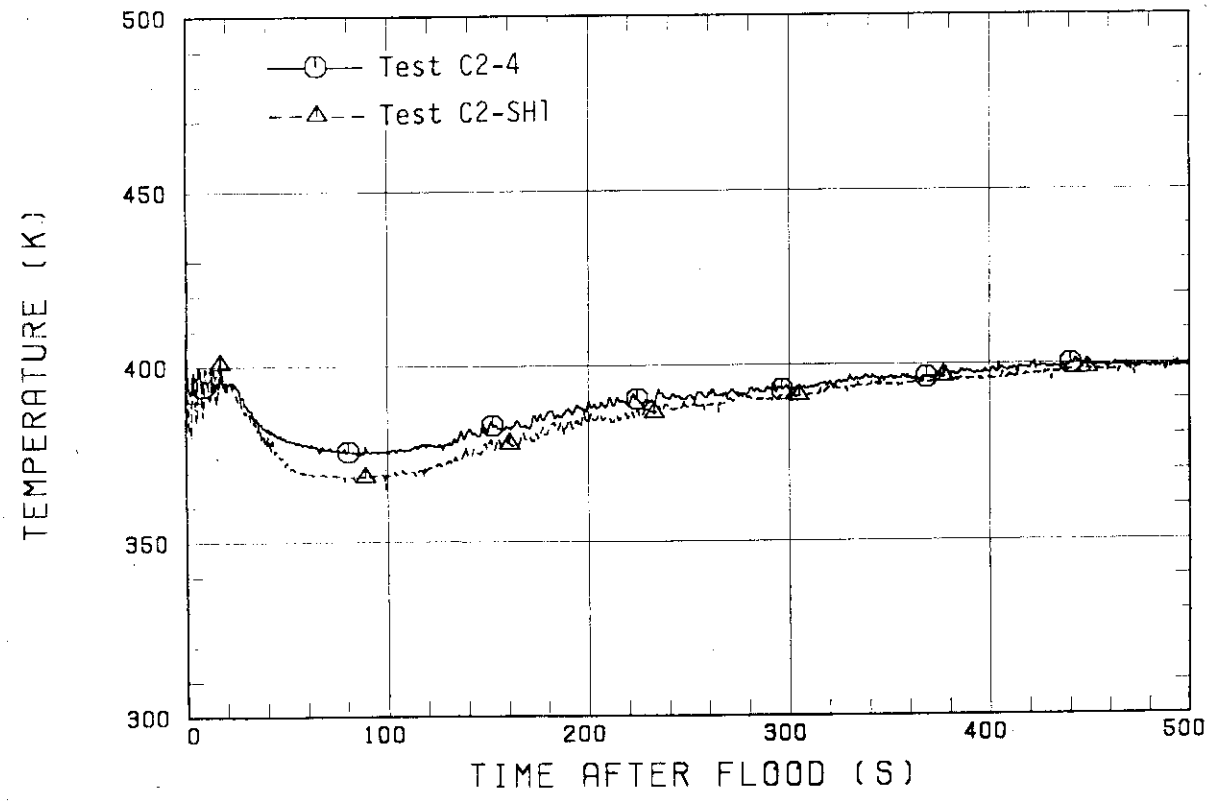

Fig. 3.17 Fluid temperatures at core inlet

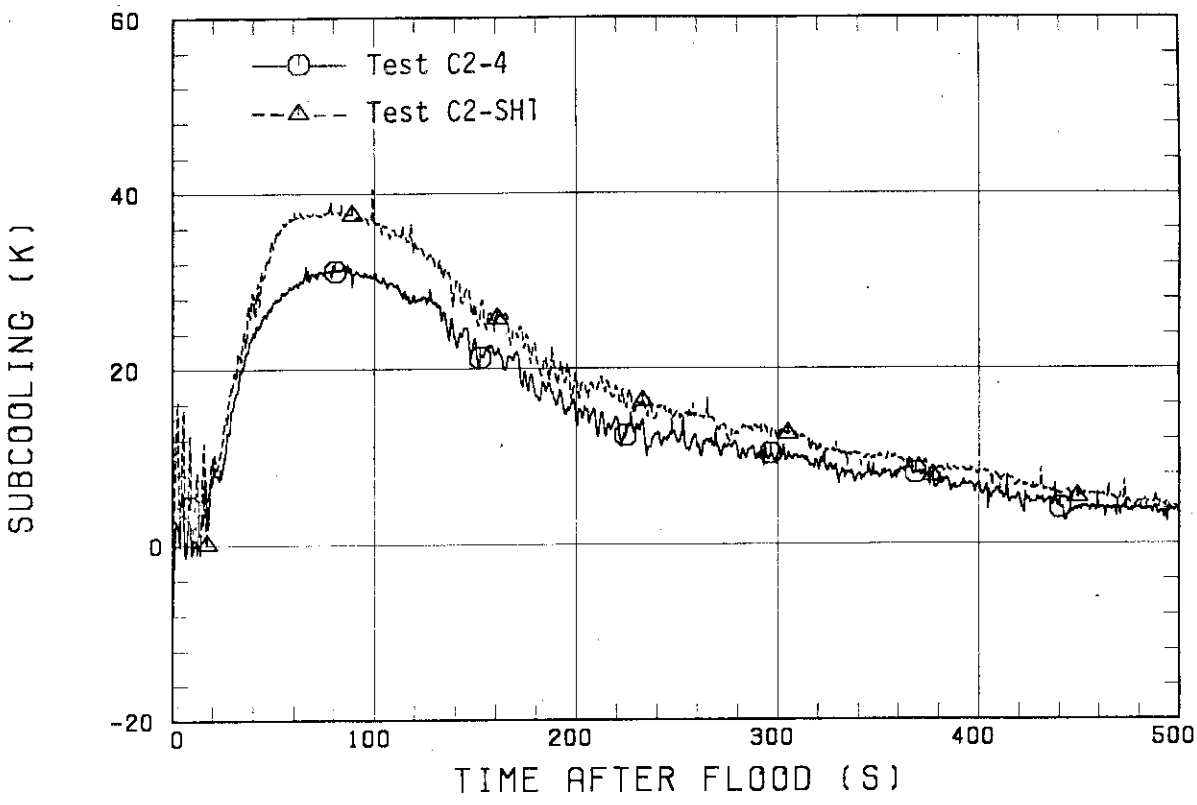

Fig. 3.18 Core inlet subcoolings

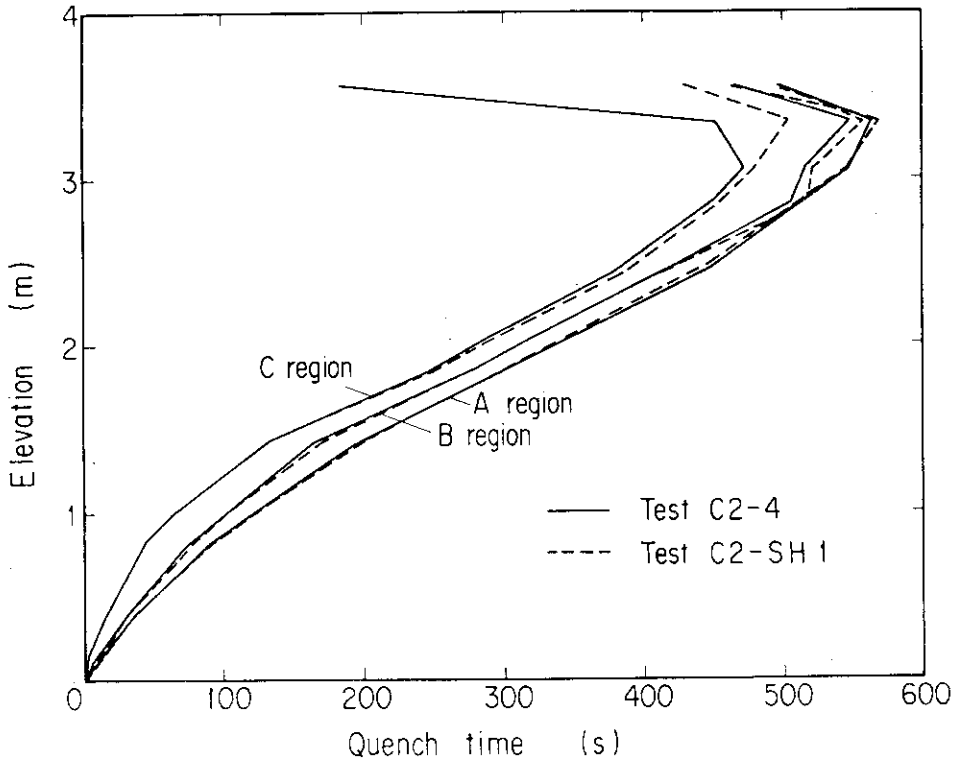

Fig. 3.19 Quench envelopes (mean values)

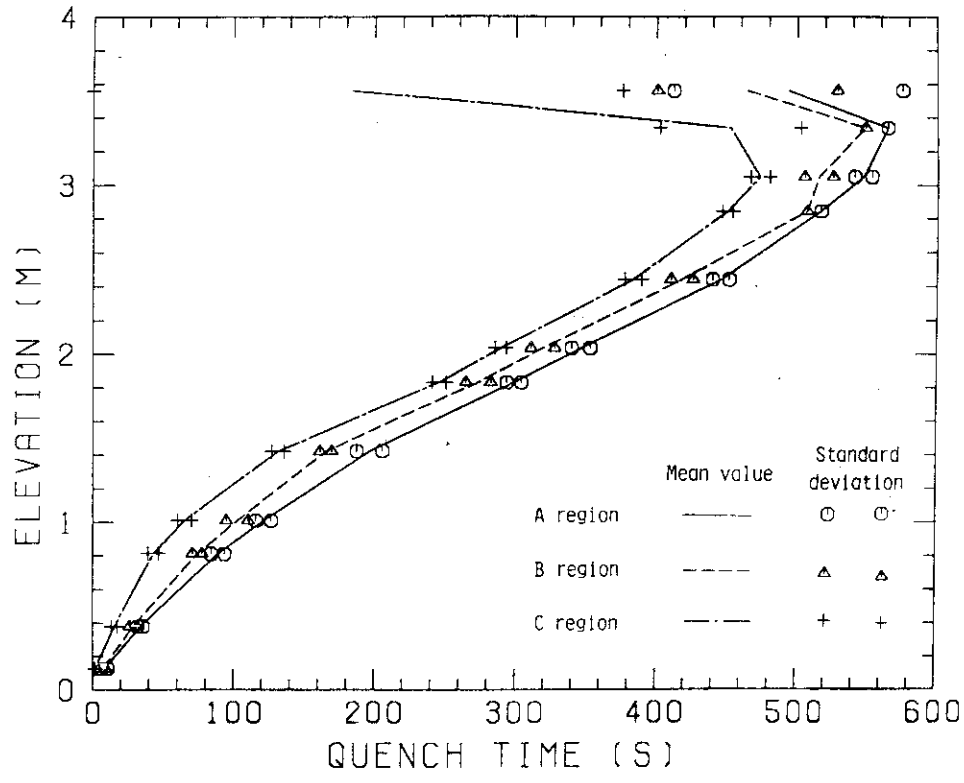

Fig. 3.20(a) Quench envelope for Test C2-4

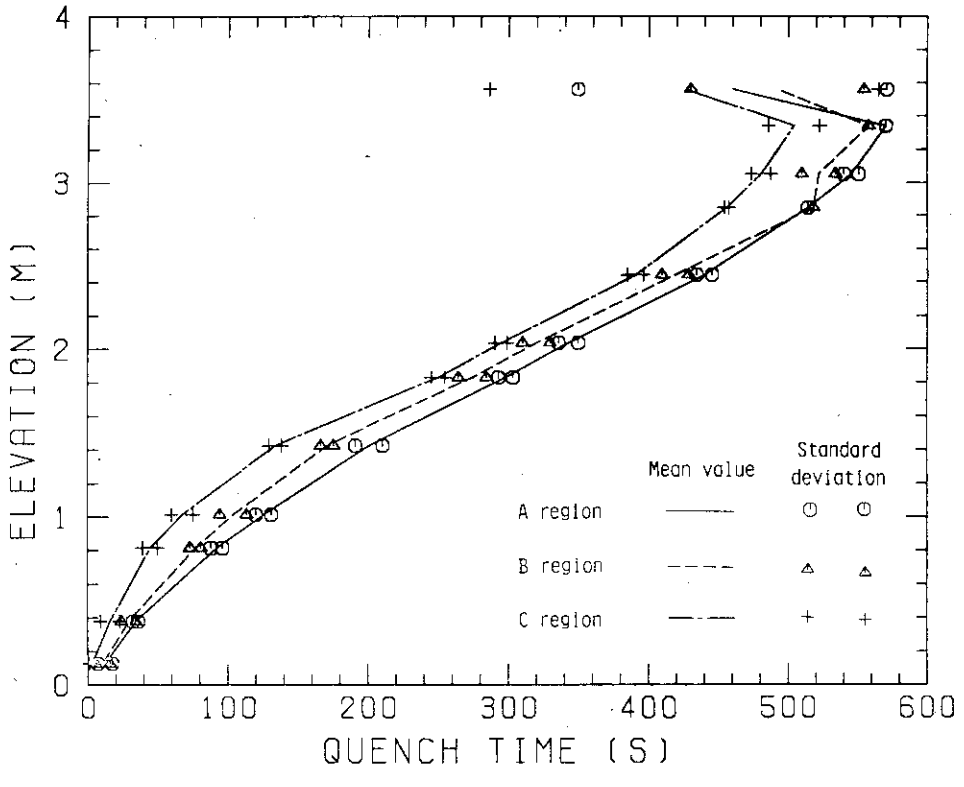

Fig. 3.20(b) Quench envelope for Test C2-SH1

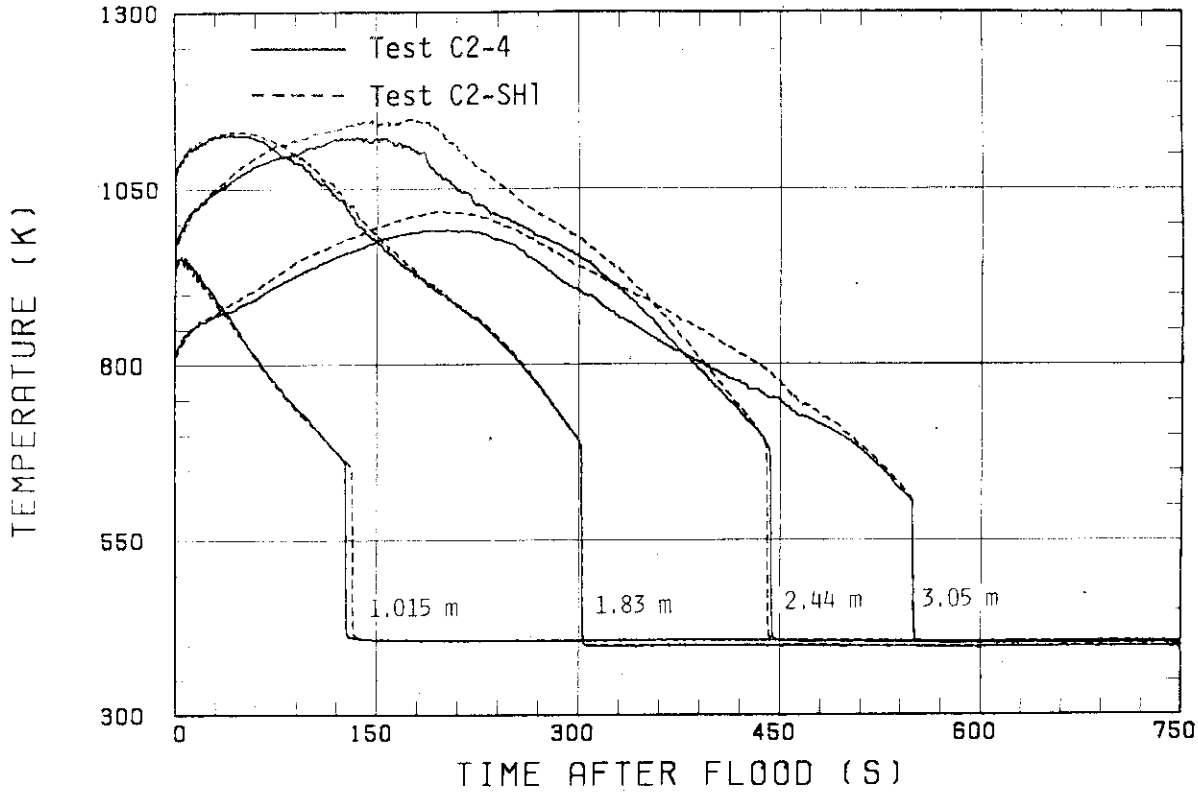

Fig. 3.21(a) Rod surface temperatures in A region

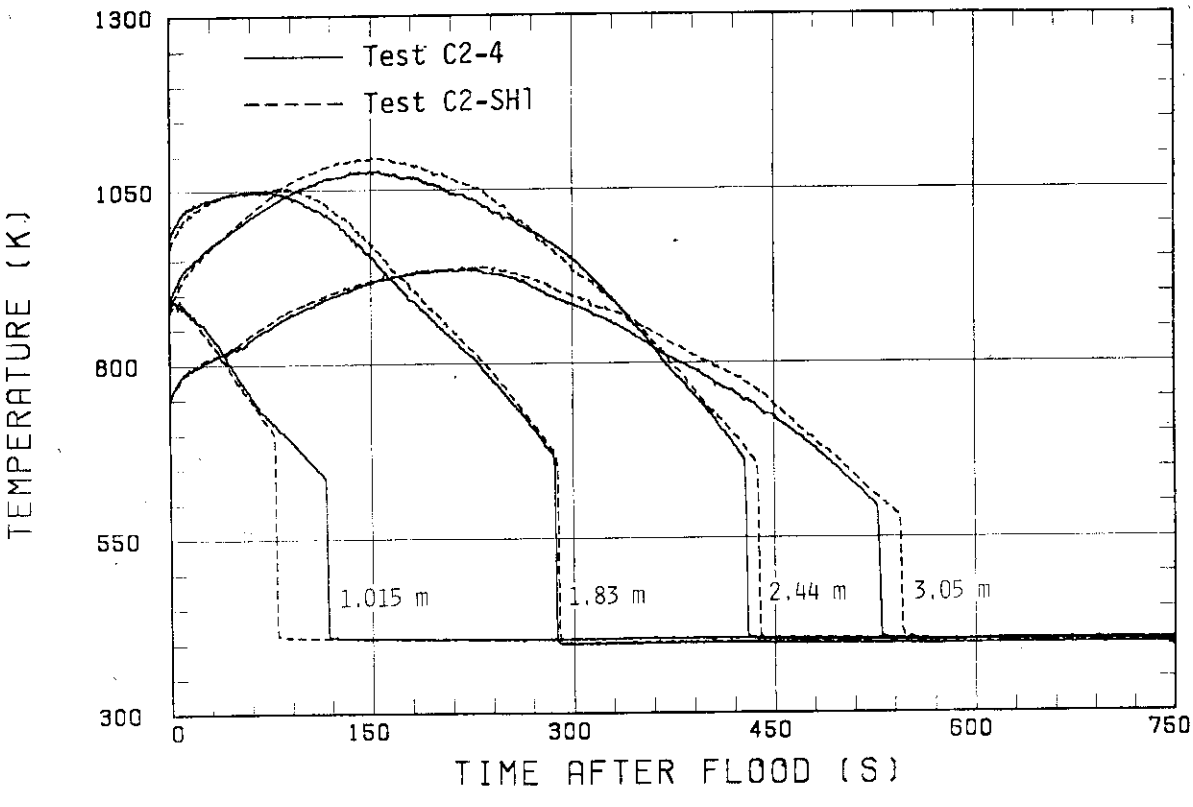

Fig. 3.21(b) Rod surface temperatures in B region

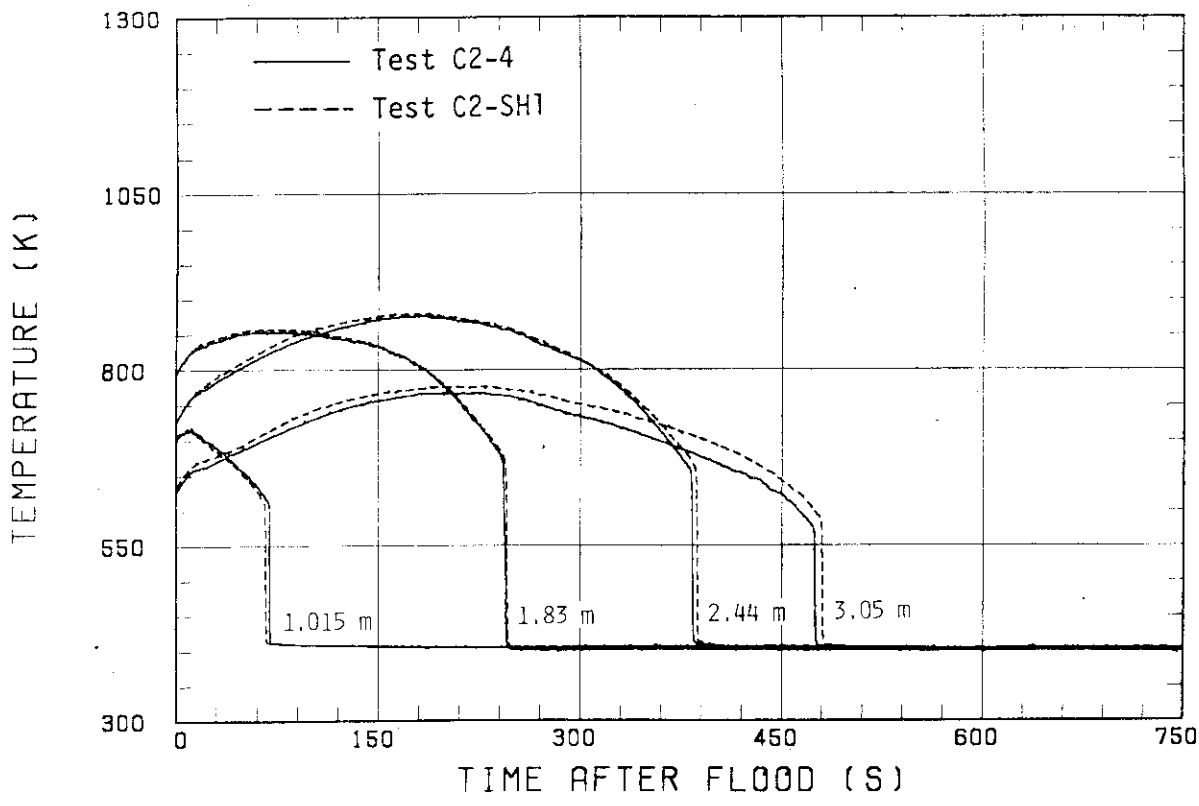

Fig. 3.21(c) Rod surface temperatures in C region

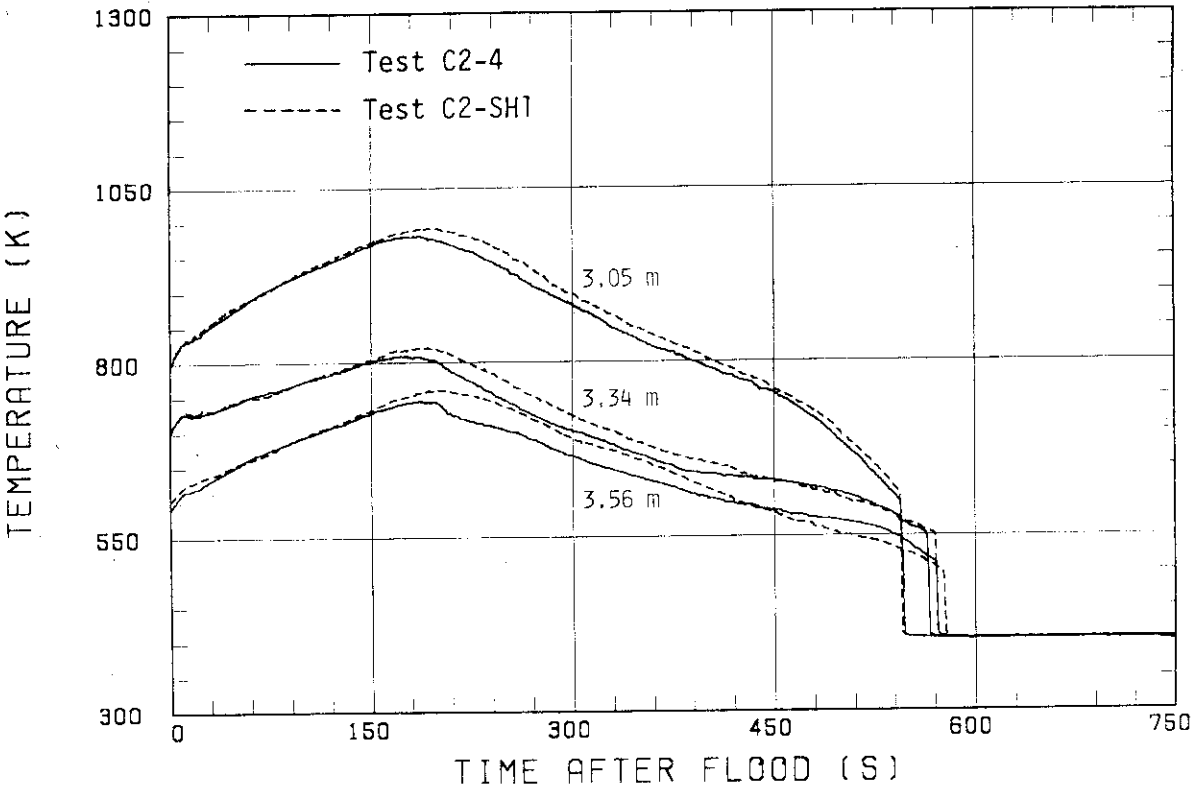

Fig. 3.22 Rod surface temperatures at top part in A region

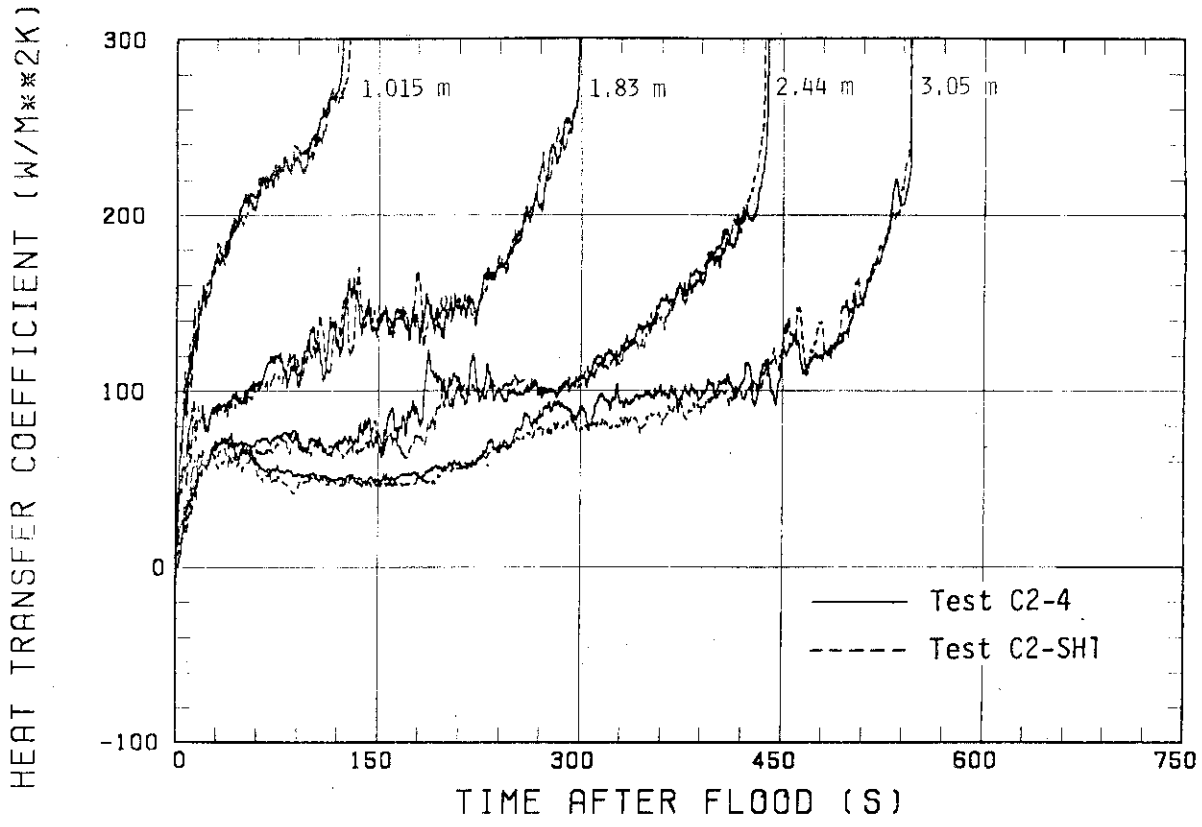

Fig. 3.23 Heat transfer coefficients in A region

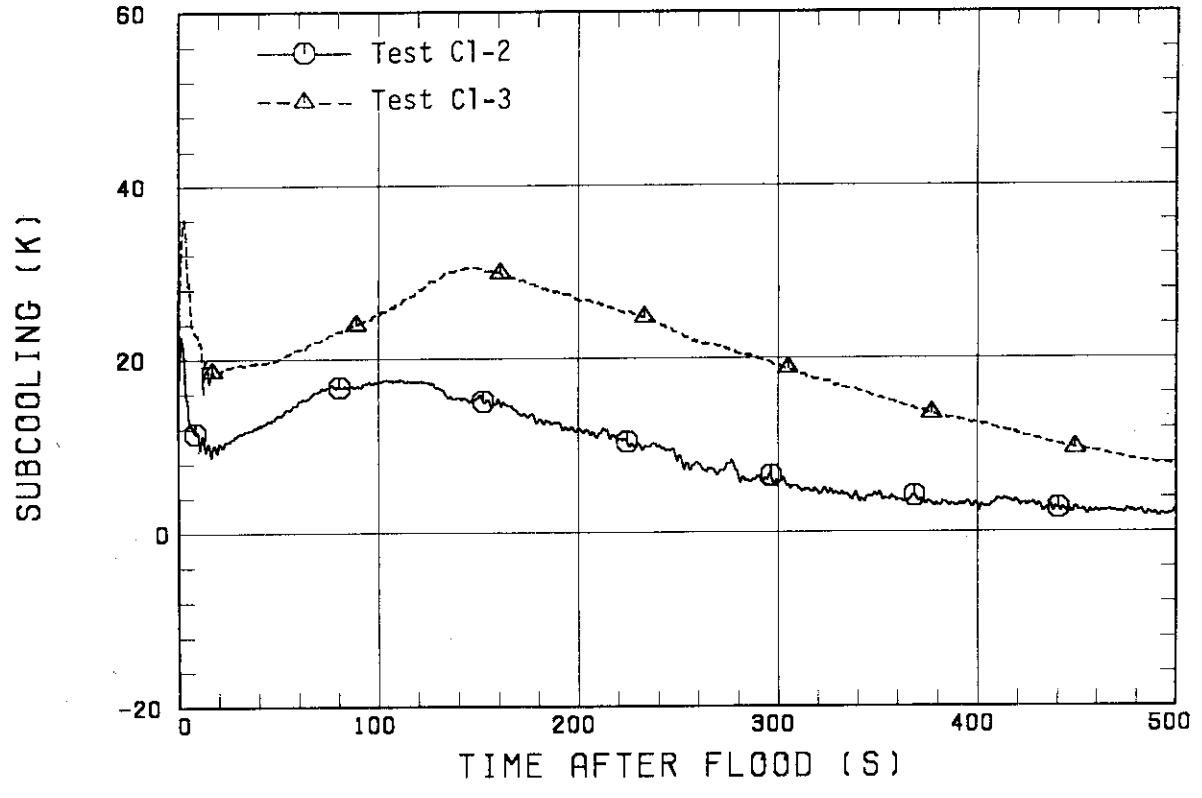

Fig. 3.24 Core inlet subcoolings for Tests C1-2 and C1-3

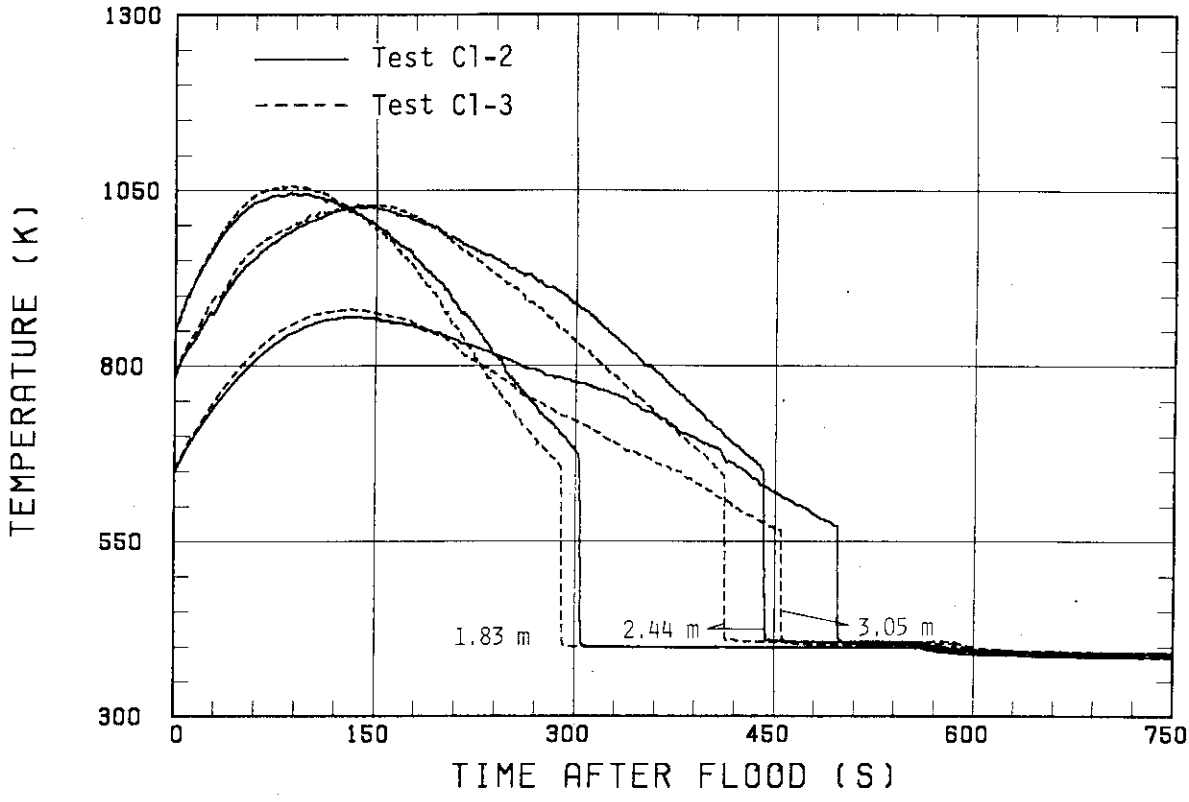

Fig. 3.25 Rod Surface temperatures of peak power rod for Tests C1-2 and C1-3

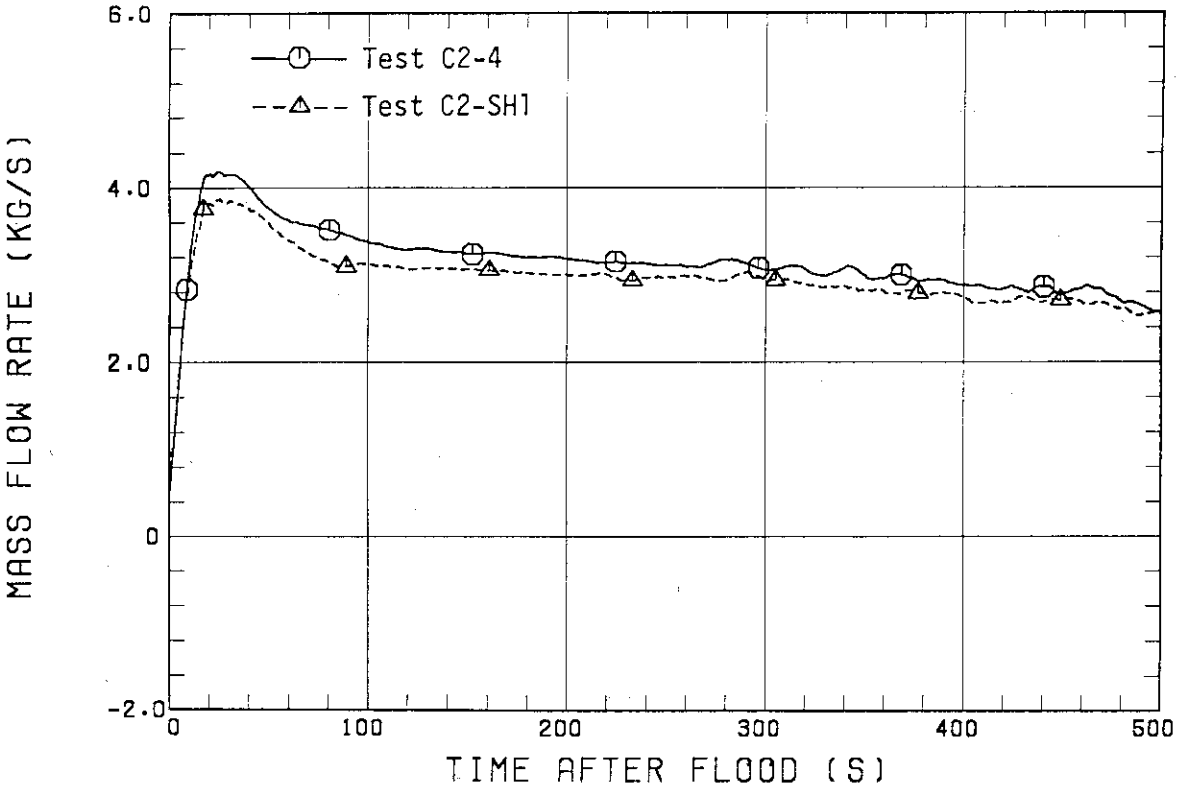

Fig. 3.26 Core outlet steam mass flow rates

4. Conclusions

In order to investigate the reproducibility of the CCTF Core-II tests, the data of the present test (Test C2-4) are compared with those of Test C2-SH1. The following results are obtained.

(1) The initial and boundary conditions for the two tests were almost identical except the temperatures of the core barrel and the lower plenum fluid. The difference in the latter is considered to result in a little difference in core inlet subcooling of about 6 K at most.

(2) The system behavior was almost identical.

(3) The core cooling behavior was also nearly identical except a little difference in the rod surface temperature in the upper part of the high power region.

(4) Taking account that the difference mentioned above in item (3) is small and can be explained qualitatively to be caused by the difference in the core inlet subcooling mentioned above in item (1), it is practically concluded that there is the reproducibility of the thermo-hydrodynamic behavior in the CCTF Core-II tests.

Acknowledgments

The authors are much indebted to Drs. M. Nozawa, S. Katsuragi, M. Hirata, and K. Hirano of JAERI for their guidance and encouragement for this program.

They would like to express their appreciation to the member of their analysis group, especially Mr. Messrs. H. Adachi, M. Sobajima, T. Iwamura, A. Ohnuki and Y. Abe of JAERI.

They also would like to express their thanks to the 2D/3D project members of USA and FRG.

They are deeply indebted to Messrs. Y. Fukaya, T. Ohyama, T. Wakabayashi, Y. Niitsuma, K. Nakajuma, T. Chiba, J. Matsumoto, K. Komori and H. Sonobe of JAERI for their contribution to the test conduction.

References

1. Hirano, K. and Murao, Y. "Large Scale Reflood Test". J. At. Energy Soc. Japan 22 [10], 681 (1980) [in Japanese].
2. Murao, Y., *et al.* "Analysis Report on CCTF Core-I Reflood Test", To be published as a JAERI-M report.
3. Sudoh, T., *et al.* "Evaluation Report on CCTF Core-II Reflood Test, First Shakedown Test, C2-SH1 (Run 53)", To be published as a JAERI-M report.
4. Akimoto, H. and Murao, Y. "Evaluation Report on CCTF Core-I Reflood Tests C1-2 (Run 11) and C1-3 (Run 12)", JAERI-M 83-090 (1983).

Acknowledgments

The authors are much indebted to Drs. M. Nozawa, S. Katsuragi, M. Hirata, and K. Hirano of JAERI for their guidance and encouragement for this program.

They would like to express their appreciation to the member of their analysis group, especially Mr. Messrs. H. Adachi, M. Sobajima, T. Iwamura, A. Ohnuki and Y. Abe of JAERI.

They also would like to express their thanks to the 2D/3D project members of USA and FRG.

They are deeply indebted to Messrs. Y. Fukaya, T. Ohyama, T. Wakabayashi, Y. Niitsuma, K. Nakajuma, T. Chiba, J. Matsumoto, K. Komori and H. Sonobe of JAERI for their contribution to the test conduction.

References

1. Hirano, K. and Murao, Y. "Large Scale Reflood Test". J. At. Energy Soc. Japan 22 [10], 681 (1980) [in Japanese].
2. Murao, Y., *et al.* "Analysis Report on CCTF Core-I Reflood Test", To be published as a JAERI-M report.
3. Sudoh, T., *et al.* "Evaluation Report on CCTF Core-II Reflood Test, First Shakedown Test, C2-SH1 (Run 53)", To be published as a JAERI-M report.
4. Akimoto, H. and Murao, Y. "Evaluation Report on CCTF Core-I Reflood Tests C1-2 (Run 11) and C1-3 (Run 12)", JAERI-M 83-090 (1983).

Appendix

Appendix A

Definitions of Tag IDs

Figure List

1. Definition of Tag. ID for clad surface temperatures and heat fransfer coefficients

Notation : TEnnYlm (temperature)

HTEmmYlm (heat transfer coefficient)

nn : Bundle number (see Fig. A.1)

m : Elevation number

	Elevation (m)	Axial power factor
3	0.38	0.651
5	1.015	1.147
7	1.83	1.40
9	2.44	1.256
A	3.05	0.854

2. Definition of power zone and boundle number

See Fig. A.1

3. Definition of Tag. ID for void fraction

See Fig. A.2

4. Definition of Tag. ID for average linear power of heater rod in each power unit zone

See Fig. A.3

5. Definition of Tag. ID for differential pressure through downcomer, upper plenum, core and lower plenum

See Fig. A.4

6. Definition of Tag. ID for differential pressure through intact and broken loop and broken cold leg nozzle

See Fig. A.5

7. Definition of Tag. ID for fluid temperature in inlet and outlet plenum and secondary side of steam generator

See Fig. A.6

8. Definition of Tag. ID for ECC water injection rate, ECC water temperature and vented steam flow rate

See Fig. A.7

9. Definition of initial temperature, turnaround temperature quench temperature, temperature rise, turnaround time and quench time. (See Fig. A.8

T_i : Initial temperature (Clad surface temperature at reflood initiation)

T_t : Turnaround temperature (Maximum clad surface temperature in each temperature history)

ΔT_r : Temperature rise ($= T_t - T_i$)

T_q : Quench temperature (Clad surface temperature at quenching)

10. Definition of quenching

See Fig. A.8

Quench time t_t is determined as

$$t_t = i \times \Delta t - \text{(reflood initiation time)}$$

In above equation, i is determined by the following criteria.

(1) Clad surface temperature is high, compared with the saturation temperature.

$$T_i > T_{sat} + \Delta T_1$$

(2) Decreasing rate of clad surface temperature is large.

$$\frac{T_{i+1} - T_i}{\Delta t} < - C_{st}$$

(3) Clad surface temperature falls around the saturation temperature.

$$T_{i + k_1} \leq T_{sat} + \Delta T_1$$

(4) If the determined i is inadequate, the value i is manually re-determined.

Δt : Data sampling period (s)

T_i : Clad surface temperature (K)

T_{sat} : Saturation temperature at the pressure in upper plenum (K)

ΔT_1 : Temperature discrepancy (K)
Default value = 50.0

C_{st} : Decreasing rate of clad surface temperature (K/S)
Default value = 25.0

k_1 : Number of referred data (-)
Default value = 6

11. Definition of Tag. ID for core inlet mass flow rate, time-integral core inlet mass flow rate and carry-over rate fraction

(1) Core inlet mass flow rate : $\dot{m}_F$
Notation : MLCRI□ (□ = N, 1 or 11)

(2) Time-intefral core inlet mass flow rate : $\int \dot{m}_F dt$
Notation : IMLCRI□ (□ = N, 1 or 11)

(3) Carry-over rate fraction : $(\dot{m}_F - \dot{m}_{CR})/\dot{m}_F$
Natation : CRF□ (□ = N, 1 or 11)

where $\dot{m}_F$: Core inlet mass flow rate (See item 12)

$\dot{m}_{CR}$: Water accumulation rate in core

Suffix	$\dot{m}_F$ based on
N	Eq.(A.2)
1	Eq.(A.1) with K=15
11	Eq.(A.1) with K=20

12. Evaluation of core inlet mass flow rate

The reflood phenomena is a relatively slow transient and a steady state condition can be applied. In a steady state condition, based on the mass balance relations of the system, the core flooding mass flow rates $\dot{m}_F$s can be written as follows:

By using the data measured at the downstream of the core inlet, $\dot{m}_F$ is derived as,

$$\dot{m}_F = \dot{m}_C + \dot{m}_U + \dot{m}_B + \Sigma \dot{m}_I \quad , \qquad (A.1)$$

where $\dot{m}_C$ and $\dot{m}_U$ are the mass accumulation rates in the core and the upper plenum respectively. The $\dot{m}_B$ and $\dot{m}_I$ are the mass flow rates in the broken loop and the intact loop, respectively.

By using the data measured at the upstream of the core inlet, $\dot{m}_F$ is derived as,

$$\dot{m}_F = \Sigma \dot{m}_{DL} - \dot{m}_D - \dot{m}_O + \dot{m}_{ECC/LP} \quad , \tag{A.2}$$

where $\dot{m}_{DL}$ and $\dot{m}_O$ are the mass flow rates of the water flowing into and overflowing from the downcomer, $\dot{m}_{ECC/LP}$ and $\dot{m}_D$ are the mass flow rate of the ECC water injected into the lower plenum and the water accumulation rate in the dowmcomer respectively.

The $\dot{m}_I$s and $\dot{m}_B$ can be obtained from the pressure drops at the pump simulators with orifices by assuming the K-factor of the orifice is constant. The values of $\dot{m}_C$, $\dot{m}_D$ and $\dot{m}_U$ can be evaluated with the differential pressure ΔP_C, ΔP_D and ΔP_U, respectively, as follows:

$$\dot{m}_n = d(\Delta P_n S_n/g)/dt \quad (n : C, D, U) \quad , \tag{A.3}$$

where g is the gravitational acceleration and S_n is the cross sectional area. The value of $\dot{m}_O$ can be obtained from the liquid level X in the Containment tank 1 as,

$$\dot{m}_O = d(X\rho_\ell S_o)/dt \quad , \tag{A.4}$$

where ρ_ℓ is the liquid density and S_o is the cross sectional area of the containment tank 1.

The value of $\dot{m}_{DL}$, $\dot{m}_{DV}$ and h, which are liquid flow rate, steam flow rate and enthalpy of two phase mixture downstream each ECC port respectively, are obtained from the following mass and energy balance relations at each ECC port under the assumption of thermal equilibrium:

$$\dot{m}_{DV} + \dot{m}_{DL} = \dot{m}_{ECC} + \dot{m}_I \quad , \tag{A.5}$$

$$(\dot{m}_{DV} + \dot{m}_{DL})i = \dot{m}_{ECC} h_{ECC} + \dot{m}_I h_f \quad , \tag{A.6}$$

$$\text{if} \quad h_g \geq h \geq h_\ell \quad , \quad (\dot{m}_{DV} + \dot{m}_{DL})h = \dot{m}_{DV} h_g + \dot{m}_{DL} h_\ell$$

$$\text{if} \quad h \geq h_g \quad , \quad \dot{m}_{DL} = 0 \quad , \tag{A.7}$$

$$\text{if} \quad h \geq h_\ell \quad , \quad \dot{m}_{DV} = 0$$

where h is enthalpy of fluid and h_ℓ and h_g are enthalpies of liquid and steam at the saturation temperature, respectively.

The fluid temperatures can be measured with thermocouples immersed in the fluid and the enthalpies h_I and h_{ECC} can be estimated.

Mass balance calculations were performed with Eqs. (A.1) and (A.2). The K-factor of the orifice in the pump simulator was evaluated in the following two ways.

The K-factor of 20 was obtained with the steam and water single phase calibration tests using the flow meter and spool piece data. The K-factor of 15 was obtained with the Pitot tube measurement in a typical reflood condition assuming the flat velocity profile in the pipings. In the differentiation, higher frequency components of the data tends to be amplified more. Therefore, in the differentiation of the differential pressure data, the smoothing procedure was used to suppress the high frequency components of the data.

In the Acc injection period, the calculated $\dot{m}_F$s with Eqs. (A.1) and (A.2) are significantly different from each other. This discrepancy may be caused by inaccuracy of the mass flow rate injected into the system and by the unaccounting of the storage of water in the cold leg pipe. The former might be introduced from the slow time response of the flow meter (time constant 1 second) and the change of the gas volume in the injection line. In this period, especially before the steam generation from the core becomes noticeable, the mass flow rate, $\dot{m}_F$, calculated with Eq. (A.1) is probably reasonable, since the calculation uses the increasing rates of the masses in the core and the upper plenum and their accuracy is good enough for our estimation.

In the LPCI injection period, the calculated $\dot{m}_F$s are slightly different from each other. Judging from the time-integral values of both $\dot{m}_F$s, their average values are nearly proportional. The discrepancy was inferred to be caused by the disregard of the bypass of steam and liquid from the upper plenum without going through the hot legs in the calculation with Eq. (A.1). And additionally the discrepancy was caused by the disregard of the steam generation in the downcomer due to the hot wall of the pressure vessel in the calculation with Eq. (A.2). It was estimated that the disregard of the downcomer steam generation causes the error of 0.25 kg/s on predicted $\dot{m}_F$. The estimation was made by comparing the results of the tests with hot and cold downcomer conditions.

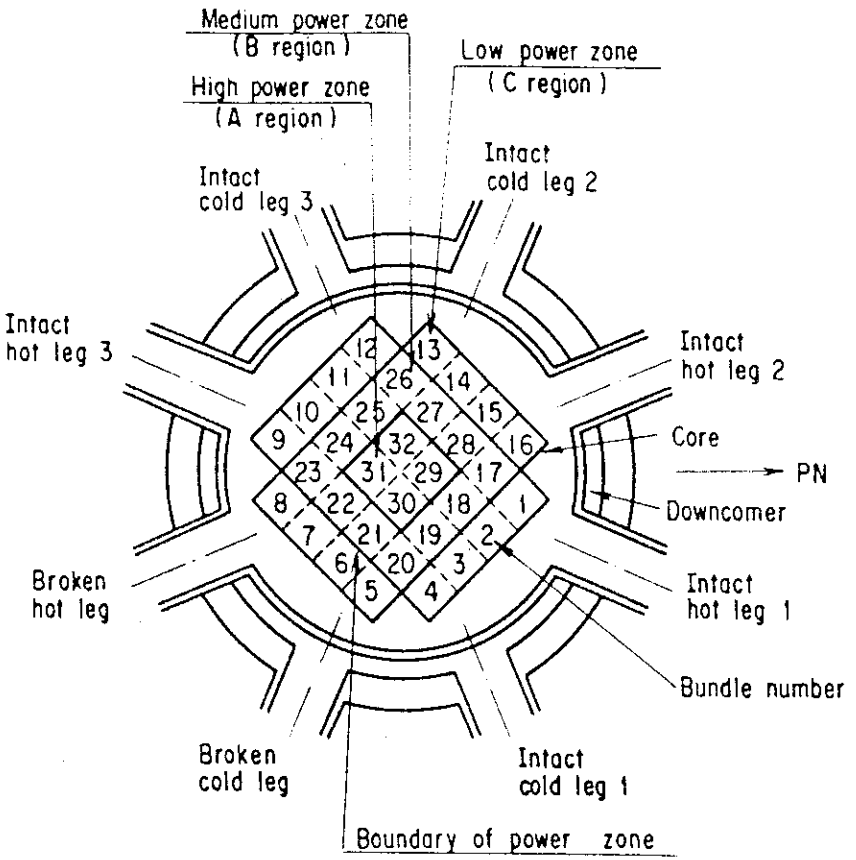

Fig. A. 1 Definition of power zones and bundle numbers

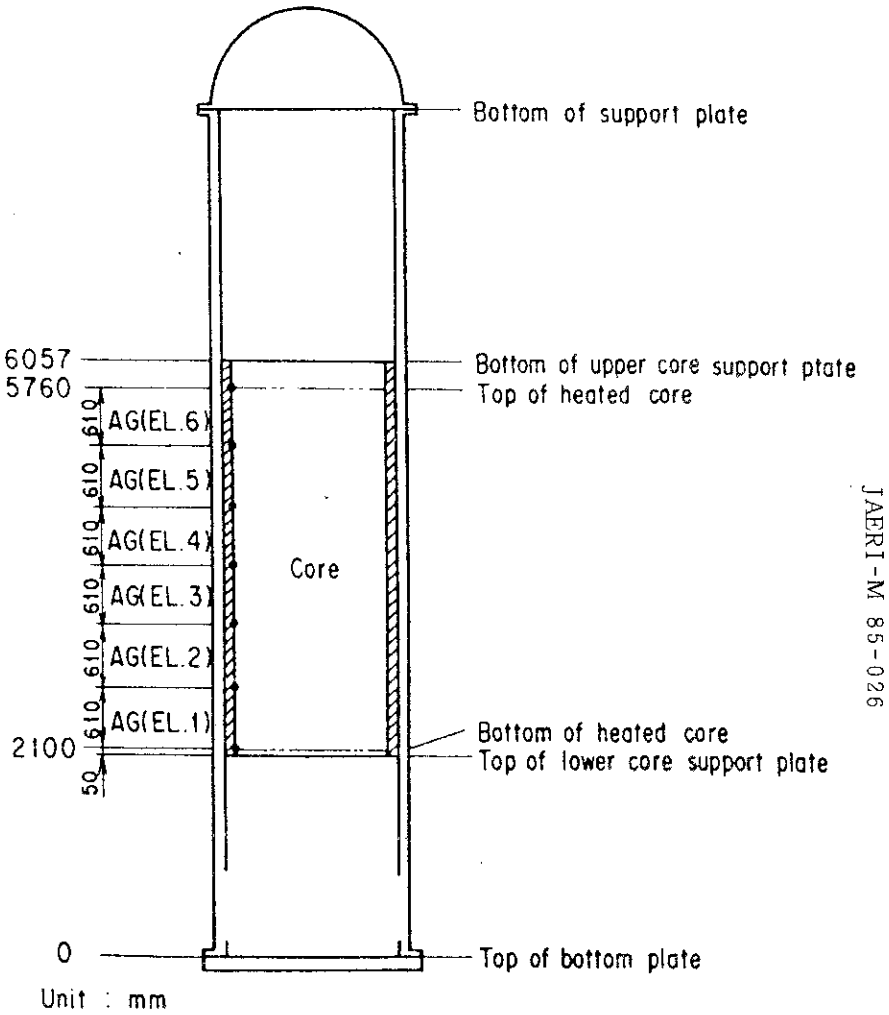

Fig. A. 2 Definition of Tag ID for void fraction (AG(EL. 1) ~ AG(EL. 6))

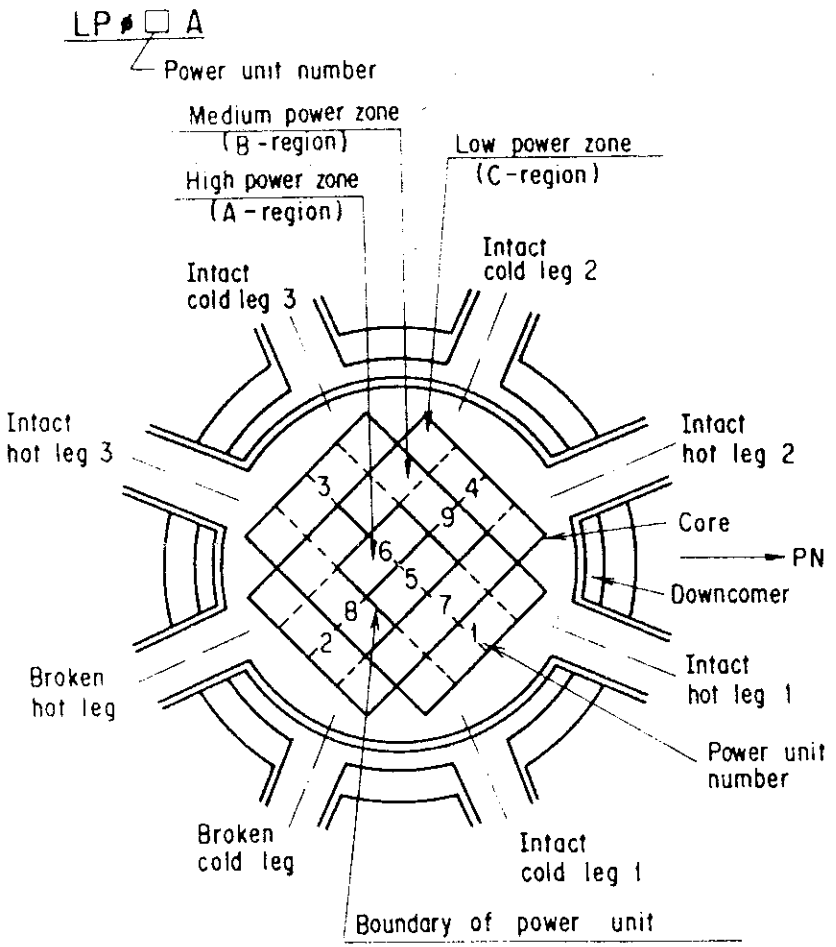

Fig. A. 3 Definition of Tag. ID for average linear power of heater rod in each power unit zone
(LP01A ~ LP09A)

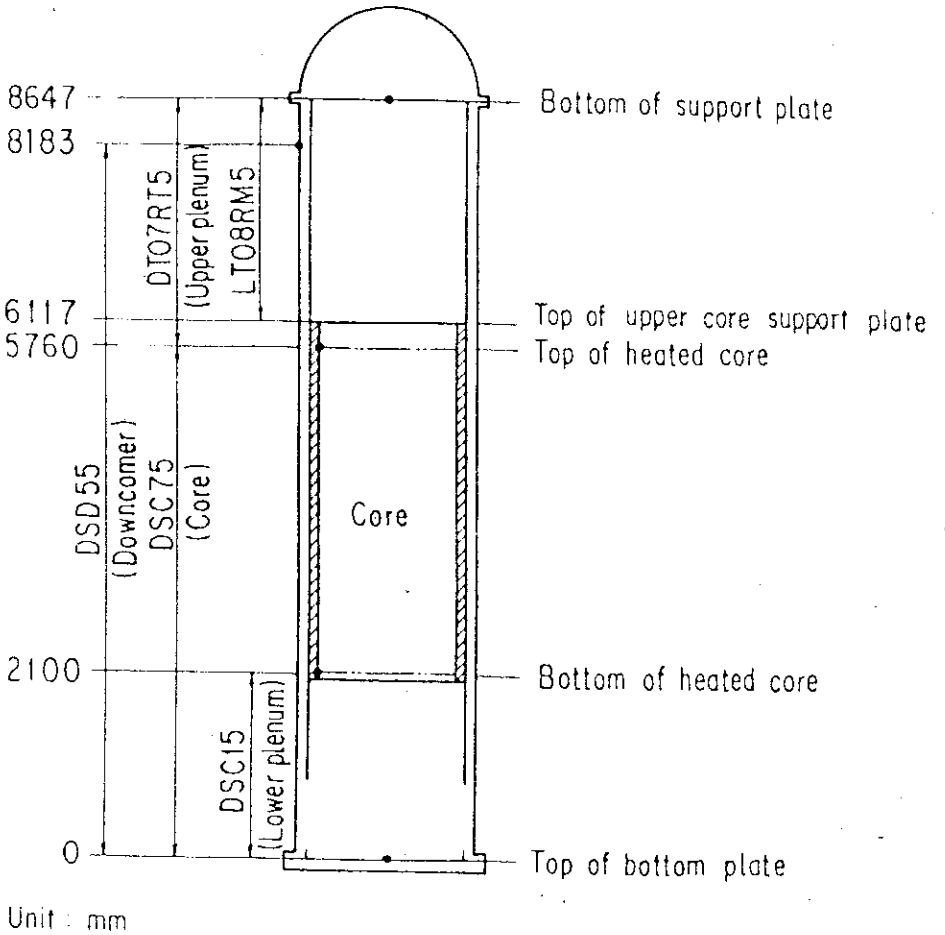

Fig. A. 4 Definition of Tag. ID for differential pressure through downcomer, upper plenum, core, and lower plenum
(DSD55, DT07RT5, LT08RM5, DSC75, DSC15)

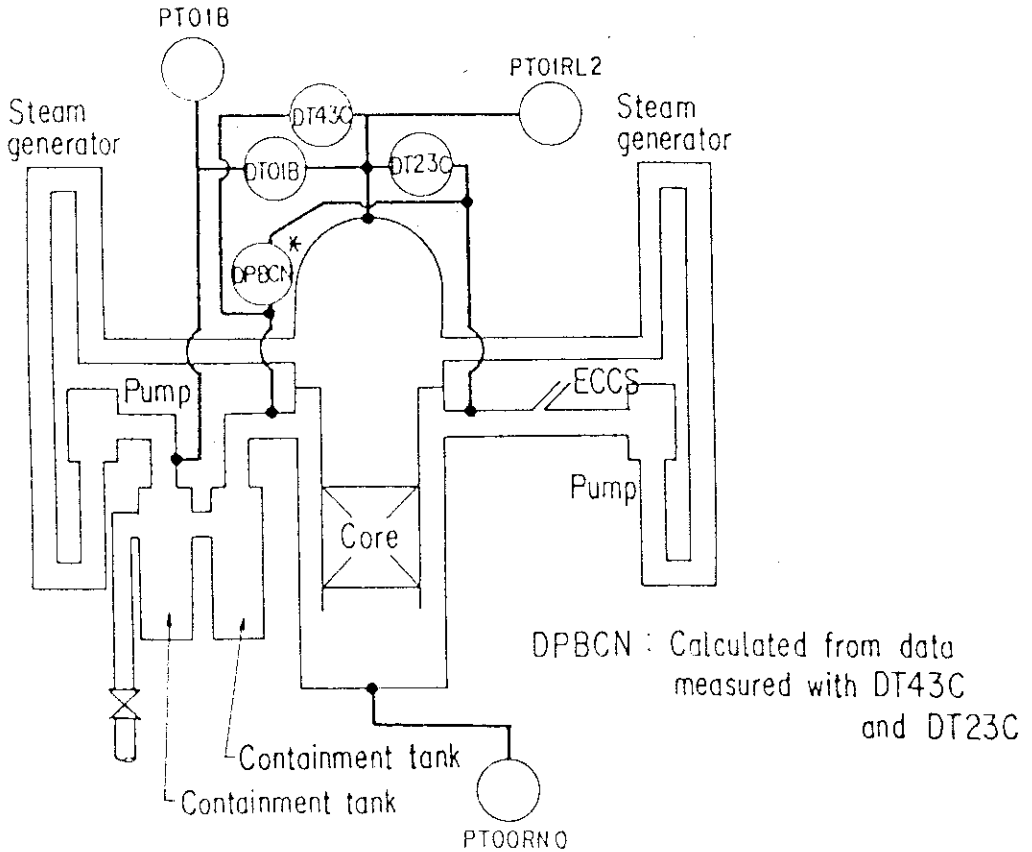

Fig. A. 5 Definition of Tag. ID for pressures in upper and lower plena and containment tank 2 (PT01RL2, PT00RN0, PT01B) and for differential pressure through intact and broken loop and broken cold leg nozzle (DT23C, DT01B, DPBCN)

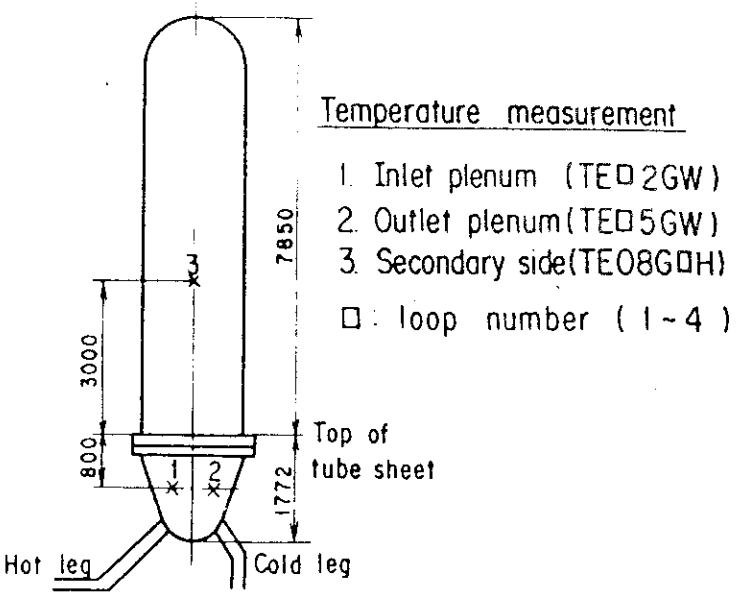

Fig. A. 6 Definition of Tag. ID for fluid temperature in inlet and outlet plenum and secondary of steam generator (TE□2GW, TE□5GW, TE08G□H)

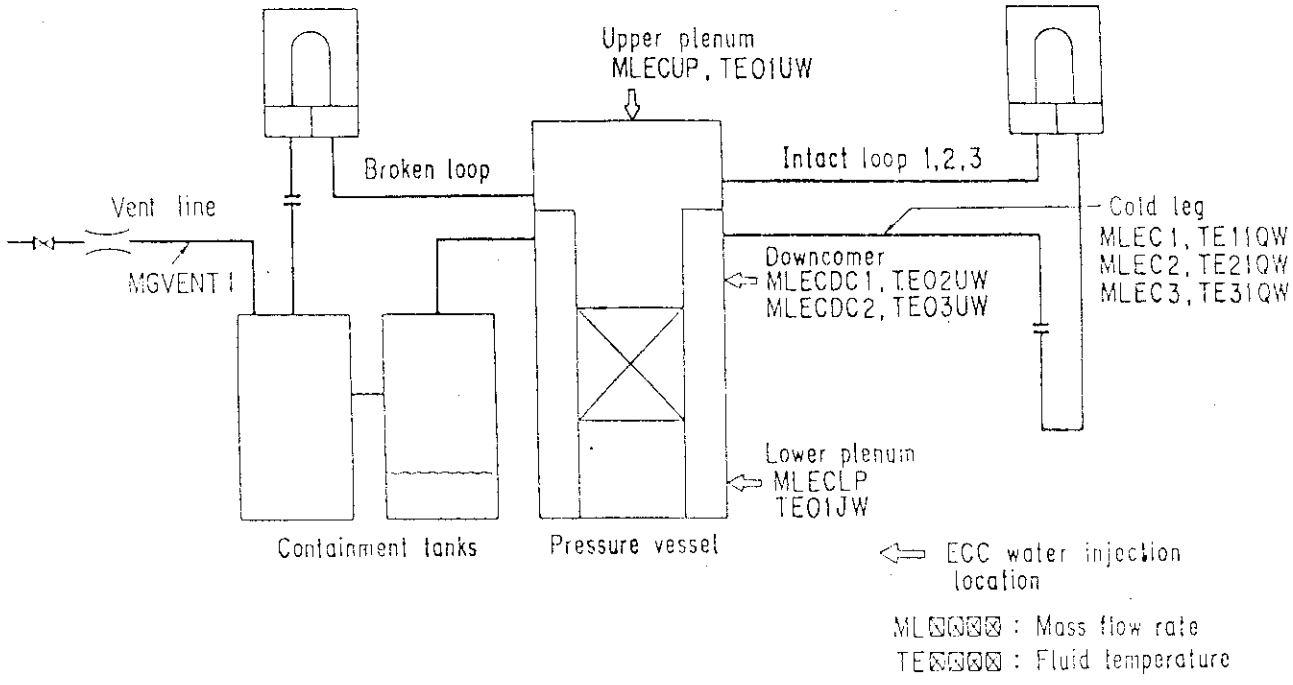

Fig. A. 7 Definition of Tag. ID for ECC water injection rate, ECC water temperature and vented steam flow rate

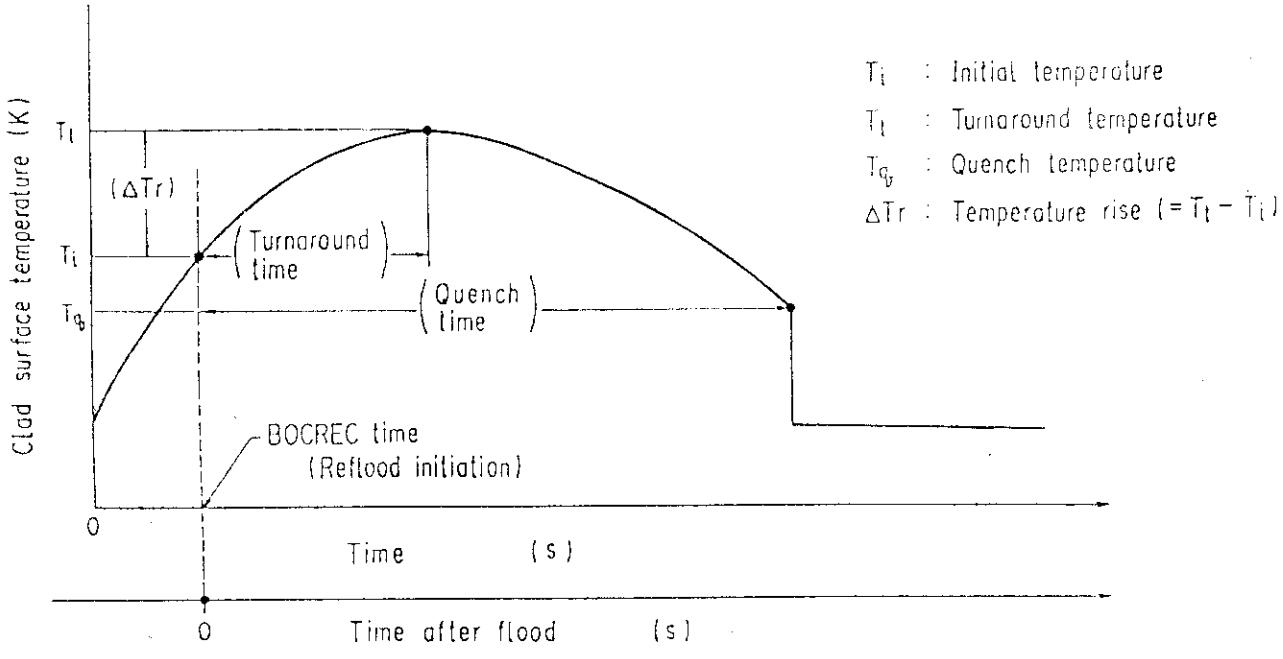

Fig. A. 8 Definition of initial temperature, turnaround temperature, quench temperature, temperature rise, turnaround time and quench time

Appendix B

Selected data of CCTF Test C2-4 (Run 62)

Figure List

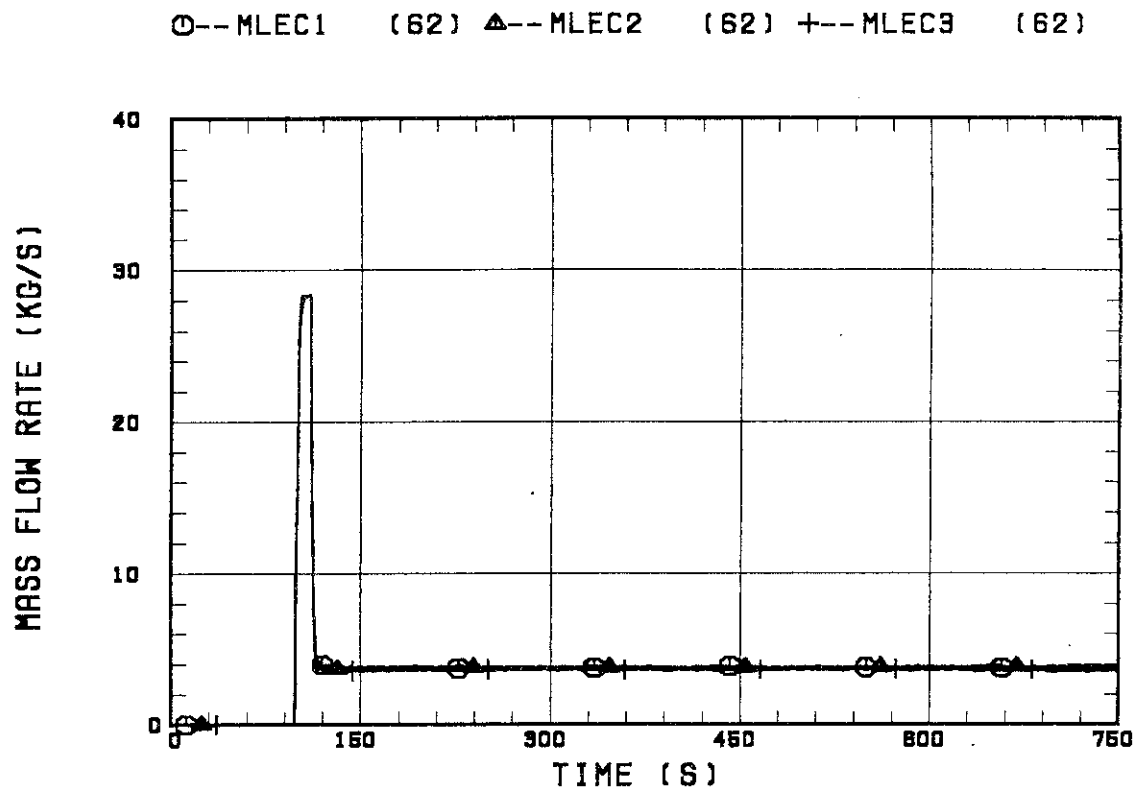

Fig. B.1 ECC water injection rates into the primary system.

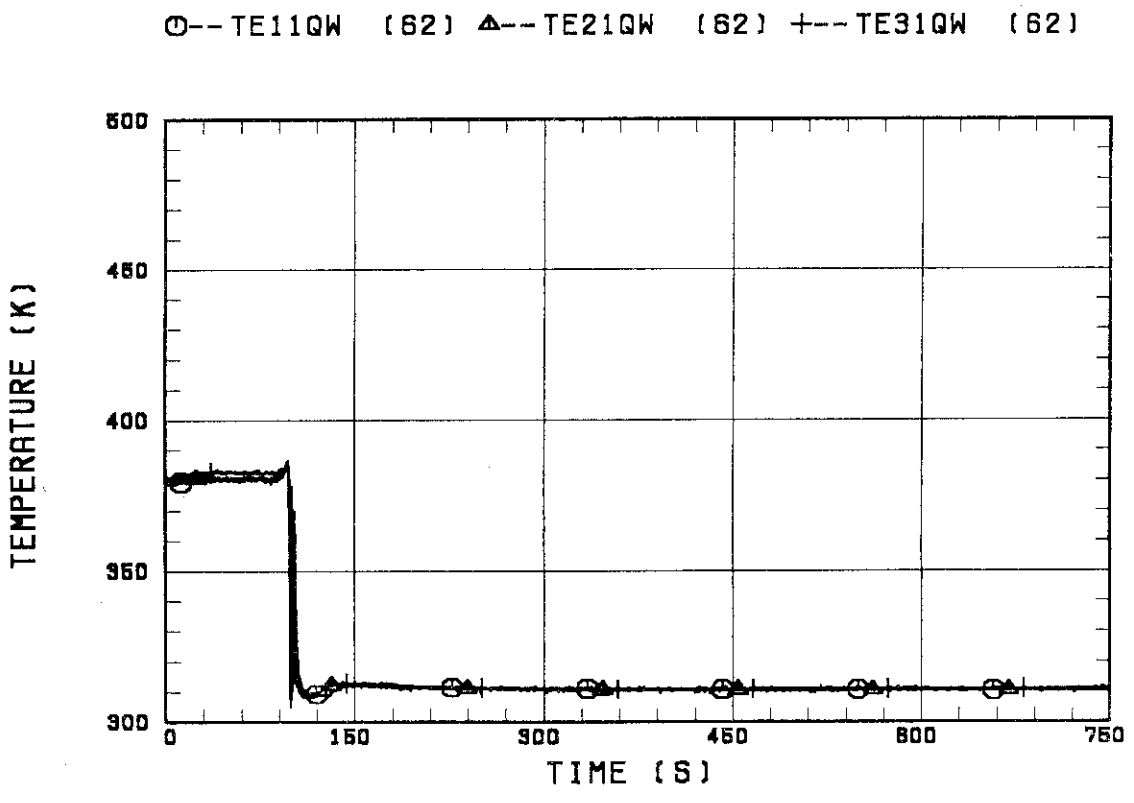

Fig. B.2 ECC water temperature.

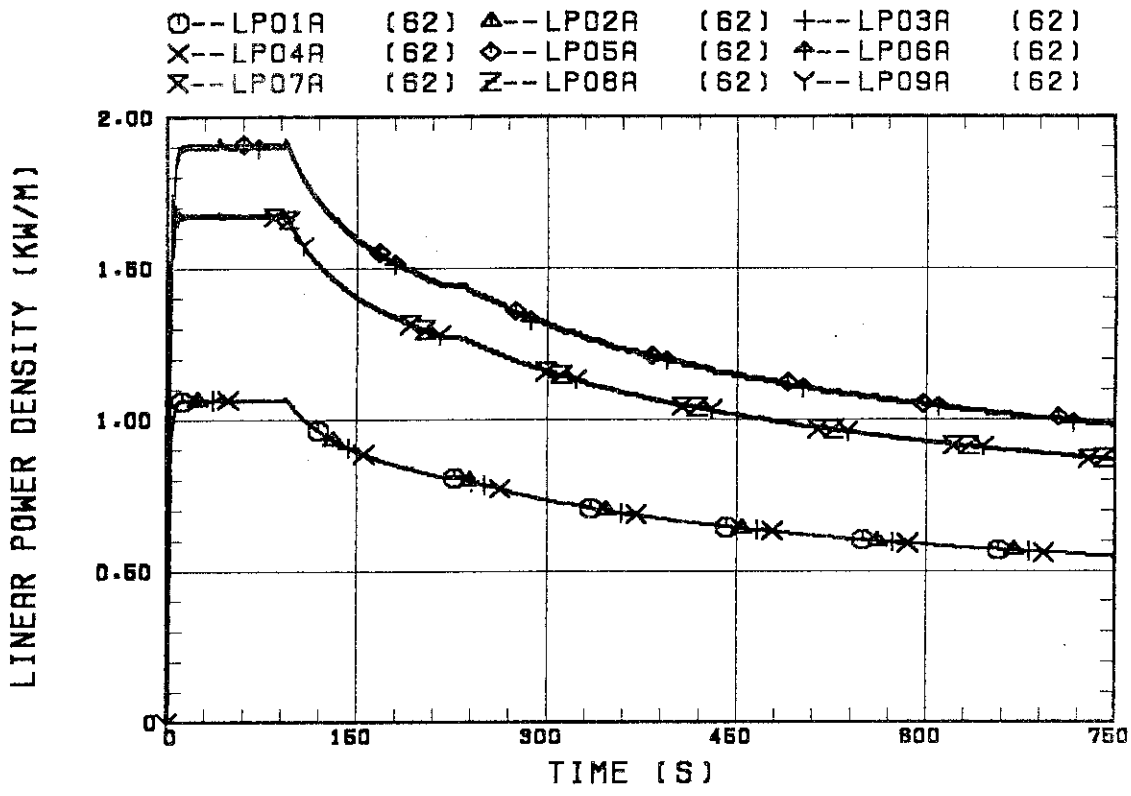

Fig. B.3 Average linear power of heater rod in each power unit zone.

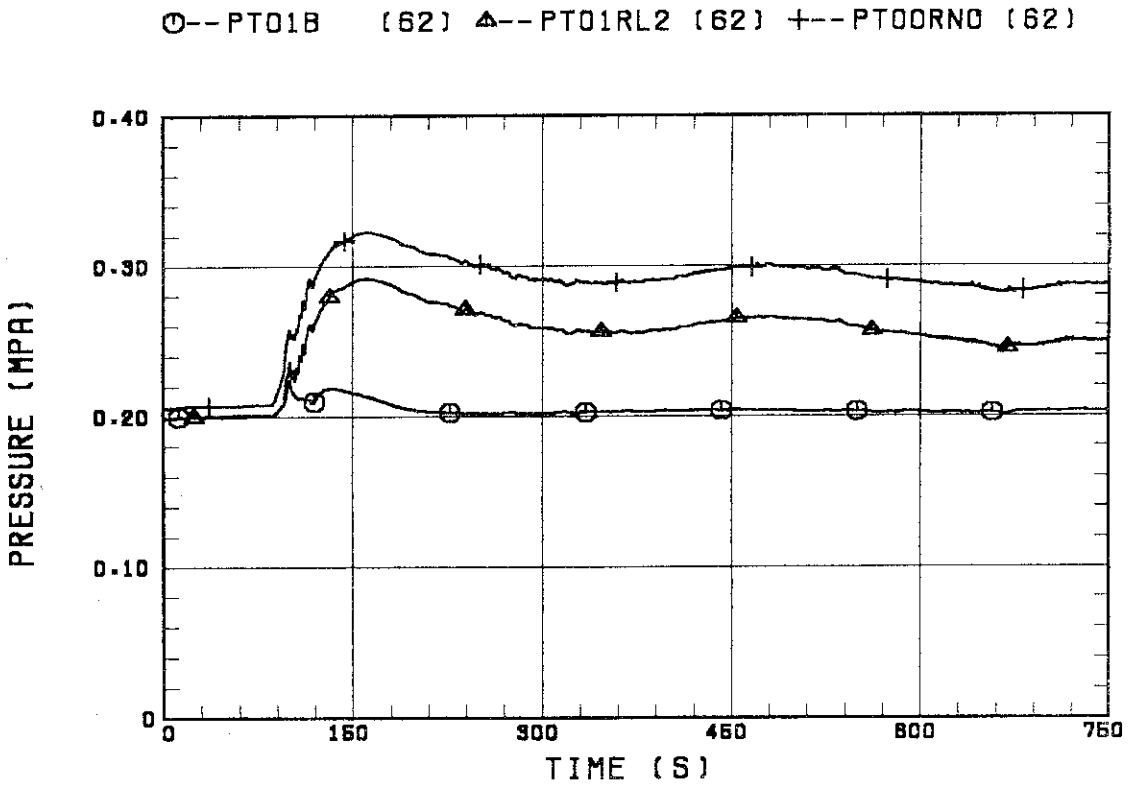

Fig. B.4 Pressure history in containment tank 2, upper plenum and lower plenum.

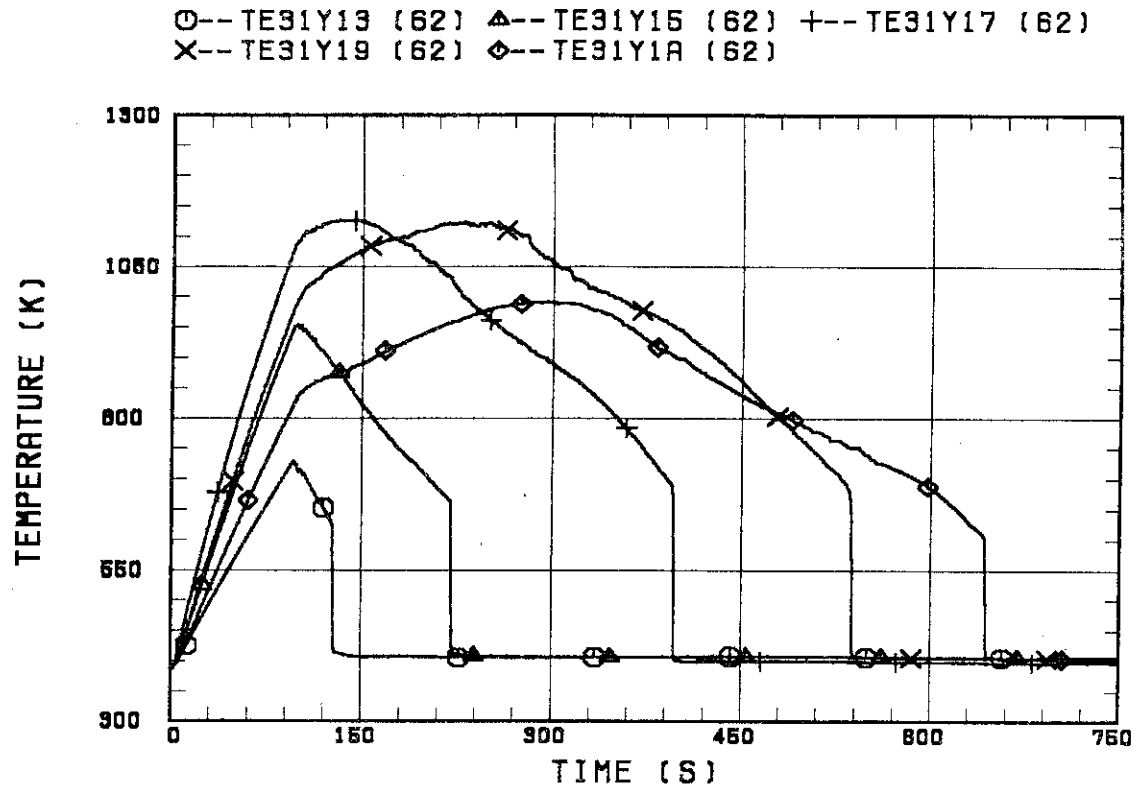

Fig. B.5 Clad surface temperature at various elevations along a heater rod in high power region (A region).

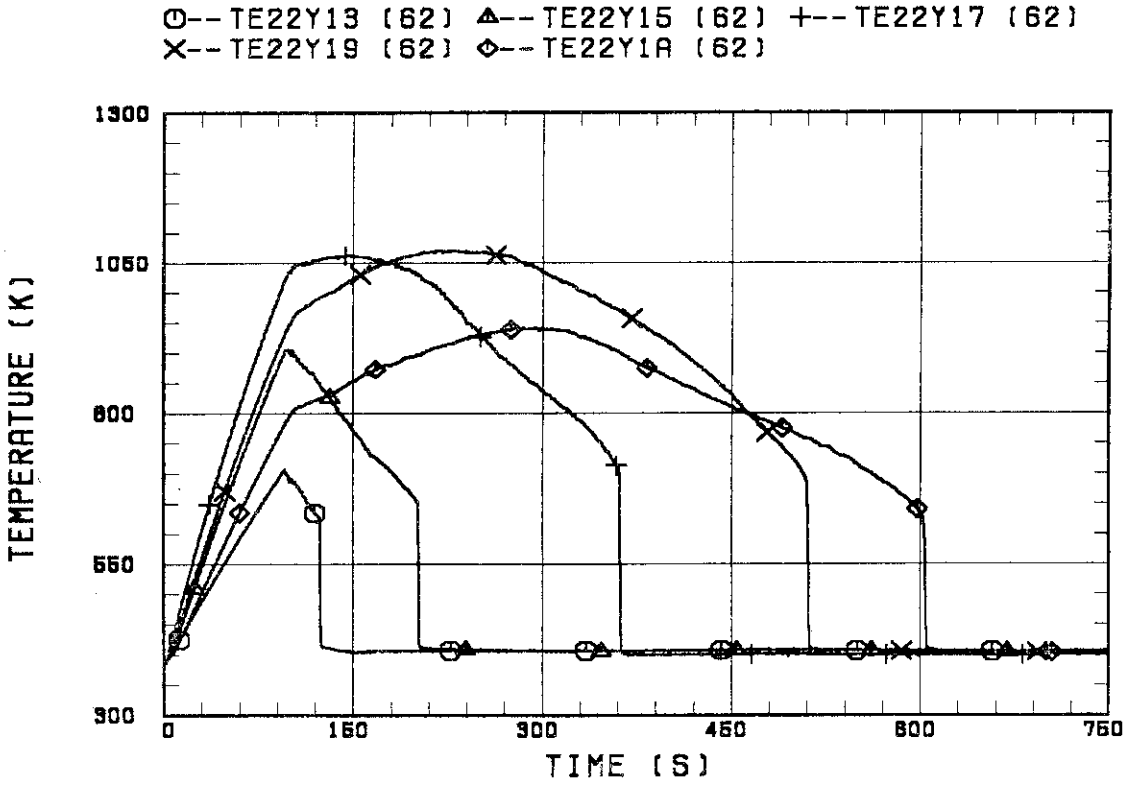

Fig. B.6 Clad surface temperature at various elevations along a heater rod in medium power region (B region).

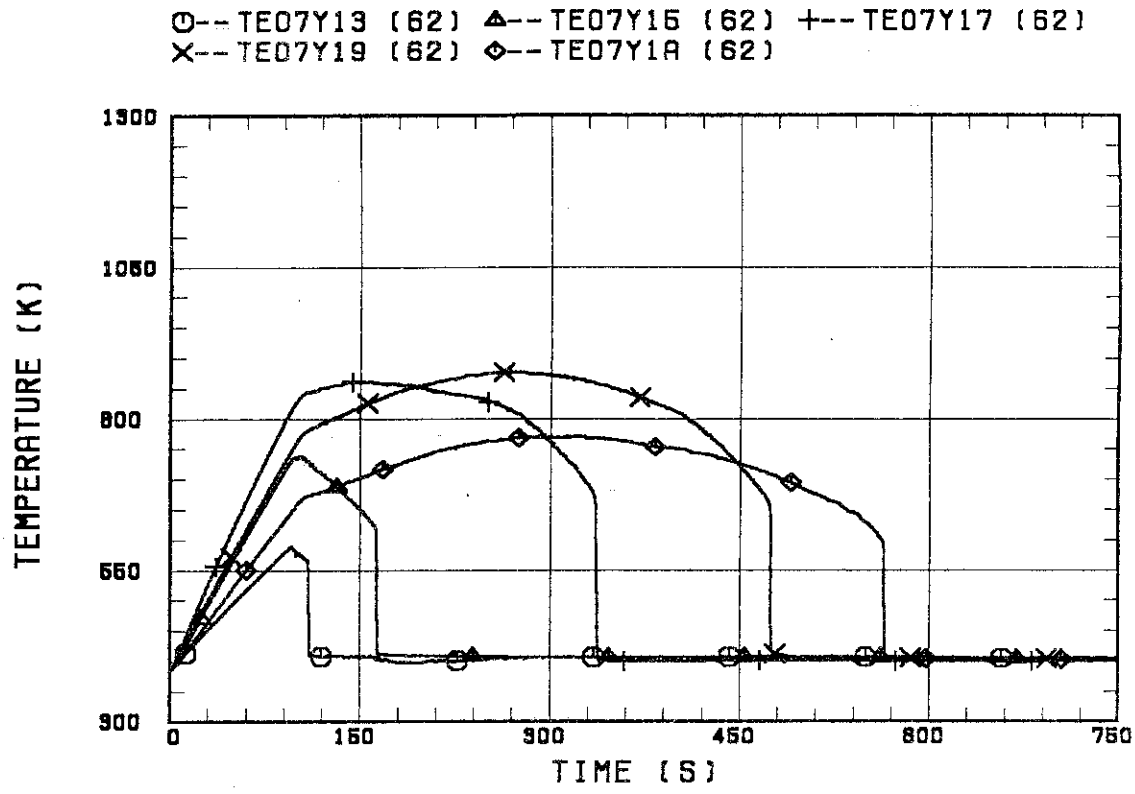

Fig. B.7 Clad surface temperature at various elevations along a heater rod in low power region (C region).

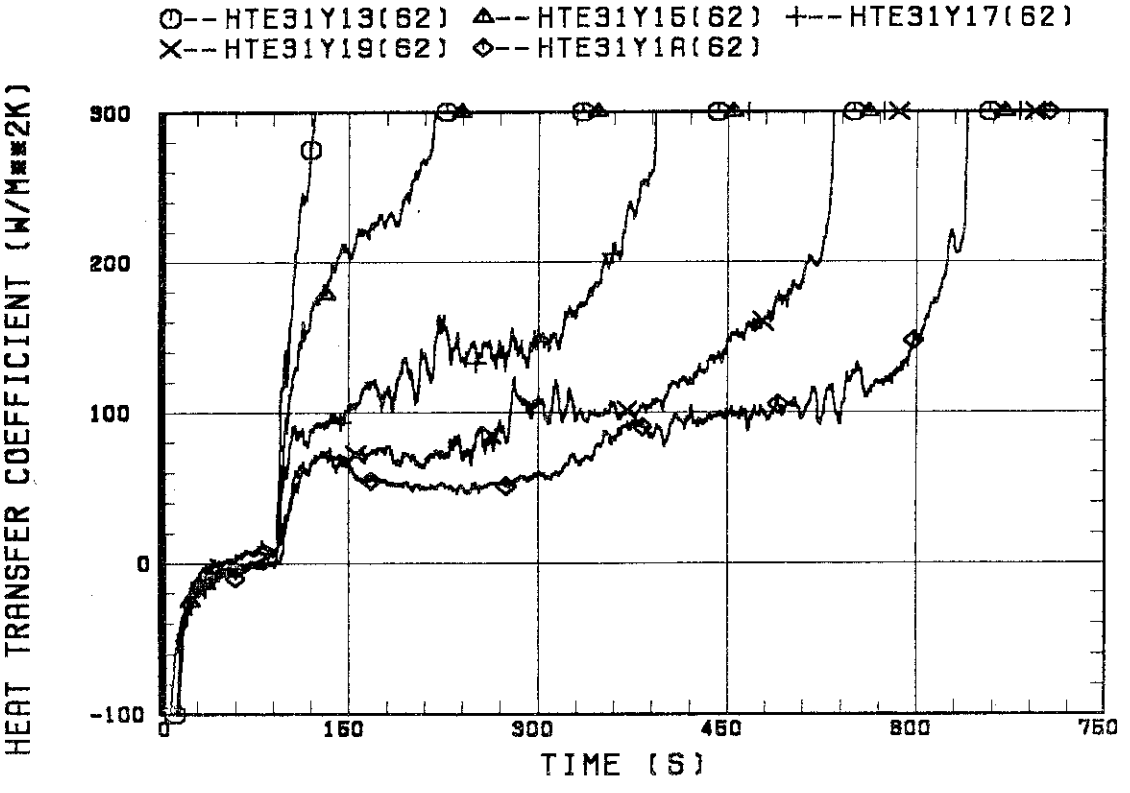

Fig. B.8 Heat transfer coefficient at various elevations along a heater rod in high power region (A region).

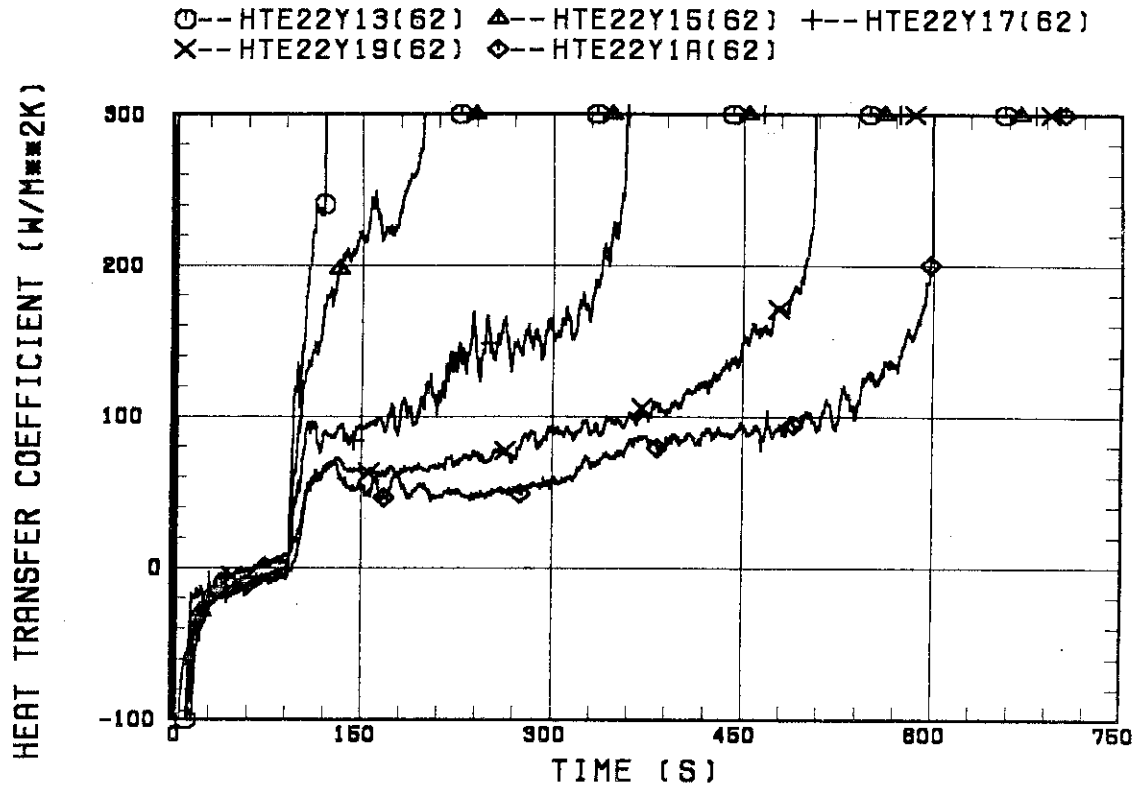

Fig. B.9 Heat transfer coefficient at various elevations along a heater rod in medium power region (B region).

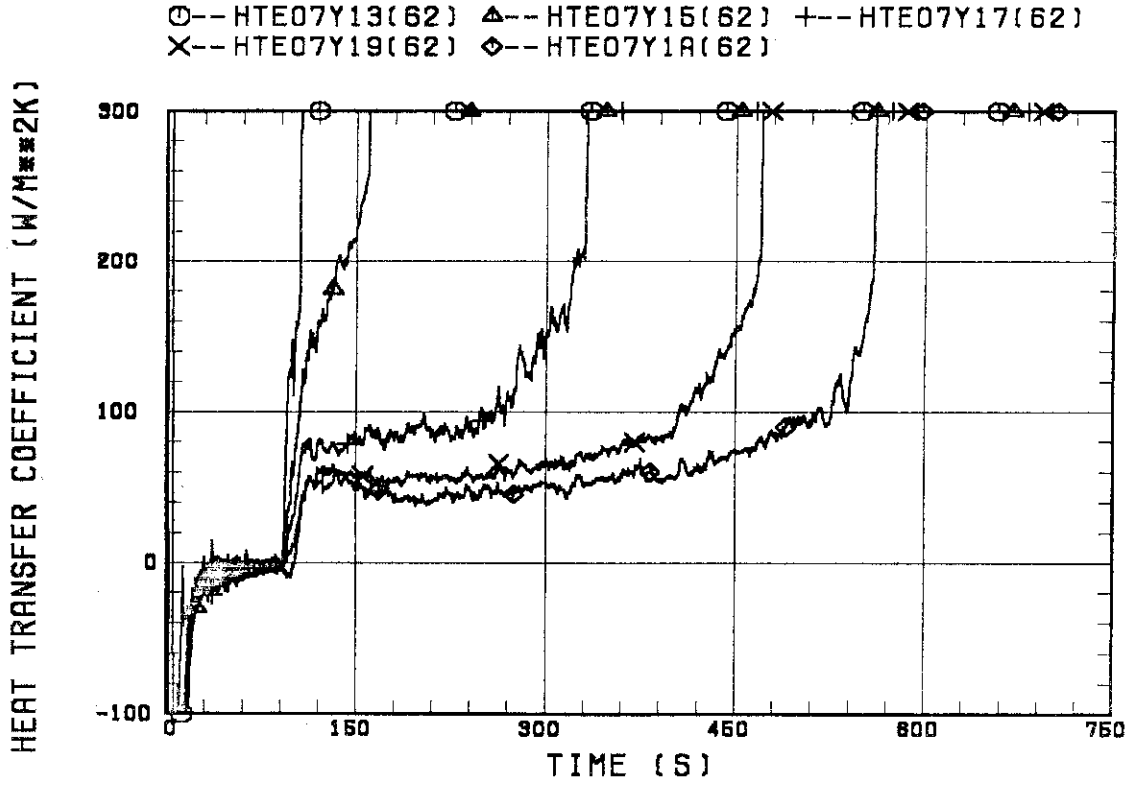

Fig. B.10 Heat transfer coefficient at various elevations along a heater rod in low power region (C region).

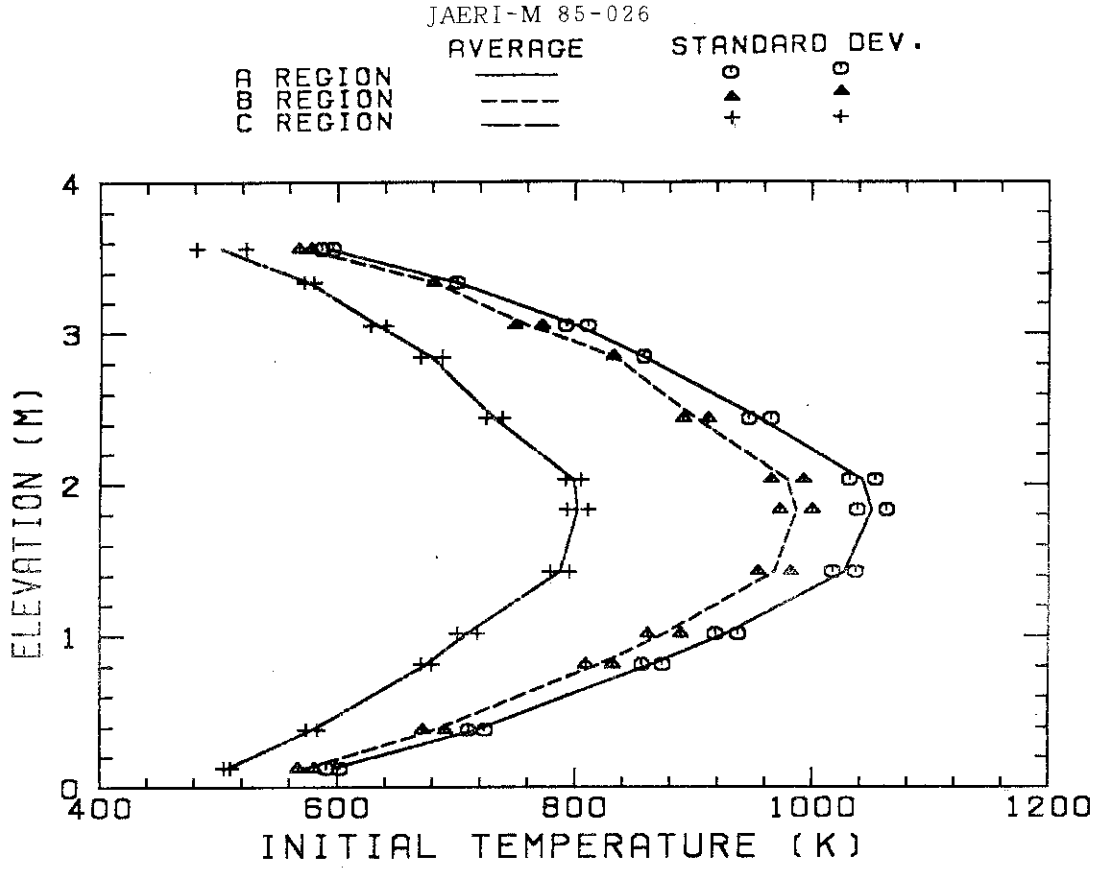

Fig. B.11 Initial clad surface temperature.

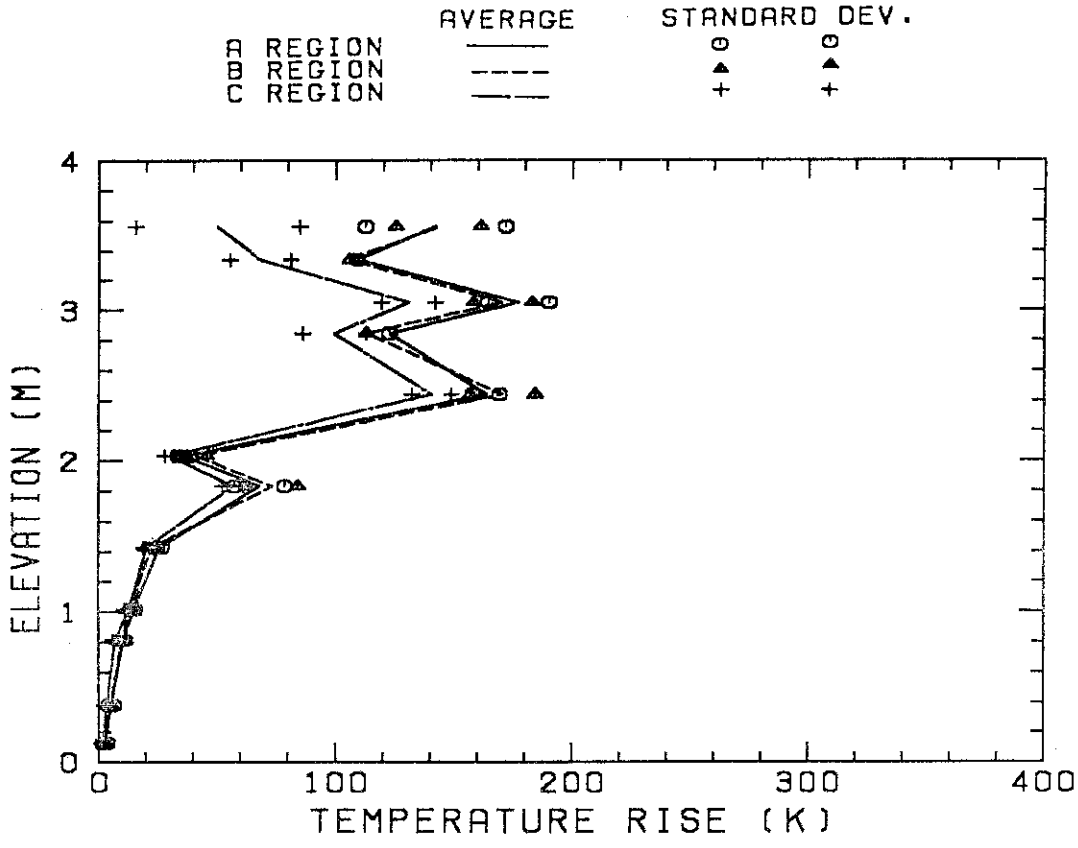

Fig. B.12 Temperature rise.

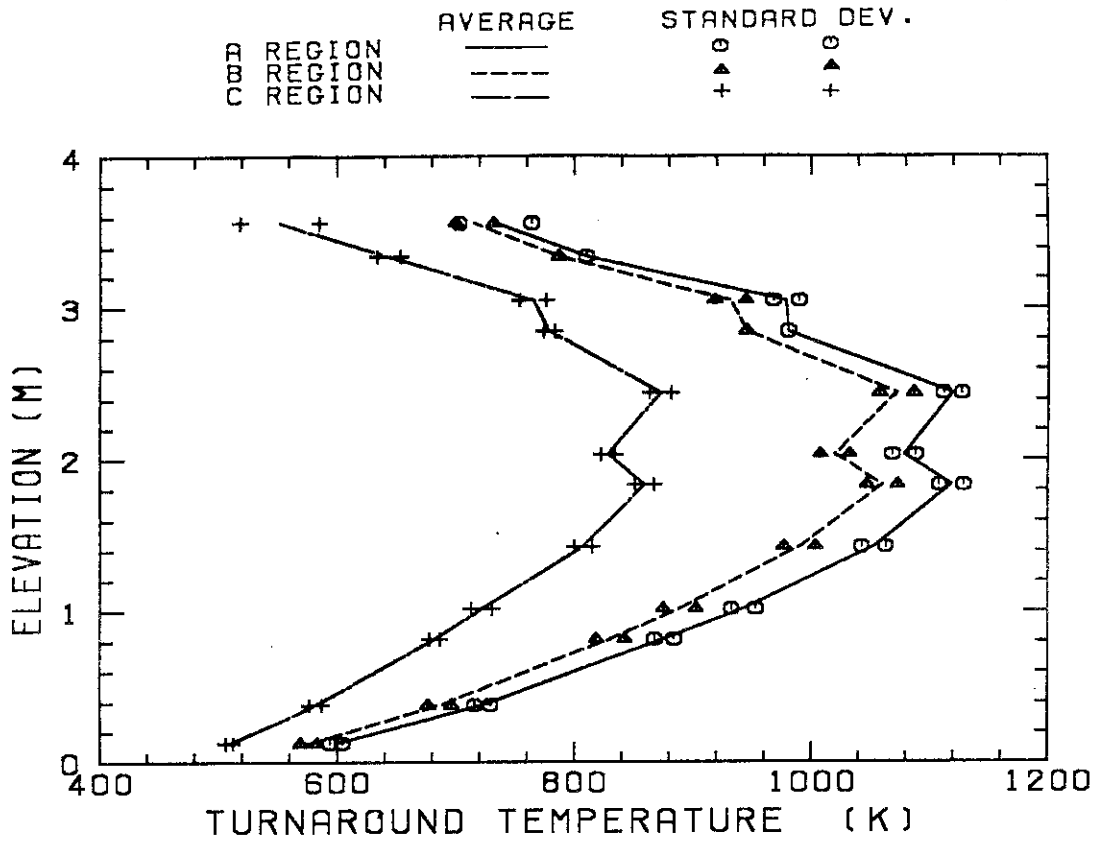

Fig. B.13 Turnaround temperature.

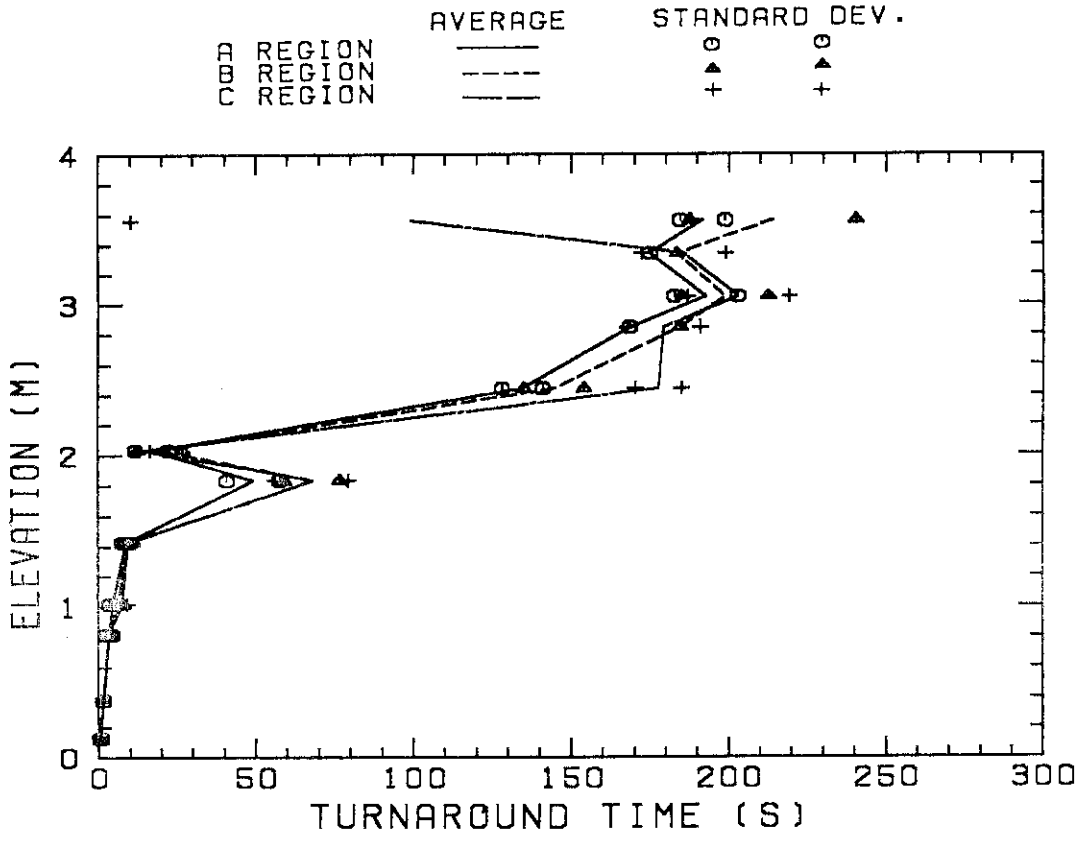

Fig. B.14 Turnaround time.

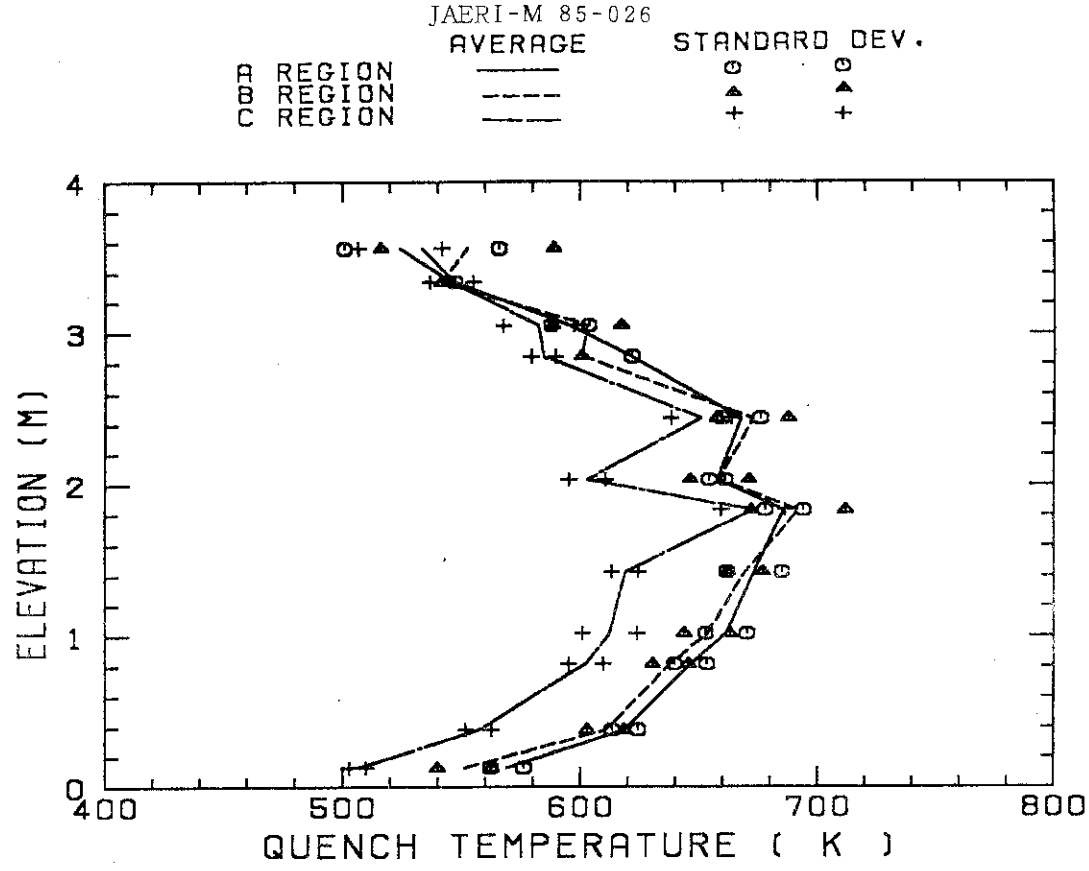

Fig. B.15 Quench temperature.

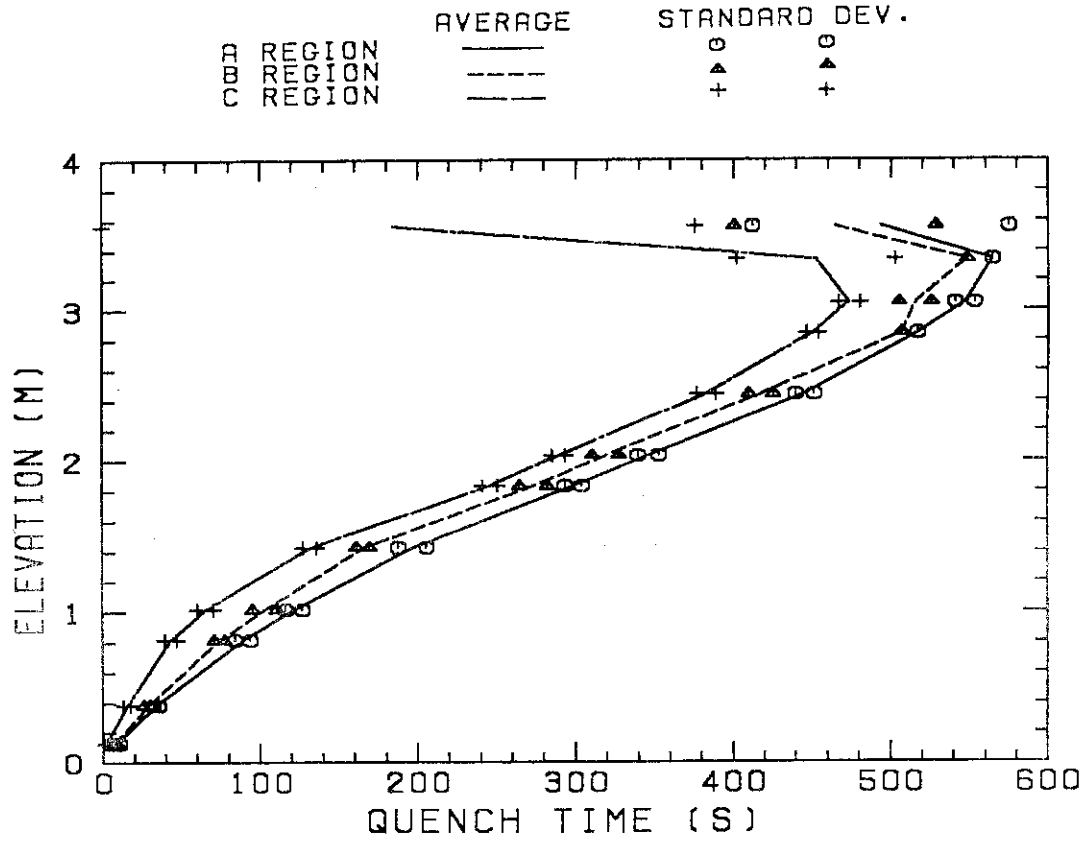

Fig. B.16 Quench time.

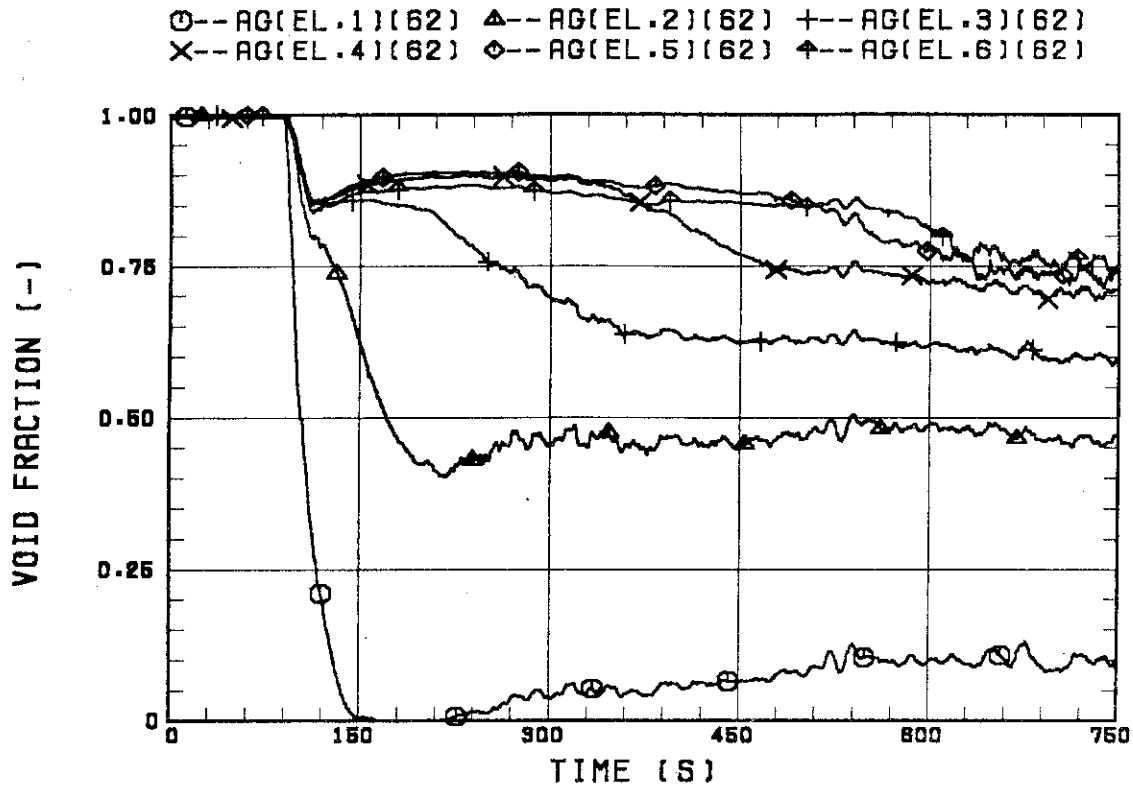

Fig. B.17 Void fraction in core.

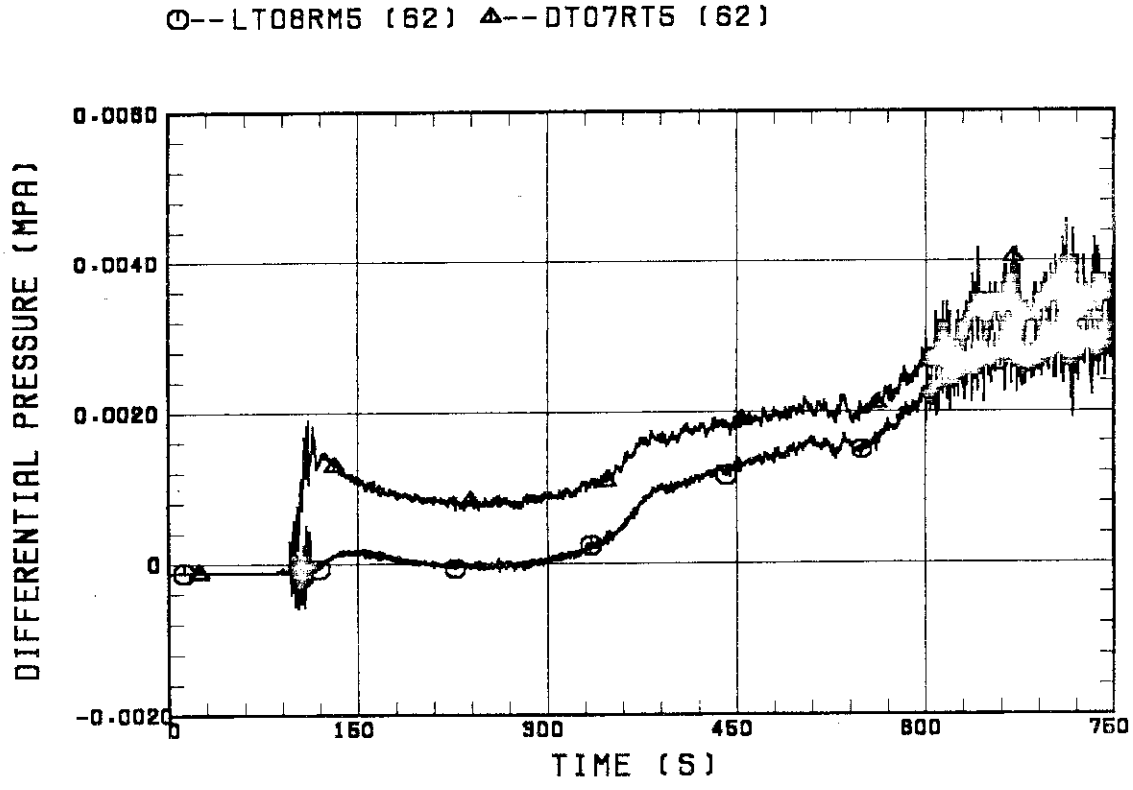

Fig. B.18 Differential pressure through upper plenum.

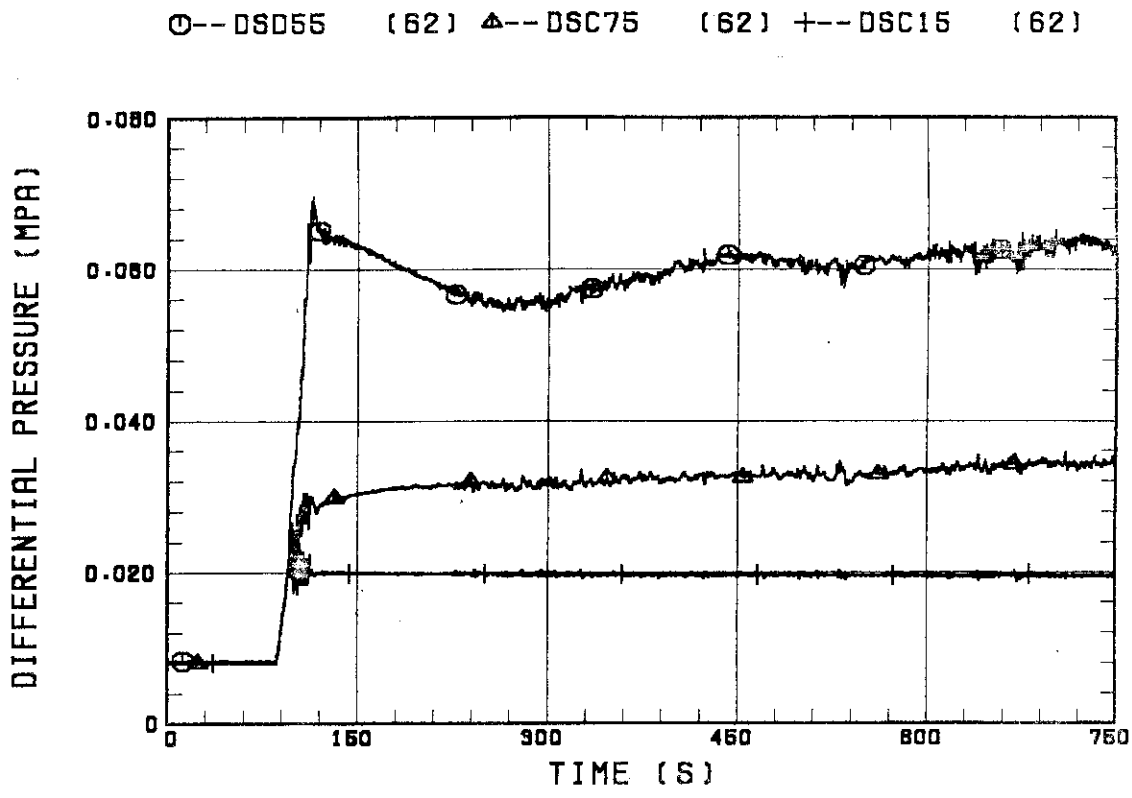

Fig. B.19 Differential pressure through downcomer, core, and lower plenum.

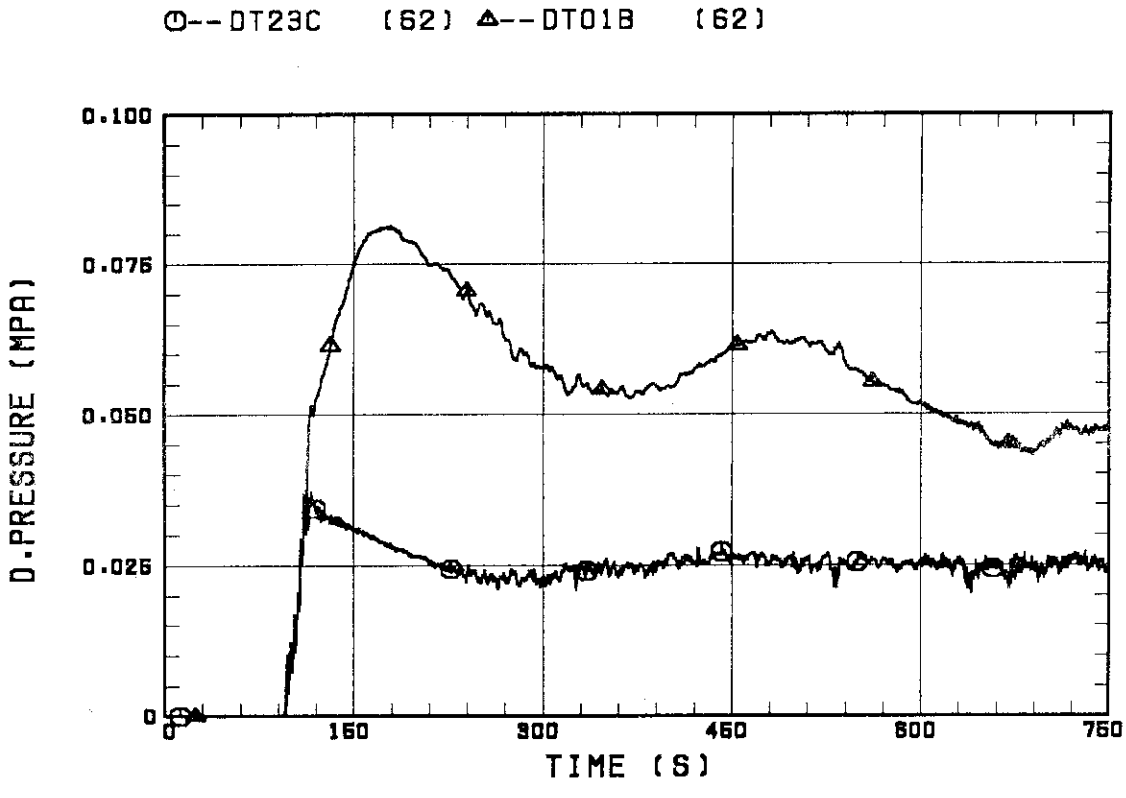

Fig. B.20 Differential pressure through intact and broken loops.

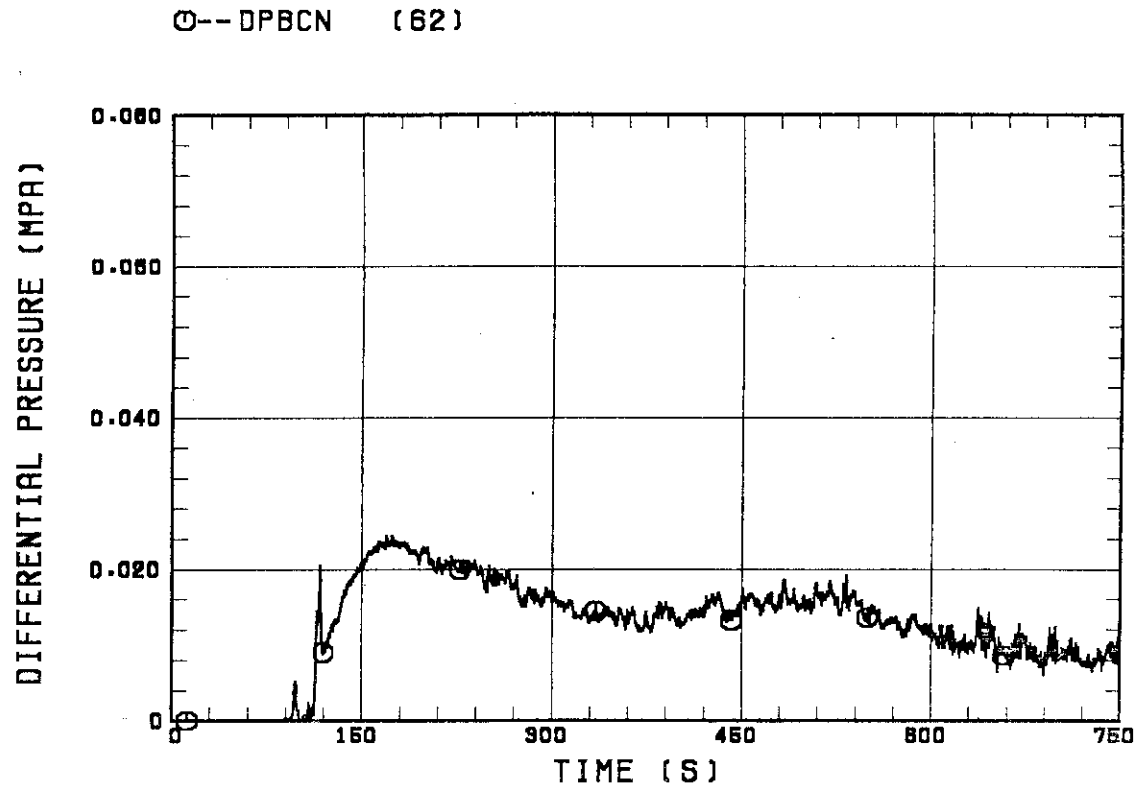

Fig. B.21 Differential pressure through broken cold leg nozzle.

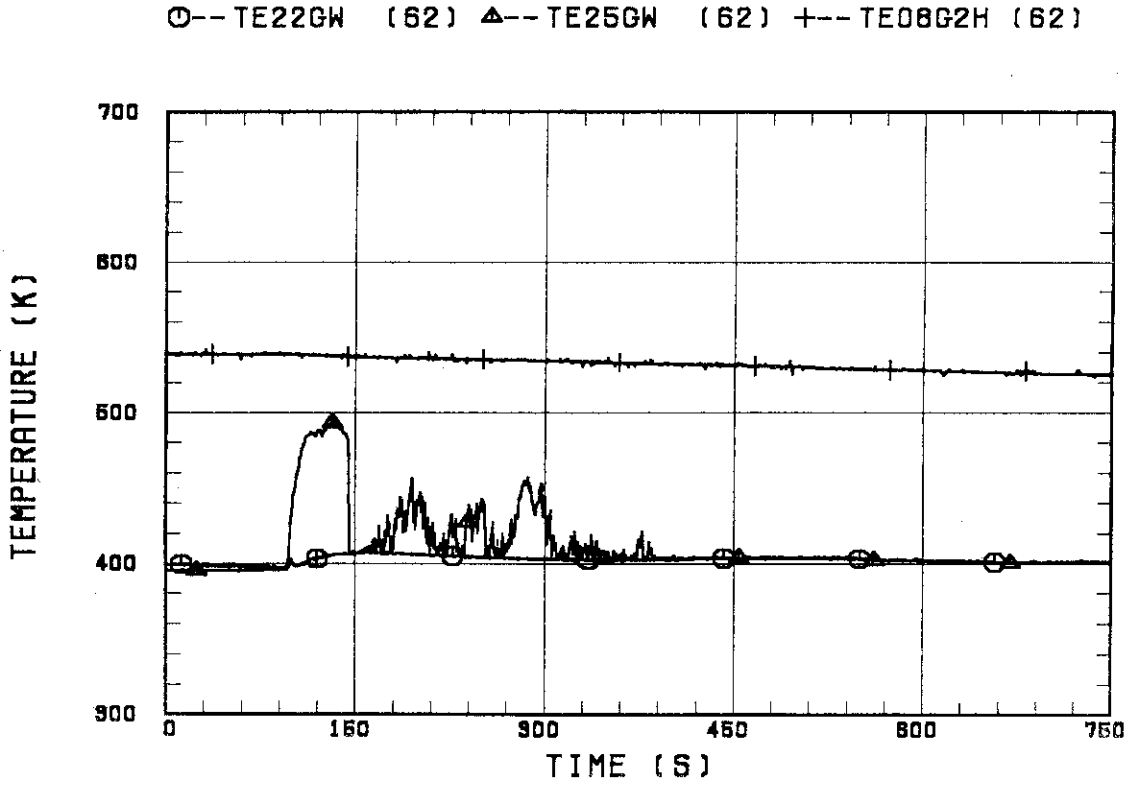

Fig. B.22 Fluid temperature in inlet plenum, outlet plenum, and secondary of steam generator 1.

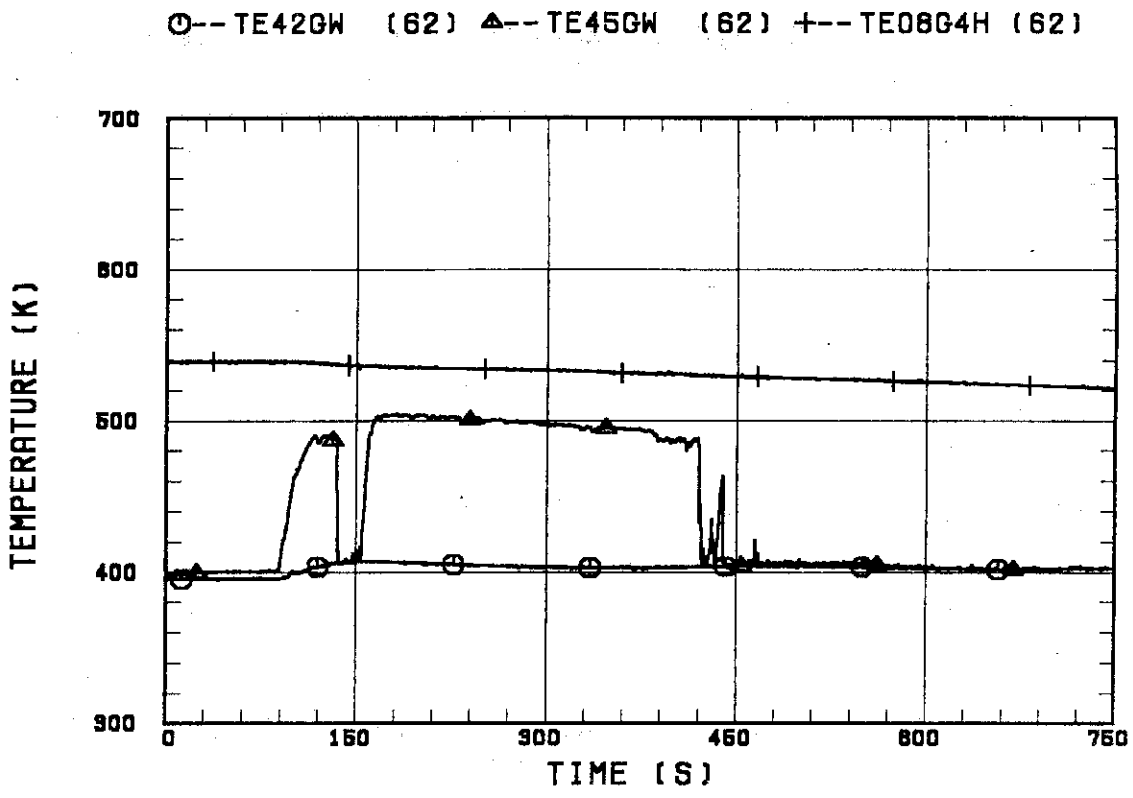

Fig. B.23 Fluid temperature in inlet plenum, outlet plenum, and secondary of steam generator 2.

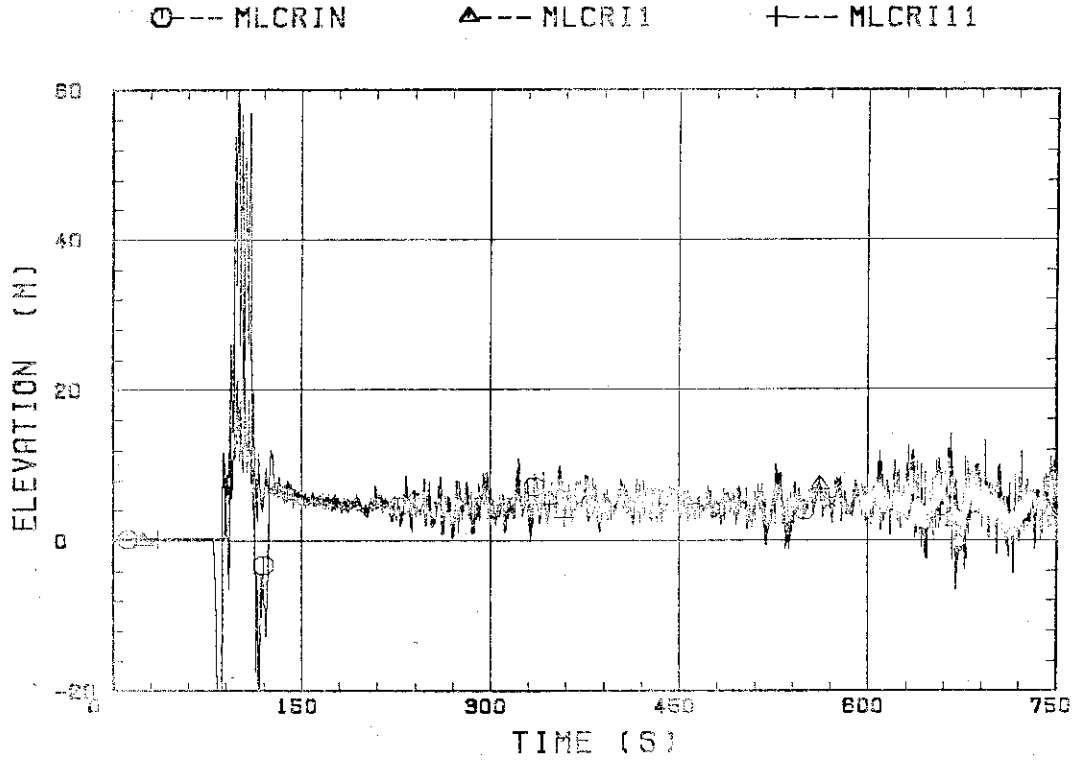

Fig. B.24 Core flooding mass flow rates evaluated with Eqs. (A.1) and (A.2)

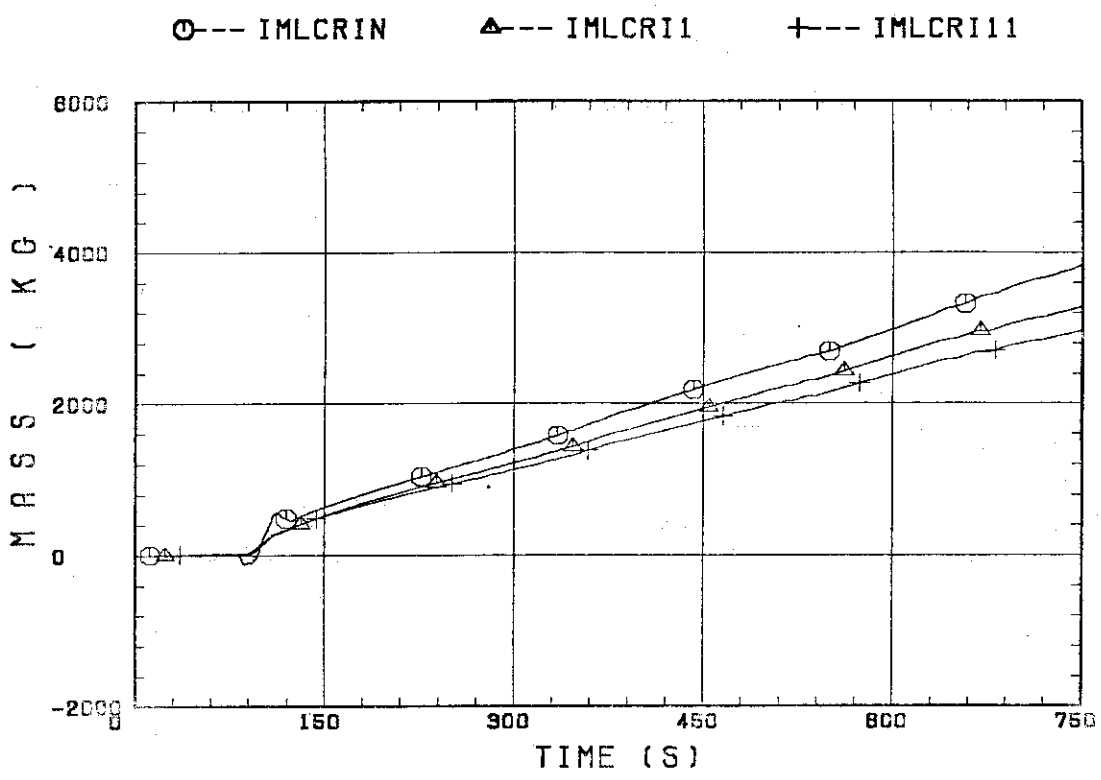

Fig. B.25 Time-integral mass flooded into core evaluated with Eqs. (A.1) and (A.2).

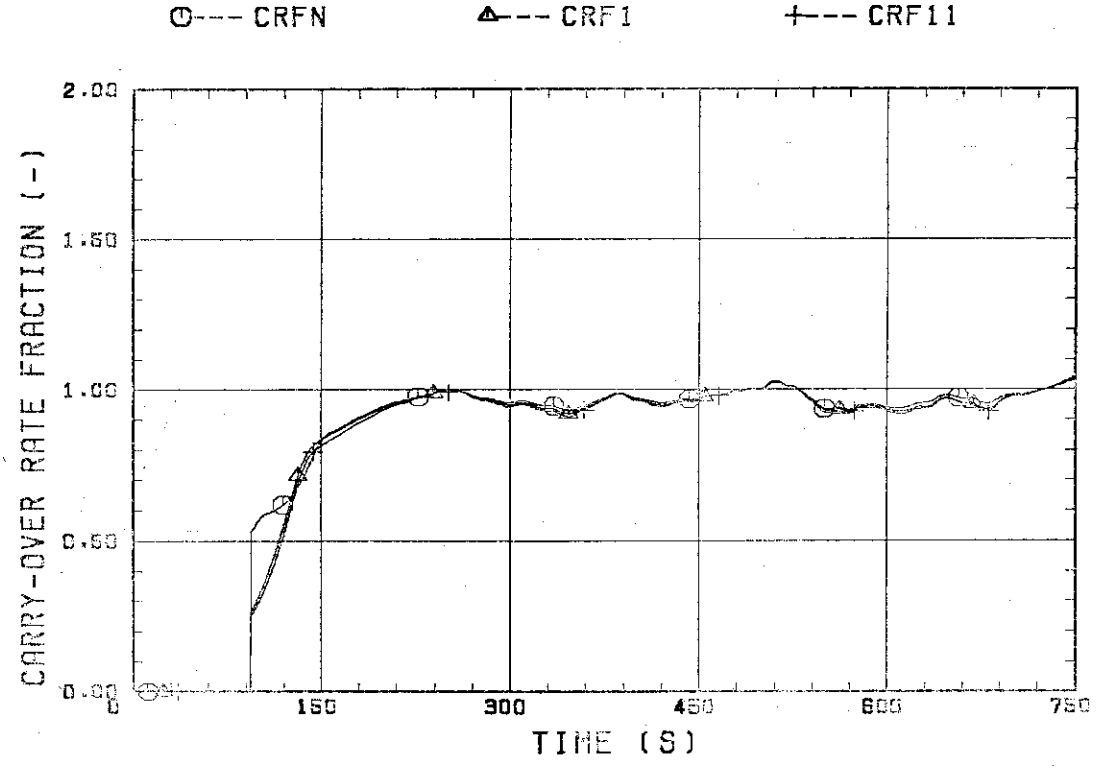

Fig. B.26 Carry-over rate fraction.

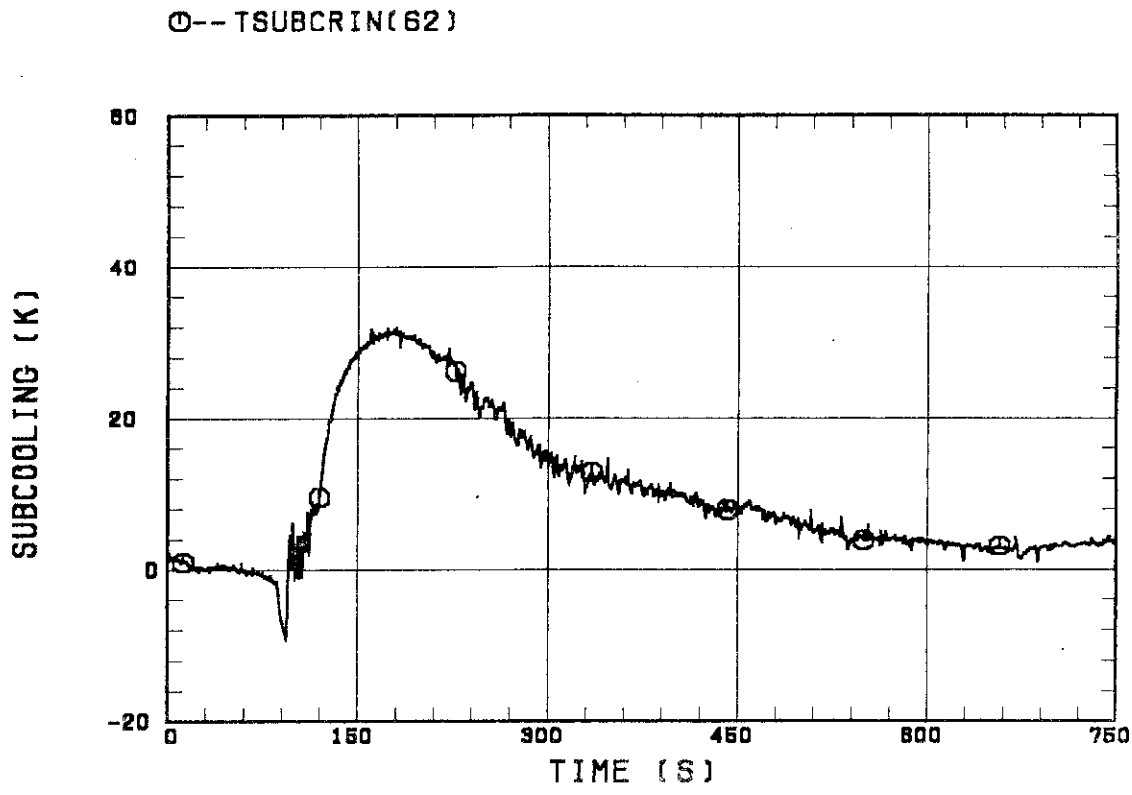

Fig. B.27 Core inlet subcooling.

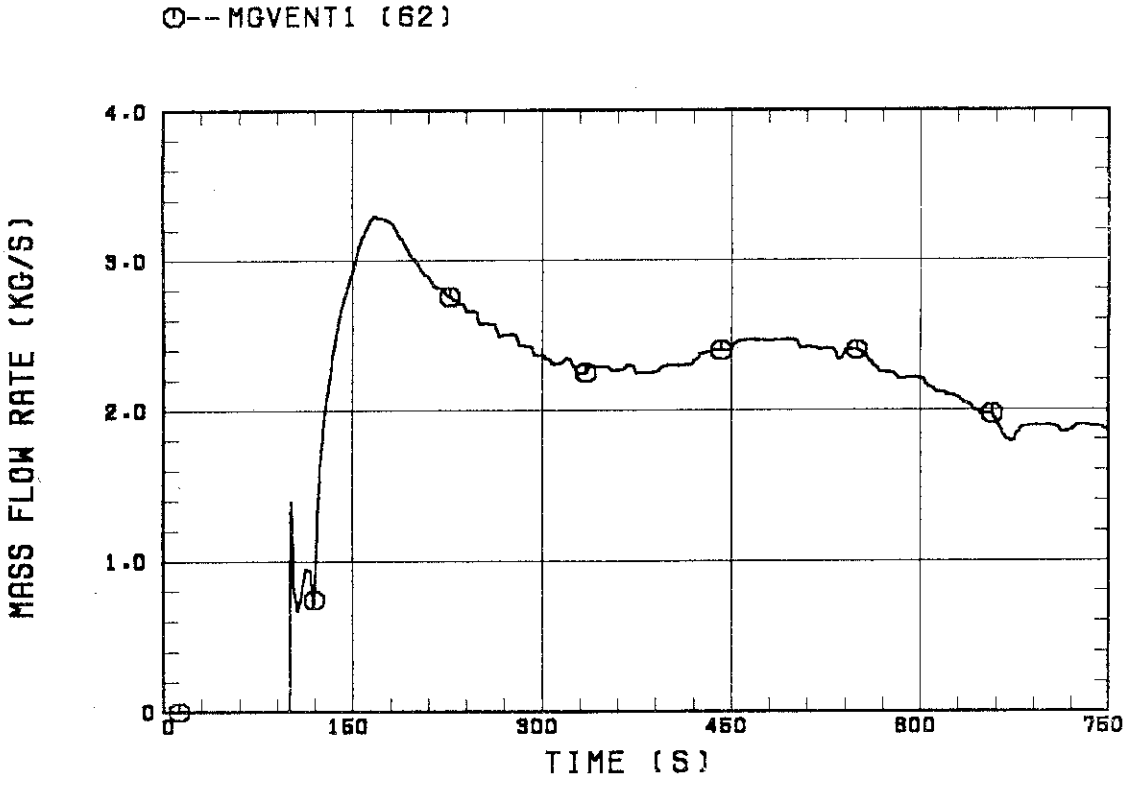

Fig. B.28 Exhausted mass flow rate from containment tank 2.